RADX: A novel single-stranded DNA-binding protein regulating telomere recombination

Thèse N° 9759

Présentée le 4 octobre 2019

à la Faculté des sciences de la vie
Unité du Prof. Lingner
Programme doctoral en approches moléculaires du vivant

pour l'obtention du grade de Docteur ès Sciences

par

Anna-Sophia BRIOD

Acceptée sur proposition du jury

Prof. V. Simanis, président du jury
Prof. J. Lingner, directeur de thèse
Prof. Y. Doksani, rapporteur
Prof. B. Luke, rapporteur
Prof. B. Fierz, rapporteur

2019

ÉCOLE POLYTECHNIQUE
FÉDÉRALE DE LAUSANNE

Acknowledgements

First, I would like to express my gratitude to my supervisor Prof. Joachim Lingner for giving me the opportunity to work on this interesting and challenging project. I am very thankful for his full support throughout these five years, his patience and understanding during difficult times and his passion and motivation which encouraged me to continue striving to discover the important functions and mechanisms behind these unknown telomeric proteins.

I also would like to thank all former and present colleagues and lab members. Eric Aeby helped me with my very first experiments and sparked my interest in CRISPR/Cas9 genome editing. Wareed, Marianna and Gabriela who always had an open ear for my questions. Many thanks to Jana, Aleksandra, Rita, Anna, Trang with whom I could share the ups and downs of this Ph.D. journey and especially to Patricia, who understood better than anyone else the challenges and the excitement I encountered and who supported me and cheered me up. I owe a special thanks to my lab and bench mate Galina, who was there for me at all times and without whom my project would not have taken this exciting turn. My gratitude also goes to Thomas, who keeps not only the lab but also all of us in check. I am especially grateful to him for all the extra work he took on when I needed help.

I would like to acknowledge the NCCR RNA&Disease network who supported me with a maternity leave compensation grant which allowed us to hire Timothy Murray, who helped me with my project and continued working and performing important experiments while I was gone.

I also would like to express my gratitude to Helene Fischer and Chantal Mellier from the EPFL Equal Opportunity Office, who provided us with financial support for a private daycare solution on the EPFL campus. Their help allowed me to return to my Ph.D. after my maternity leave under the best possible conditions.

Thank you to Tatiana Dubi, Sandra Roux and Nicole De Montmollin helping me to navigate administrative duties and requirements.

I am grateful to the members of my thesis exam committee, Ylli Doksani, Brian Luke, Beat Fierz and Viesturs Simanis, who provided important feedback for my thesis and project.

Many experiments would not have been possible without the support of the EPFL Flow Cytometry Facility, the Proteomics Core Facility and the Bioimaging and Optics Platform.

Thank you to Florence Delie, Yves Dupertuis, Eric Allémann and Claude Pichard from the university of Geneva and the HUG for believing in me and allowing me to make my first research experiences in Switzerland.

I would like to thank my friends Eva, Chrissi, Corgi, Cori, Anja, Angi, Sophie and Patricia who are there for me at all times, to celebrate my successes and to cheer me up during difficult times. Thank you to Antonin and Aurélie, my life would not be the same without you.

I am incredibly thankful to my parents, who supported me all along and never once doubted my capabilities to reach my goals. I am grateful to my husband's family in Lausanne, Jean-Denis, Anne-Francoise, Maminette, Adrien, Lin, Francois et Isaline, who were always there for me.

Most importantly I thank my husband Pascal for his tremendous support, for always believing in me, sharing his positivity as well as his illustrator skills with me and encouraging me to never give up. Thank you, Olivia, for your love and your smiles and for making each day count.

Abstract

Telomeres are specialized nucleoprotein structures present at the ends of linear chromosome. The telomeric DNA part is comprised of 5-15 kilo base pairs of double stranded TTAGGG repeats and it contains at the 3'end a single-stranded G-rich overhang of 50-400 nucleotides. Telomeric DNA associates with a large number of proteins, which inhibit DNA damage checkpoint activation, DNA repair activities and nucleolytic degradation. To better understand the complex roles which telomeres play in genome stability, premature aging and cancer development we explored the telomeric proteomic environment with BioID.

We employed a CRISPR/Cas9 based knock-in approach to integrate the promiscuous biotin ligase BirA at the genomic loci of the telomeric components *TRF1*, *TRF2* and *POT1*. Thus, we expressed the fusion proteins from native promoters aiming at retaining native expression levels. Upon incubation with Biotin, the promiscuous biotinylase can label proximal proteins, which can be selectively purified and identified via mass spectrometry. Our BioID results indicated that TRF1, TRF2 and POT1 share a large number of common protein partners. In addition to already known telomere components, we identified a significant number of novel telomeric proteins. Among those newly identified proteins, we found RADX, an RPA-like single-stranded DNA-binding-protein, which counteracts RAD51 at stalled replication forks.

Even though RADX had so far only been characterized for its role in DNA replication we observed colocalization of ectopically expressed 3xFlag-RADX with telomeres throughout the cell cycle. The colocalization decreased when the RADXs single-stranded DNA-binding domain was mutated. We therefore hypothesize that RADX binds the single-stranded G-rich telomeric strand either as displaced strand in the t-loop or as single-stranded telomeric overhang. Chromatin-immunoprecipitation experiments suggest that RADX plays a distinct role in telomere replication, since upon treatment with the replication stress inducing reagent hydroxyurea we observed increased binding of RADX specifically to telomeres. Notably, RADX depletion on its own did not alter telomere integrity and telomere length but upon co-depletion with POT1, telomere fragility, sister-chromatid associations and telomere length increased strikingly. POT1 and POT1/RADX depletions lead to increased associations of the recombinase RAD51 with telomeres and consequently silencing of RAD51 rescued telomere integrity and elongation implying the regulatory role of RADX for RAD51.

In summary my thesis describes the proteomic microenvironment of different telomeric proteins, identifies the novel telomeric protein RADX and characterizes its role at telomeres. My findings provide important insights into how homologous recombination and RAD51 loading is suppressed at telomeres.

Keywords

Telomeres, BioID, RADX, POT1, RAD51, homologous recombination, telomere fragility, telomere proteome, DNA replication

Zusammenfassung

Telomere befinden sich an den Enden linearer Chromosomen, bestehen aus etwa 5.000-15.000 Basenpaaren doppelsträngiger repetitiver DNA-Sequenz und enden mit einem einzelsträngigen Überhang von 50-400 Nukleotiden. Telomere DNA assoziiert mit einer Vielzahl von Proteinen, welche die Aktivierung von Zellzyklus-Kontrollpunkten, DNA-Reparaturaktivitäten und nukleolytische Degradierung hemmen. Deshalb haben Telomere eine bedeutende Rolle in der Genomstabilität, dem vorzeitigen Altern und der Krebsentstehung. Um diese Aufgaben besser zu verstehen untersuchte ich das telomere Proteom mit BioID.

Ich verwendete einen CRISPR/Cas9-basierten Knock-In-Ansatz, um die promiskuitive Biotin-Ligase BirA in den Genen der Telomerproteine TRF1, TRF2 und POT1 zu integrieren. Das erlaubte mir die Fusionsproteine von nativen Promotern zu exprimieren und die natürlichen Expressionsniveaus aufrecht zu erhalten. Nach Inkubation mit Biotin kann die promiskuitive Biotinylase proximale Proteine markieren, die dann selektiv isoliert, aufgereinigt und mittels Massenspektrometrie identifiziert werden können. Meine BioID-Ergebnisse zeigten, dass TRF1, TRF2 und POT1 eine große Anzahl gemeinsamer Proteinpartner teilen. Zusätzlich zu den bekannten Telomerbausteinen habe ich eine signifikante Anzahl neuer telomerer Proteinen identifiziert, darunter auch RADX.

RADX wurde bisher nur in der DNA-Replikation beschrieben, aber ich beobachtete, dass ektopisch exprimiertes RADX während des ganzen Zellzyklus mit Telomeren kolokalisiert. Ich sah weniger Assoziationen, wenn das einzelsträngige-DNA-Bindemotif von RADX modifiziert war und gehe deshalb davon aus, dass RADX den einzelsträngigen telomeren Überhang bindet. Chromatin-Immunopräzipitationsexperimente zeigten eine erhöhte Telomer-RADX-Bindung nach Behandlung mit dem Replikationsstress-induzierenden Reagenz Hydroxyharnstoff, was auf eine spezifische Rolle in der Telomerreplikation hindeutet. Bemerkenswert ist auch, dass die RADX-Depletion alleine keine Auswirkung auf Telomerintegrität und Telomerlänge hat, aber wenn zusätzlich POT1 entfernt wird, nahm Länge und Fragilität der Telomere deutlich zu. Außerdem führte Depletion von POT1 und POT1/RADX zu einer erhöhten Assoziation der Rekombinase RAD51 mit dem Telomer. Wurde RAD51 ausgeschaltet, war Telomerintegrität und Telomerlänge wiederhergestellt, was die wichtige regulatorische Rolle von RADX für RAD51 impliziert.

Zusammenfassend habe ich die proteomische Mikroumgebung verschiedener telomerer Proteine beschrieben und ein neuartiges Protein RADX identifiziert. Zusätzlich habe ich seine telomere Rolle charakterisiert und wichtige Erkenntnisse zur homologen Rekombination und RAD51-Bindung am Telomer geliefert.

Schlagwörter

Telomere, BioID, RADX, POT1, RAD51, Homologe Recombination, Telomerfragilität, Telomerproteom, DNA Replication

Contents

1. Introduction

1.1. Historical background

Telomeres are at the ends of linear chromosomes and are found in all eukaryotes. Hermann Müller and Barbara McClintock were the first to recognize that the linear ends of chromosomes are physiologically very different from X-ray-induced DNA-double-strand-breaks (DSB) (McClintock, 1941; Muller, 1938). This important discovery was made even before it was known that chromosomes harbor genetic information in the form of DNA. When in 1953 Watson and Crick shared their structural model of DNA consisting of a double helix with specific base pairings they also suggested a possible mechanism for DNA replication (Watson and Crick, 1953), which was then further characterized by Meselson and Stahl as semi-conservative DNA replication in 1958 (Meselson and Stahl, 1958). Each strand of the double helix serves as a template for the newly synthesized strand. This means, a newly divided daughter cell has an exact copy in terms of sequence and length of the chromosome of its mother cell. Yet further studies on the replication mechanism and on polymerases revealed that the replication machinery cannot fully replicate the DNA at the very end of the chromosome. Therefore, chromosomes will shorten with each round of division. This concept of the so called end-replication problem was introduced by Watson in 1972 (Watson, 1972).

In the late 1970s the repetitive telomeric sequence 5'-T_2G_4 -3' and the fact that the G-rich strand is longer than the C-rich strand was discovered by Elizabeth Blackburn (Blackburn and Gall, 1978) and David Prescott (Klobutcher et al., 1981) in ciliated protozoa. Further experiments lead to the discovery that the chromosome ends of all eukaryotes consist of simple repeats, but that the number of telomeric repeats can vary enormously depending on the organism. This repetitive nature of chromosome ends acts as a buffer to protect important genetic information from getting lost due to the end replication problem.

In 1985 Elisabeth Blackburn and Carol Greider discovered the enzyme telomerase, which can add repeats to the end of telomeres and elongate them, providing a solution to the end-replication problem (Greider and Blackburn, 1985).

Today we know that intact human chromosomes finish with an array of 5-10kb of TTAGGG repeats and a G-rich overhang of 50-400 nucleotides (nt) (Lazzerini-Denchi and Sfeir, 2016). Furthermore, telomeres are transcribed generating the long-non-coding RNA TERRA (Azzalin

et al., 2007). Telomeres shorten around 50-200 bp per cell division and when a telomere becomes too short it elicits a signal which instructs the cell to stop dividing and enter senescence (Fagagna et al., 2003). This provides an important mechanism to limit lifespan and acts as proliferative barrier to tumor growth. Most malignant tumors use a telomere maintenance mechanism, based on telomerase in 80-95% or alternative telomere lengthening (ALT) in 10-15% of all cases, to overcome this obstacle and become immortal (Bryan et al., 1997; Kim et al., 1994). Therefore, telomeres play a major role in aging, premature aging disorders and cancer development.

1.2. Telomere structure

1.2.1. Telomeric proteins

Telomeres protect the linear chromosome ends form being recognized as DNA-double-strand-breaks and consequently triggering checkpoint signaling, nuclease-mediated degradation and fusions. Required for this protection is the telomeric duplex DNA, the 3'-G-rich overhang and most importantly proteins that are recruited to the telomeric DNA (Figure 1).

The most abundant proteins at telomeres are part of the shelterin complex. It consists of the telomeric repeat binding factor 1 (TRF1), telomeric-repeat binding factor 2 (TRF2), TRF1-interacting nuclear factor 2 (TIN2), repressor/activator protein 1 (RAP1), TIN2-interacting protein 1 (TPP1) and protection of telomeres 1 (POT1). This complex is found only at telomeric DNA, does not accumulate at other sequences and is present throughout the cell cycle, which discriminates it from other proteins found at telomeres (de Lange, 2005).

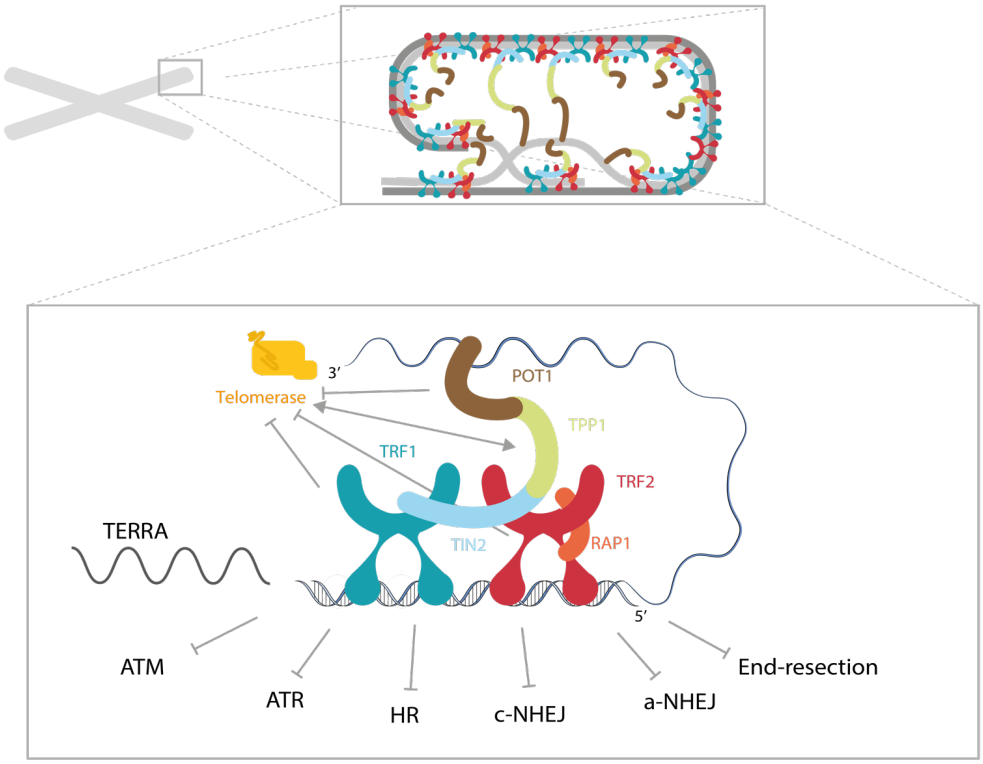

Figure 1. Telomere structure and protective function

Telomeres are nucleoprotein structures consisting of duplex DNA, a single-stranded 3'- overhang, telomeric proteins and the long non-coding RNA TERRA. Intact telomeres inhibit ATM- and ATR-checkpoint-signaling, homologous recombination (HR), classical- (c-) and alternative- (a-) non-

> homologous end-joining (NHEJ) as well as nuclease mediated end-resection. Telomerase, which is recruited by TPP1, can elongate the 3′ overhang.

The structure of the shelterin subunits provides important explanations for their function. The complex is anchored to double-stranded TTAGGG repeats via TRF1 and TRF2, which share sequence homology, especially in their DNA-binding myb-domain (Broccoli et al., 1997). Further, both proteins form homodimers via their TRFH domain (Fairall et al., 2001). The TRFH domain of TRF2 is also the harbor for interactions with several other proteins important for telomere biology like the exonuclease Apollo (van Overbeek and de Lange, 2006) and the helicase RTEL1 (Sarek et al., 2015) or more general proteins harboring a F/YxLxP motif (Kim et al., 2009). Both proteins differ in their N-terminus. TRF1 has an acidic N-terminal domain, whereas in contrast TRF2 is rich in basic Arginine and Glutamine (GAR) amino acids. TRF1 and TRF2 contain also flexible hinge domains, which allows them to act as architectural factors and to change the higher-order structure of DNA (Fairall et al., 2001) and indeed TRF2 can form a t-loop structure, when provided with a telomeric substrate *in vitro* (Griffith et al., 1999). The t-loop is a lariat structure, where the ss 3'-overhang invades the double-stranded repeat part (Figure 1). T-loops were also observed *in vivo* by super-resolution microscopy and their abundance is greatly reduced upon TRF2 depletion (Doksani et al., 2013) further strengthening the hypothesis that TRF2 mediates their formation. RAP1 contains a myb-domain but lacks direct DNA binding ability. Instead it is recruited to telomeres via a direct interaction with TRF2 mediated by its hinge domain (Takai et al., 2010) (Figure 2).

TRF1 and TRF2 do not interact directly with each other but are linked via TIN2, which also recruits TPP1 (Ye et al., 2004). TPP1 recruits telomerase by its TEL patch in its oligonucleotide/oligosaccharide-binding (OB)-fold and binds POT1 via its C-terminal domain (Nandakumar et al., 2012). POT1 is mainly recruited to telomeres by interaction with TPP1, which stabilizes its interaction with the single-stranded telomeric DNA through its OB-folds (Takai et al., 2011) (Figure 2).

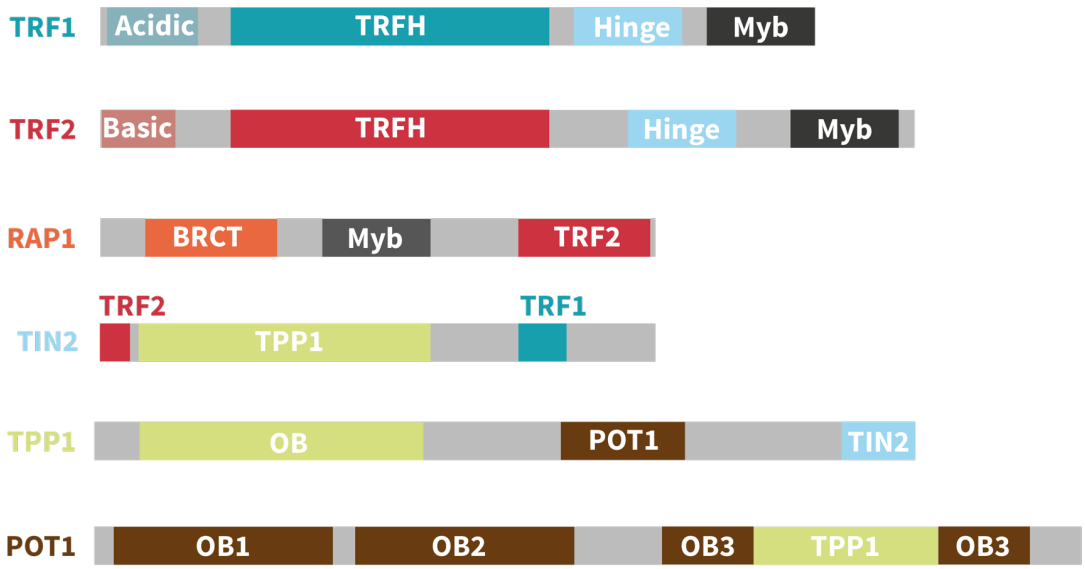

Figure 2. Shelterin proteins and their domain organization

See main text for description. Adapted from (de Lange, 2018).

The shelterin complex is highly conserved in mammals, only rodents have two POT1 orthologues, POT1 a and b, which both interact with TPP1 and are present in similar amounts, but differ in their function. POT1a is similar to human POT1 in preventing the activation of DNA damage response pathways at telomeres, whereas POT1b is mainly involved in preventing aberrant resection at the overhang (Hockemeyer et al., 2006).

Not only POT1 can bind single-stranded telomeric DNA via its OB-folds but also the CST-complex, which consist of CTC1, STN1 and TEN1. The CST-complex has an important function in the fine-tuning of telomere overhang length (Wu et al., 2012) and the regulation of telomerase (Chen et al., 2012). Further, proteins containing an OB-fold-DNA-binding motif are not only very common among telomeric proteins, but also in DNA replication and homology-directed repair. The most prominent and abundant OB-fold containing protein in replication is RPA, which acts as the first responder to ssDNA, and RAD51, together with BRCA2, is involved in homologous recombination (Bhat and Cortez, 2018). All three proteins are also found in low abundance at normal telomeres and can contribute to telomere maintenance (Badie et al., 2010; Takai et al., 2011).

Likewise, proteins involved in DNA damage signaling and processing, DNA repair, DNA replication as well as chromatin modification and transcription regulation are present at telomeres and execute important functions. Their binding and activity are often tightly regulated by shelterin proteins to sustain telomere stability and integrity. In the subsequent sections several telomeric proteins and their functions will be discussed in more detail.

1.2.2. Transcription at telomeres

Telomeres contain heterochromatin marks (Deng et al., 2009), no coding gene sequence and were therefore thought to be transcriptionally silent for a long time. Now it is evident that this is not true and that most, if not all telomeres, transcribe the long non-coding TElomeric Repeat-containing RNA TERRA (Azzalin et al., 2007). TERRA is a RNA-polymerase II-transcript containing telomeric and subtelomeric repeats. Its transcription is mostly initiated in the subtelomeres and proceeds into the TTAGGG-tract (Porro et al., 2014a). TERRA's functions are not fully understood but several lines of evidence point to interactions with chromatin-remodeling-factors, like SUV39H1, HP1 and LSD1, which promote increased deposition of He3K9me3, characteristic of transcriptionally silent heterochromatin (Arnoult et al., 2012; Deng et al., 2009; Porro et al., 2014a).

TERRA can also form R-loops at telomeres, a DNA-RNA hybrid structure formed co-transcriptionally, where the RNA invades the double-stranded DNA and is stabilized through base pairing (Arora et al., 2014). R-loops, if not properly resolved, were found to be problematic for DNA replication and lead to DNA-double-strand-breaks genome-wide (Gan et al., 2011). Interestingly, higher levels of TERRA and R-loops are found in ALT cells and yeast survivors relying on homologous recombination for telomere maintenance, and therefore R-loops are proposed to favor homologous recombination. Consequently, telomere length maintenance is compromised in these cells upon RNaseH overexpression, which resolves these R-loops (Arora et al., 2014; Balk et al., 2013).

TERRA can also influence telomere maintenance in telomerase-positive yeast cells through regulation of exonuclease EXO1 (Pfeiffer and Lingner, 2012) and was shown to inhibit telomerase *in vitro* (Redon et al., 2013), but further studies are necessary to understand TERRA's involvement in telomere length maintenance in telomerase-positive human cells.

1.2.3. Telomere replication and overhang processing

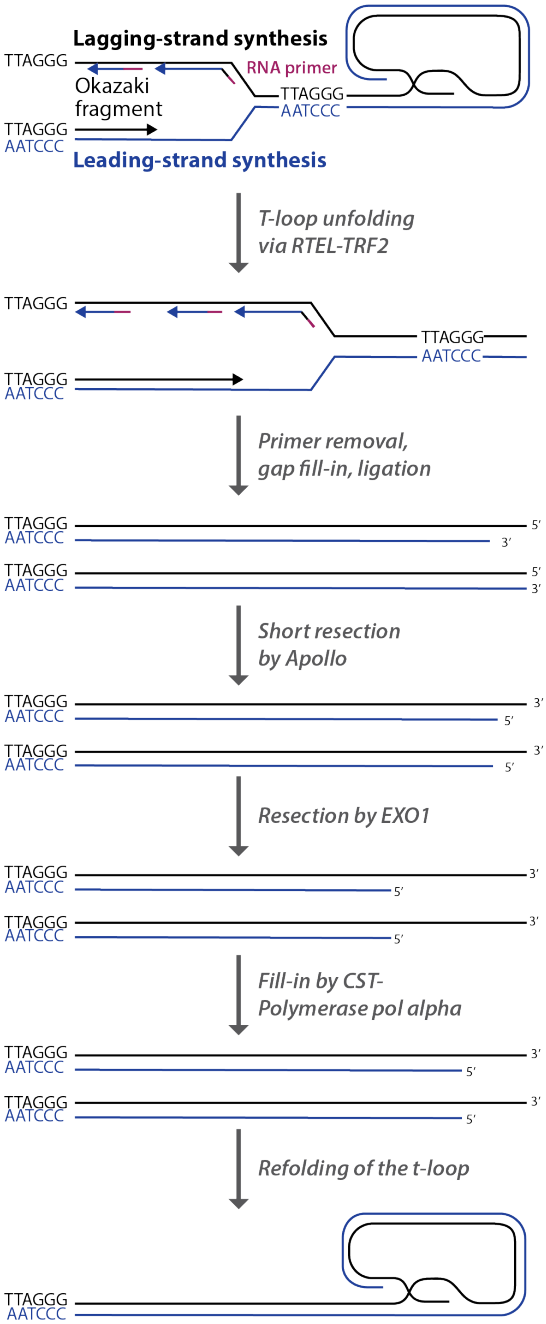

Figure 3. Telomere replication and overhang generation

See main text for description. Adapted from (Arnoult and Karlseder, 2015)

Telomere replication proceeds from the subtelomere and progresses towards the chromosome end (Sfeir et al., 2009). Therefore, the G-rich strand serves as a template for lagging-strand-synthesis and the C-rich strand is the template for the leading-strand-synthesis. Once the majority of the telomere is replicated the replication fork reaches the t-loop, which needs to be dismantled by TRF2-recruited helicase RTEL1 to allow replication fork progression. Otherwise the t-loop can be processed by SLX4, leading to telomere shortening and t-circles (Sarek et al., 2015).

At the end of telomere replication, the 3'G-rich overhang has to be re-established. The lagging strand telomere possesses already a short 3'-G-rich overhang due to the terminal RNA-primer-removal of the Okazaki fragment, but the leading strand finishes with blunt ends. TRF2 can recruit Apollo, which cleaves 5' to 3' to generate a short 3' overhang. Once short overhangs are generated, POT1 binds and inhibits further resection by Apollo. Now, Exo1 can bind on both leading and lagging strand and remove long ranges of nucleotides in the 5' to 3' direction. To fine-tune the overhang length to around 50-300, the CST complex is recruited, via POT1, to mediate fill-in synthesis by DNA polymerase α (Wu et al., 2012). Telomerase can also bind and elongate the 3'overhang, which is terminated by the CST complex and this event

also triggers fill-in synthesis (Chen et al., 2012). Finally the t-loop can be refolded by TRF2 (Doksani et al., 2013) (Figure 3).

Overhang formation is necessary to form the protective t-loop and to allow the binding of telomerase, but aberrant resection must be limited to prevent telomere erosion. Protection of the overhang is redundantly achieved by shelterin or by 53PB1 upon shelterin depletion (Sfeir and de Lange, 2012).

1.2.4. Telomere replication problems

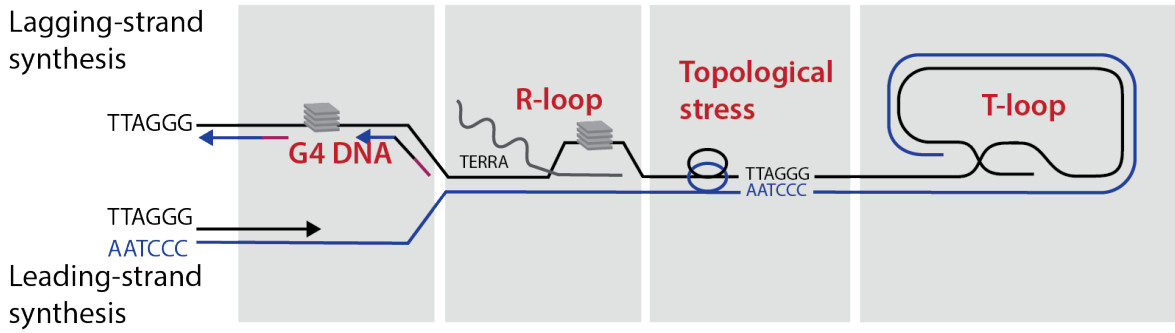

Figure 4. Possible obstacles to telomere replication

G4 DNA, R-loops, topological stress and the t-loop can lead to replication fork stalling, formation of DNA single- and double-strand-breaks, stretches of ssDNA and condensation defects which can manifest as abnormal telomeres in metaphase chromosomes.

Telomeres, due to their structure and function, are by nature difficult to replicate. Several obstacles, like G-quadruplex secondary structures (G4) formed by the TTAGGG repeats, topological stress and loops formed by the compact heterochromatin, TERRA-R-loops and the distal t-loop, need to be removed or dismantled to allow replication fork progression (Figure 4).

Therefore, telomeres are often compared to common fragile sites, which are specific chromosome regions difficult to replicate and prone to display abnormalities in metaphase chromosome analysis. Treatment with low doses of the polymerase inhibitor aphidicolin can exacerbate this phenotype at common fragile sites (Glover et al., 1984) and at telomeres (Sfeir et al., 2009). Abnormal telomeres in metaphase spreads were first observed upon TRF1-

deletion in mouse-embryonic fibroblasts (MEFs) and can exhibit sister-chromatid fusions, telomere signals outside of the DAPI staining, several telomeric signals at one chromosome arm, the loss of the telomeric signal, or a broad smear of the telomeric signal (Sfeir et al., 2009) (Figure 5).

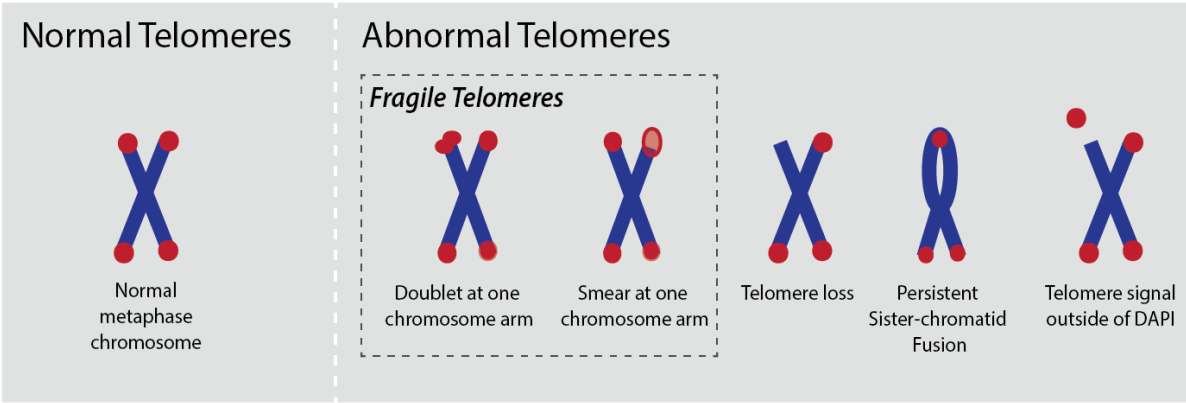

Figure 5. Telomere phenotypes in metaphase chromosomes

In analysis of metaphase chromosomes, the telomeric signal should be linked to the DAPI-stained-DNA and be present at each chromosome arm with similar intensity to qualify as a normal telomere. Abnormal telomeres are classified as fragile telomeres, persistent sister-telomere-associations, telomeric signal outside of the DAPI signal or as a lost telomere with no telomeric signal at one chromosome arm.

Fragile telomeres are commonly referred to as a subgroup of abnormal telomeres and are defined by a several telomeric signals or by a broad smear at one chromosome arm (Sfeir et al., 2009). The abundance of fragile telomeres upon TRF1 depletion can depend on the cell type and telomere length. In MEFs with telomeres raging from 40-50 kb long fragility increases from 5% to 20% upon TRF1 deletion (Sfeir et al., 2009). In HELA cells with over-elongated telomeres of around 30 kb, we observed fragility of 10-15 % upon TRF1 depletion with background levels of 5% whereas HELA cells with telomere lengths between 6-10kbs fragility increases from 2% to 7 % upon TRF1 depletion (unpublished data).

So far it is unclear if these differences in fragility scores are because the longer telomeres are more prone to accumulate replication defects, or if the telomeric signal of shorter telomeres is too weak to allow detection of all fragile telomeres, specifically if the smears or a doublets are very small. Moreover, it has not been elucidated at the molecular level how telomere replication defects lead to the formation of fragile telomeres. The most prominent hypotheses include that

telomere fragility reflects altered packaging or condensation defects, chromatin-gaps and DNA-breaks or stretches of single-stranded DNA (Sfeir et al., 2009; Zimmermann et al., 2014).

Distinct proteins are necessary to facilitate telomere replication. TRF1 was already mentioned to be necessary for proper telomere replication and its depletion results in replication defects and replication fork stalling. It fulfills its protective function in collaboration with the helicases BLM and RTEL1, which are both necessary to resolve secondary structures and their depletions show fragility, which is epistatic to TRF1 deletion (Sfeir et al., 2009). Further, the helicase RTEL1 and its interaction with PCNA is important to unwind G4 structures during replication, which otherwise causes replication fork stalling and fragility (Vannier et al., 2013). The helicase WRN and the CST-complex are also proposed to assist telomere replication, since their depletion results in telomere fragility, but their precise function is not understood (Chen et al., 2013; Crabbe et al., 2004; Stewart et al., 2012).

The role and participation of POT1 in replication remains unclear. Cancer-associated POT1 mutations induce replication fork stalling and telomere fragility epistatic to CST depletion, but the mechanism behind it is not fully understood (Pinzaru et al., 2016). Theoretically POT1 can bind the ssDNA-telomeric DNA at the replication fork and suppress RPA-binding at stalled replication forks. In support of this hypothesis it was shown that increased tethering of POT1 to TRF2 can suppress DNA damage foci formation at telomeres due to TRF1 deletion (Zimmermann et al., 2014). Yet, pull-downs of telomeric replication forks followed by proteomic analysis in our lab raise the hypothesis that POT1 might be excluded from the replication fork in favor of RPA (unpublished data). Supportive of this hypothesis is the observation that TERRA and hnRNPA1 can orchestrate a switch from POT1 to RPA in vitro (Flynn et al., 2011).

In this thesis I present a different model by which lack of POT1 can lead to telomere fragility.

1.3. Chromosome end-protection

The natural ends of chromosomes and DNA-double-strand-breaks are fundamentally different. In contrast to DSBs, intact telomeres prevent the activation of DNA damage signaling and the DSB repair activities. DNA damage signaling can be monitored by the TIF (telomere-dysfunction-induced foci) assay in which accumulated DNA damage marker γH2AX or 53BP1 can be stained with antibodies and visualized in immunofluorescence experiments. DNA damage repair via non-homologous end-joining (NHEJ) can be observed as telomere fusions in metaphase chromosome analysis and homologous recombination (HR) is typically analyzed by telomere length changes and the CO-FISH assay, in which leading and lagging strand telomeres are labeled with different fluorophores (Bailey et al., 2001).

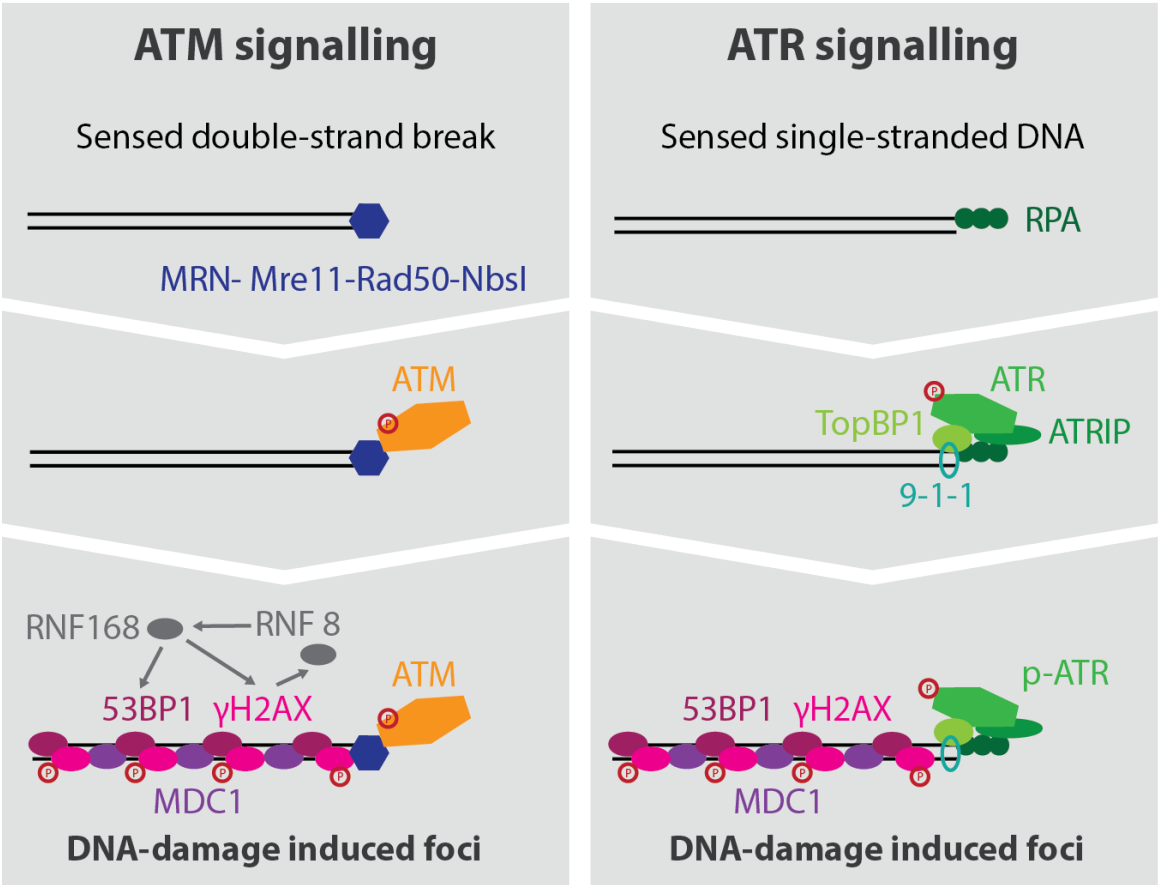

Figure 6. Main steps of ATM-and ATR-signaling

Schematic explaining the main steps of ATR and ATM activation. A DSB is typically sensed by the MRN complex, which recruits the ATM kinase through interaction with MRE11. Upon binding, ATM autophosphorylates and phosphorylates histone H2AX which transduces the signal locally at the

chromatin by recruitment of MDC1 and RNF8. They further amplify the signal by binding RNF168 and recruitment of 53BP1.

Single-stranded DNA is bound by RPA, which can associate with the ATRIP-ATR complex and induce autophosphorylation of ATR. The RAD9-HUS1-RAD1 (9-1-1)-complex is loaded onto the adherent ss-ds-DNA junction and recruits TOPBP1, promoting phosphorylation of H2AX and recruitment of MDC1 and 53BP1.

1.3.1. Suppression of ATM-signaling

The ATM signaling cascade starts with the loading of the MRE11-RAD51-NBSI (MRN) complex onto the free ends created by DNA-double-strand-breaks (DSB). This leads to the autophosphorylation of ATM and downstream effectors H2AX as well as recruitment of MDC1, RNF168 and 53BP1 (Figure 6). CHK2 phosphorylation leads to upregulation of p53, which is stabilized upon phosphorylation by checkpoint kinases, induction of p21 and consequently cell cycle arrest (Karlseder et al., 2004).

The most important protein preventing ATM activation is TRF2, which carries out this function in several redundant ways. Upon TRF2 depletion, as well as the expression of a dominant-negative-mutant lacking the basic and the TRFH domain, abundant TIFs and fusions are observed (van Steensel et al., 1998). It was shown that TRF2 can inhibit the ATM kinase directly itself (Karlseder et al., 2004) as well as crucial downstream effectors. Through a motif within the hinge region termed iDDR (inhibitor of the DDR pathway) TRF2 prevents RNF168 recruitment and therefore accumulation of 53BP1 (Okamoto et al., 2013). Furthermore, TRF2 promotes the formation of the t-loop, which physically hides the chromosome ends and blocks loading of the MRN complex (Doksani et al., 2013). Finally, TRF2 was also described to inhibit ATM activation by a topological mechanism where the DNA is wrapped around the TRFH domain (Amiard et al., 2007; Benarroch-Popivker et al., 2016).

1.3.2. Prevention of ATR-signaling

Typically, the ATR kinase pathway is activated by the binding of RPA to single-stranded DNA. This initiates a cascade with RPA binding ATRIP and ATR, which leads to loading of TOPBP1 and the 9-1-1 (RAD9-Hus1-RAD1) complex onto the ss-ds-DNA junction (Zou and Elledge, 2003). Auto-phosphorylation of ATR and downstream targets like CHK1 and H2AX as well as the recruitment of 53BP1 and MDC1 lead to cell cycle arrest at the G1/S or G2/M transition (de Lange, 2010) (Figure 6).

ATR activation is primarily inhibited by POT1, which excludes RPA from binding to the single-stranded overhang. Interestingly the affinity of POT1 and RPA for single-stranded DNA is very similar, but POT1 is much more abundant at the telomere due to its recruitment via TPP1. Accordingly, depletion of TPP1 or TIN2 abrogates the POT1 recruitment and also leads to ATR-dependent TIFs (Gong and de Lange, 2010; Takai et al., 2011).

Moreover, replication problems can lead to RPA loading, which triggers the ATR-dependent DNA damage signaling. Consequently, TRF1 deletion induces ATR-dependent TIF formation, but only if the cells go through S-phase. In contrary to POT1 deletion, which leads to ATR-signaling in any phase of the cell cycle (Gong and de Lange, 2010; Sfeir et al., 2009).

Even if POT1 levels do not decrease at the telomere upon TRF1 deletion increased tethering of TIN2-TPP1-POT1 via the RAP1-binding motif to TRF2 can significantly reduce DNA damage signaling and fragility in TRF1-deleted cells. The phenotype is not fully suppressed implicating that partly the replication defect might be due to the lack of recruitment of BLM or other factors necessary to resolve topological stress (Zimmermann et al., 2014). Additional studies are necessary to further characterize TRF1's role in preventing replication defects and associated ATR-signaling at telomeres.

1.3.3. Inhibition of telomere fusions

The most deleterious outcome upon telomere deprotection is telomere fusion. Chromosome fusions can create dicentric chromosomes inducing breakage-fusions-bridge cycles and lead to extensive chromosome rearrangements, which induce genome instability and tumor formation (Maciejowski and de Lange, 2017).

Inhibition of classical non-homologous end-joining (c-NHEJ)

Key steps of the c-NHEJ cascade at telomeres are overhang processing to form blunt-ends, followed by the loading of the KU70/80 heterodimer, recruitment of DNA-PKcs and the LIG4-mediated joining of chromosome ends (Arnoult and Karlseder, 2015). Interestingly, the KU complex, which is such an essential part of the c-NHEJ pathway, is also constitutively present at telomeres. It is recruited via TRF1, TRF2 and RAP1 and must have an important role in telomere protection as its deletion leads to rapid telomere loss (Wang et al., 2009). The KU 70/80 heterotetramerization, which tethers opposite DNA ends together to allow ligation, is

blocked by TRF2, which also plays a major role in preventing c-NHEJ (Ribes-Zamora et al., 2013). Furthermore, the t-loop is thought to render it sterically difficult for KU70/80 dimers to load and provides an additional TRF2-mediated repression mechanism of fusions in G1-phase.

The role of RAP1 in NHEJ is not fully understood. It is bound and recruited to the telomere via TRF2 and does not induce fusions upon deletion. But fusion formation upon expression of a dominant negative mutant of TRF2 lacking the basic, the hinge and the myb domain can be repressed if RAP1 is tethered to the telomere independently of TRF2 (Sarthy et al., 2009). Therefore, there might be a potential role for RAP1 in the inhibition of c-NHEJ in the TRF2 pathway.

Inhibition of alternative non-homologous end-joining (a-NHEJ)

A-NHEJ provides a backup repair pathway for double-strand breaks, where MRE11 and CtIP resect the 5' end. End-joining is mediated by PARP1, LIG3 and DNA polymerase θ (Rai et al., 2010). Telomeric DSBs are ideal chromosome regions for a-NHEJ, since they present perfect homology around the break site and indeed internal telomeric double-strand breaks were observed to be repaired preferentially by PARP1/LIG3-mediatet end-joining and HR over c-NHEJ (Doksani and de Lange, 2016). Aside double-strand break repair low levels of a-NHEJ at intact telomeres are observed when the ssDNA overhang is deprotected upon TPP1 or POT1 depletions and codepletion of TRF2 and KU, but full activation is only possible upon suppression of TRF2, TPP1-POT1, KU and 53BP1 (Rai et al., 2010; Sfeir and de Lange, 2012).

1.3.4. Inhibition of Homologous recombination (HR)

Homologous recombination is an error-free repair pathway for DNA DSBs after replication, when the sister-chromatids can be used as templates. It requires end-resection, which is initiated by the MRN complex and which precedes the loading of RPA. Upon creation of a 3' overhang, BRCA2 and BRCA1 assist the exchange of RPA with RAD51, which mediates strand-invasion into the homologous sequence (Zhao et al., 2019). After further processing either a single or double Holiday junction can form, which is further resolved by SLX1-SLX4-

MUS81-EME1 or GEN1 and leads to sequence exchange, called crossover, or dissolution by BLM/TOP3A/RMI1/RMI2 resulting in a non-crossover event (West et al., 2015) (Figure 7).

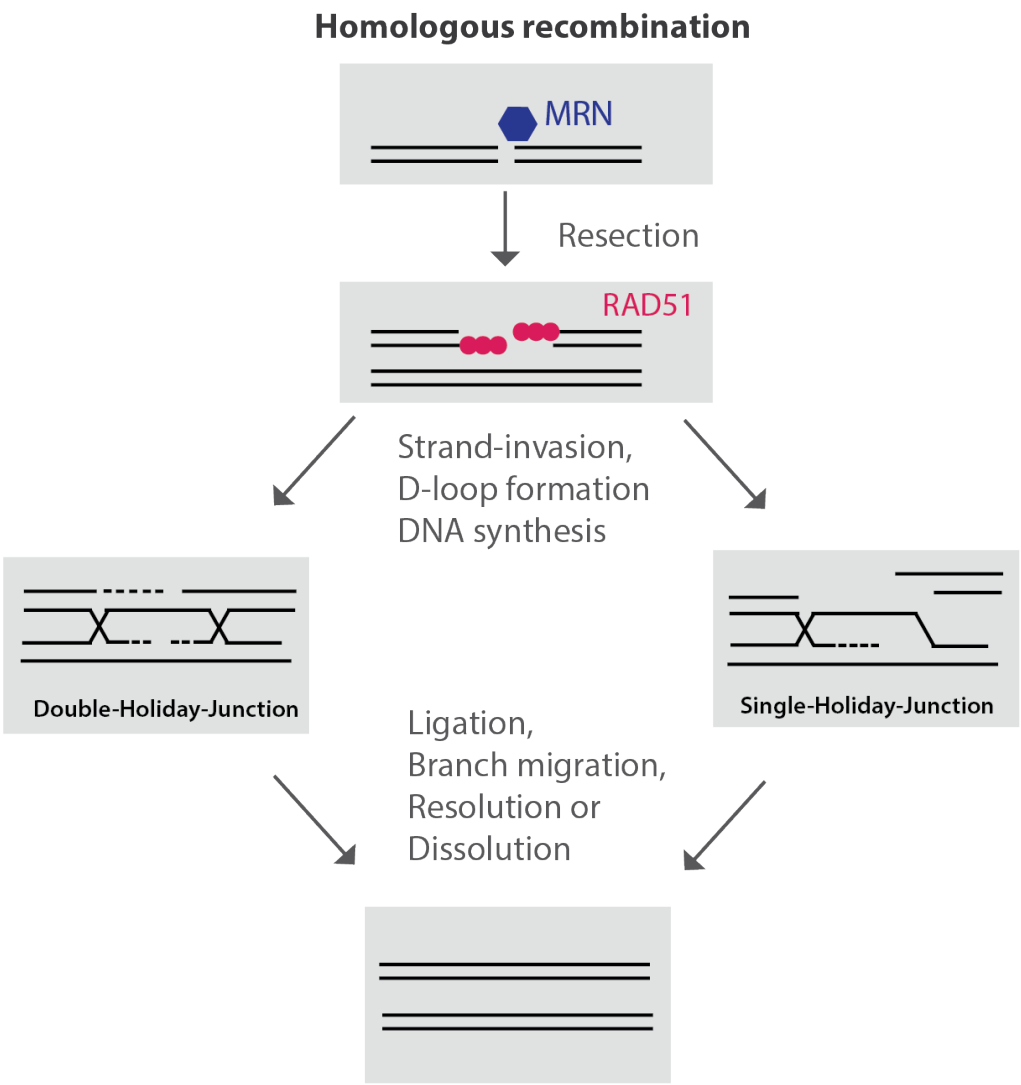

Figure 7. Basic steps of homologous recombination

In S/G2 phase of the cell cycle the MRN complex can be recruited to DSBs and promote resection. This generates stretches of ssDNA and allows the loading of RAD51, which promotes strand-invasion to a double-or single-holiday junction with the possibility of sequence exchange before resolution or dissolution.

Telomeres, due the many kilobases of identical repeats and the 3' single-stranded overhangs, are ideal substrates for HR. However HR activities need to be prevented as they can lead to altered telomere length and excision of the t-loop by XRCC3 and NBS1 (Compton et al., 2007;

Wang et al., 2004) (Figure 8). KU does not only block alt-NHEJ, but it also assists to protect from HR. Only upon deletion of KU and TRF2, RAP1 or POT1a/b high levels of telomere sister-chromatid exchange are observed in MEFs (Celli et al., 2006; Palm et al., 2009; Sfeir and de Lange, 2012). Single deletions of TRF2 or RAP1 do not lead to HR. For POT1a deletion the results are controversial. A small significant increase in telomere sister-chromatid exchange was observed by some investigators (Wu et al., 2006), but not by others (Palm et al., 2009).

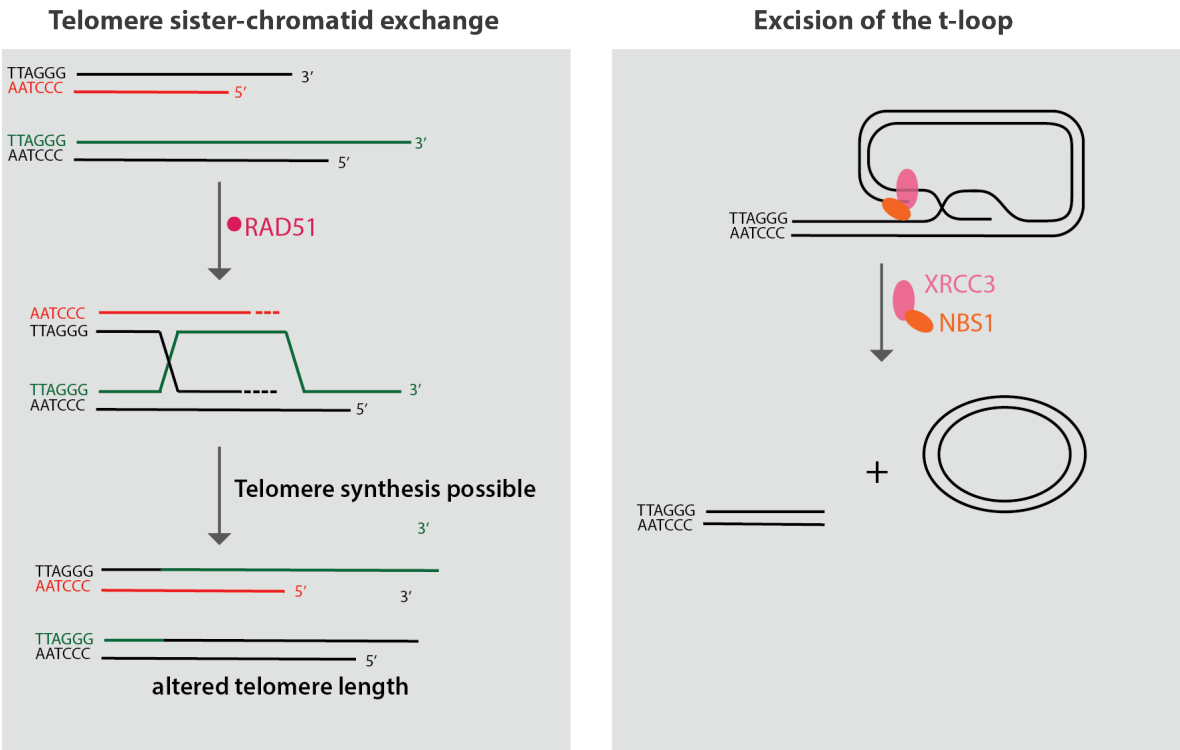

Figure 8. Manifestations of homologous recombination at telomeres

On the left side telomeric sequences can be exchanged between sister-chromatids or between different chromosomes and can potentially lead to telomere length changes. On the right side the t-loop, which resembles a holiday junction can be processed by XRCC3 and NBS1, which leads to telomere shortening and accumulation of released t-loops.

1.4. Telomere length maintenance

Telomeres shortens about 50-200 bp per round of replication mostly due to exonuclease processing (Lingner et al., 1995). This progressive shortening is a mechanism for cells to limit their proliferation. Too short telomeres provide insufficient protection from the DNA damage response pathways and will induce DNA damage signaling leading to cell cycle arrest and senescence or apoptosis (Fagagna et al., 2003). Therefore, telomere shortening acts as a barrier to uncontrolled proliferation and tumorigenesis (Smogorzewska and de Lange, 2004; Zhao et al., 2009). Germline cells, self-renewing stem cells and almost all cancer cells have a telomere length maintenance mechanism to overcome this problem and escape the proliferation limit (Kim et al., 1994).

1.4.1. Telomerase

Among cells, which have acquired a telomere length maintenance, 80-85 % of them rely on telomerase for telomere elongation. Telomerase synthesizes telomeric DNA de novo by using its integral RNA hTR as a template and the 3'overhang as a primer (Greider and Blackburn, 1985). The telomerase holoenzyme is composed of a reverse transcriptase moiety hTERT, an RNA moiety TERC and accessory proteins Dyskerin, NOP10, NHP2, BHP2, GAR1 and TCAB1, which mediate biogenesis and trafficking (Schmidt and Cech, 2015).

On one side telomerase is primarily recruited to telomeres via the TEL-patch on TPP1 (Nandakumar et al., 2012). TIN2 may encourage telomerase binding, through recruiting TPP1 to telomeres (Abreu et al., 2010) as well as on its own since mutations outside the TRF1 or TPP1 binding domain also lead to a dyskeratosis congenital phenotype with compromised telomerase function and telomere shortening (Frank et al., 2015). ATM-and ATR-signaling were also found to be important for telomerase localization to telomeres and extension (Lee et al., 2015; Tong et al., 2015).

On the other side TRF1, TRF2 and POT1 act as negative regulators of telomere length. Overexpression of TRF1 and TRF2 in the telomerase positive cancer cell line HTC75 (Smogorzewska et al., 2000) and overexpression of POT1 in HT1080 (Colgin et al., 2003) lead to telomere shortening and the expression of a dominant negative TRF1 allele leads to telomere elongation (vanSteensel and deLange, 1997). Moreover, POT1-binding to the single-stranded

overhang can physically block telomerase elongation *in vitro* (Kelleher et al., 2005) and the expression of a dominant negative POT1 mutant deleted for the OB-folds, POT1$^{\Delta OB}$, leads to telomere elongation *in vivo* (Loayza and De Lange, 2003). Interestingly, if POT1 is in association with TPP1 it increases telomerase repeat addition processivity by reducing primer dissociation rate and increasing translocation efficiency *in vitro* (Latrick and Cech, 2010).

Furthermore, Apollo positively regulates telomerase access by generating the 3'overhang necessary for its binding (Wu et al., 2012) while the CST complex acts as a terminator of telomerase activity (Chen et al., 2012).

1.4.2. Alternative lengthening of telomeres (ALT)

The majority of cancer cells rely on telomerase as a telomere maintenance mechanism, but 10-15 % use the homology-directed repair based alternative-lengthening mechanism ALT to prevent telomere shortening. A key feature of ALT is the clustering of telomeres in APBs (ALT-associated PML bodies), which are thought to be the hotspots for telomere recombination. Consequently, ALT cell lines display high levels of telomere sister-chromatid-exchanges, heterogeneous telomere length, increased TERRA levels, high levels of ECTR (Extra chromosomal Telomere Repeat Containing DNA), and rely on homologous recombination factors, like RAD51, RAD52, MRN, RAD9, RAD17, RPA for survival (Pickett and Reddel, 2015).

It is not clear, which factors decide on what mechanism a cancer cell will rely on for telomere length maintenance. TERT promoter mutations might lead to ALT activation and tissues with physiologically continuously repressed telomerase expression, such as mesenchymal stem cells, were found to favor the formation of a tumor relying on the ALT pathway (Gocha et al., 2013). Additionally, the transcriptional regulator and chromatin remodeller ATRX was observed to be disrupted in the majority of ALT cancers even if an ATRX deletion on its own is insufficient to induce ALT (Jiao et al., 2011). The mechanism of ATRX's ALT inhibiting capacity is not fully understood, but there is evidence that ATRX interacts with DAXX and binds to He3K9me3. The loss of ATRX or DAXX can limit H3.3 incorporation and this can disrupt the telomere heterochromatin which could in turn facilitate telomere recombination (Lewis et al., 2010).

Moreover, ALT telomeres contain variations of the canonical TTAGGG repeats. They might arise from recombination with subtelomeric loci and lead to lower TRF2-binding and higher binding of DNA damage response proteins. These variant repeats can also form binding sites for nuclear hormone receptors, including TR4 and COUP-TF2, which again favor changes of the telomeric chromatin structure and provide a platform for HR (Conomos et al., 2014).

The activation of ALT is certainly a multistep process making it difficult to determine and differentiate between cause and consequence. Further studies are needed to deepen our understanding of this complex mechanism.

1.5. BioID– proximity dependent biotin identification

BioID is a method based on proximity-dependent protein biotinylation to identify the proteomic environment. A modified biotin ligase from *Escherichia coli* BirA, creates a cloud of active biotin (biotin and ATP combined to form biotinoyl-5'-AMP), with an estimated radius of 10 nm. This modified BirA can be fused to a protein of interest to label vicinal proteins in the presence of biotin (Roux et al., 2012), preferable at free primary amines of lysine residues (Streaker and Beckett, 2006) (Figure 9).

Biotinylation is a rare modification in mammalian cells. Therefore, the presence of only few endogenously biotinylated proteins, mostly present in the cytoplasm and mitochondria, allows to specifically enrich for interacting proteins in the nucleus. These proteins can then be selectively purified by streptavidin binding and analyzed by mass spectrometry.

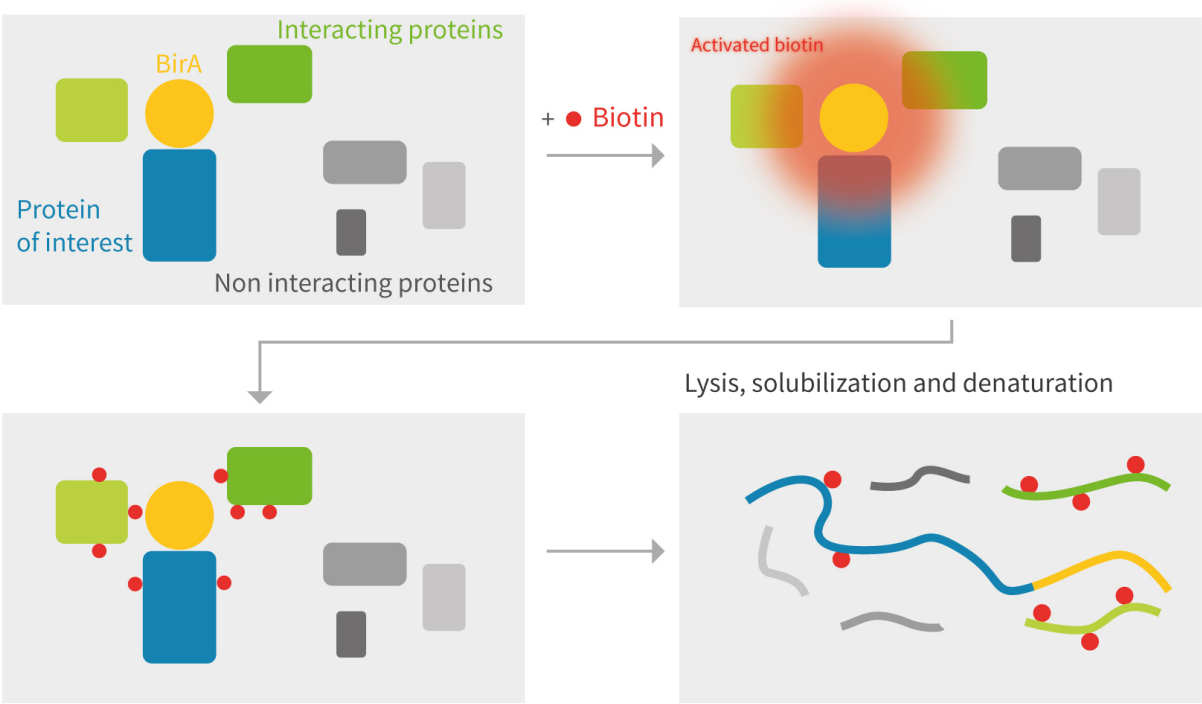

Figure 9. Model for BioID method

A promiscuous biotinylase is fused to a protein of interest and expressed in HEK293T cells. The addition of biotin to the medium leads to the activation of biotin by the formation of biotinoyl-5' AMP, which results in biotinylation of proximal proteins. Interacting proteins can then be selectively isolated following stringent cell lysis, protein denaturation and solubilization steps.

Determinant factors for the success of an affinity purification are solubility of the studied protein complex and the possibility to maintain interactions through the purification process. The BioID system provides the possibility to covalently modify vicinal proteins and to take advantage of the strong streptavidin-biotin-binding. Therefore, it is not necessary to maintain the native protein complex with its interactions through the different purification steps. Harsh lysis and extremely stringent washing conditions (up to 2% SDS and 500 mM NaCl) bring also poorly soluble proteins into solution and render them accessible to immunoprecipitation as well as remove many post-lysis artifacts and contaminants.

Two very prominent techniques to identify telomeric proteins, PICH (Déjardin and Kingston, 2009) and QTIP (Grolimund et al., 2013), rely on chemical crosslinking with formaldehyde to fix a snapshot of interactions at one time point. The crosslinking conditions, specifically duration and concentration, represent a compromise between capturing weak and transient interactions and preventing "overcrosslinking" and fixing proteins in large insoluble complexes. BioID does not have these limitations in terms of "overbiotinylation" and transient interactions will accumulate with biotin labeling over time. It can therefore act as a complementary method and identify a new set of telomeric proteins.

Yet one major limitation of this method is that the identification of a proximal protein depends on the accessibility of a primary amine (mostly lysines) for biotinylation, which can lead to false negatives. The biotinylation might also in theory impact the function of the labeled protein by for example by blocking additional modifications such as acetylations. Further it is critical to optimize expression of the BirA fusion protein. It should be similar or lower than endogenous levels to avoid artifacts coming from overabundant and aggregated BirA fusion proteins.

BioID has been successfully applied to a variety of structural proteins and organisms (Kim and Roux, 2016), as well as at the telomere by overexpression of BirA-TRF1 in the ALT cell line U2OS and the telomerase-positive cell line HELA with long telomeres. They were able to identify a large number of known as well as novel telomeric proteins (Garcia-Exposito et al., 2016). In this thesis I will present an approach where I have tagged endogenous TRF1, TRF2 and POT1 with BirA to identify novel telomeric proteins and determine the microenvironment of these shelterin components.

1.6. **RADX and replication**

RADX was first described to localize to stalled replication forks and to counteract RAD51 loading onto them. RADX contains three RPA-like OB-folds which mediate its binding to single-stranded DNA (Dungrawala et al., 2017; Schubert et al., 2017). RADX is not an essential protein for cultured cancer cells and its deletion in U2OS and HEK293T is viable, but Dungrawala et al observed increased γH2AX signaling and accumulation of DSBs upon RADX depletion. This increase can be rescued by depletion of the endonuclease MUS81, which can cleave at stalled replication forks. This finding is coherent with DNA replication fiber analysis showing decreased fork elongation rate and an increase in asymmetric forks upon RADX depletion, suggesting it can prevent replication fork collapse (Dungrawala et al., 2017; Schubert et al., 2017). Additionally RADX depletion increases RAD51 loading on stalled replication forks in S-phase, which can lead to replication fork reversal mediated through SMARCAL1 and ZRANB3 and promote fork collapse and DNA double-strand break formation (Dungrawala et al., 2017).

Further, depletion of RADX was able to rescue the MRE11- or DNA2- dependent nascent strand degradation in BRCA2-or BRCA1-deficient cells observed by DNA fiber analysis in fork protection assays. Consequently, RADX depletion conferred increased chemoresistance to hydroxyurea, cisplatin and camptothecin in RAD51-deficient and olaparib in BRCA2-deficient cells (Bhat et al., 2018; Dungrawala et al., 2017). Interestingly, only a mild but not significant increase in homologous recombination was observed upon RADX depletion (Bhat et al., 2018; Dungrawala et al., 2017).

It was further suggested that RADX protein levels and therefore its ability to counteract RAD51 must be tightly regulated since also the overexpression of RADX leads to nascent strand degradation and increased double-strand break accumulation (Bhat et al., 2018; Dungrawala et al., 2017). Likewise, the amount of RAD51 binding to stalled replication forks can also lead to different outcomes with more RAD51 required for fork protection than fork reversal (Bhat et al., 2018). These findings underline the importance of the RADX-RAD51 balance for proper DNA replication.

1.7. Thesis outline

I have performed BioID with endogenous CRISPR-Cas9 tagged shelterins to identify novel telomeric proteins, which helps us to deepen our understanding of telomere biology. We successfully identified several previously not described proteins to associate with telomeres and further focused on RADX, a newly characterized OB-fold containing protein involved in DNA replication. We show that RADX binds telomeric DNA throughout the cell cycle and prevents RAD51-loading in cooperation with POT1. Increased RAD51-binding to telomeres leads to homologous recombination, which manifests in telomere fragility, sister-chromatid-associations and increased telomere length.

Along with the characterization of RADX, I identified that the elongation seen upon POT1-deletion is dependent on RAD51 and BRCA2, which suggests the activation of an ALT-like homologous recombination-based elongation mechanism, largely independent of telomerase.

Overall this thesis provides important information on how the POT1-RADX-RAD51-interplay regulates homologous recombination at telomeres.

2. RADX sustains POT1 function at telomeres to counteract RAD51 binding, which triggers telomere fragility

Manuscript in preparation

Anna-Sophia Briod, Galina Glousker, Joachim Lingner

2.1. Abstract

The 3' terminal DNA extensions at chromosome ends can become engaged into multiple biochemical reactions during DNA replication, telomerase-mediated telomere extension, homology directed DNA repair, nucleolytic processing and DNA damage checkpoint activation. To keep these activities in check, telomeric 3' overhangs can be hidden in t-loop structures or they associate with specialized proteins such as POT1. Here, we explore the telomeric microenvironment using a proximity-dependent labeling approach and identify the oligonucleotide/oligosaccharide-binding (OB)-fold containing protein RADX. RADX binds single-stranded telomeric DNA throughout the cell cycle along with POT1, suppressing accumulation of fragile telomeres, which are indicative of telomere replication defects. Telomere fragility in POT1 and RADX double-depleted cells was due to accumulation of the RAD51 recombinase at telomeres. Thus, RADX represents next to POT1 a second OB-fold containing single-strand telomere binding protein contributing to telomere protection. RADX sustains POT1 function to suppress untimely RAD51 binding at telomeres preventing telomere replication defects.

2.1.1. Highlights

- We applied BioID to identify the telomeric microenvironment
- RADX was shown to associate with single-stranded telomeric DNA throughout the cell cycle
- Fragility and sister-chromatid associations upon POT1 and POT1/RADX loss are homologous recombination dependent
- POT1 and RADX cooperate to suppress RAD51 loading onto telomeres
- Increased RAD51 binding at telomeres leads to telomere elongation

2.1.2. Author contributions

A-SB carried out all experiments except for the development of the *POT1* conditional knockout cell line, which was done by GG. A-SB and JL wrote the paper. All authors conceptualized the experiments.

2.2. **Introduction**

Intact telomeres suppress at chromosome ends DNA repair activities, nucleolytic degradation and DNA damage checkpoint activation (de Lange, 2018; Lazzerini-Denchi and Sfeir, 2016). In humans, unharmed telomeres have a length of 5,000-15,000 bp of 5'-TTAGGG-3'/5'-CCCTAA-3' telomeric DNA repeats ending in a single stranded 3' overhang of 50-400 nucleotides. Telomeres associate with the shelterin proteins consisting of TRF1 and TRF2 which bind as homodimers to double-stranded telomeric DNA (de Lange, 2018) and POT1 which binds to the single-stranded 5'-TTAGGG-3' repeats (Baumann and Cech, 2001). The shelterin components TIN2, RAP1 and TPP1 are recruited to telomeres through protein-protein interactions with TRF1, TRF2 and POT1. In addition to shelterin components, which are abundant at telomeres presumably covering large parts of telomeric DNA, additional factors have been identified at chromosome ends through genetic, molecular biological and biochemical approaches. More recently telomeric protein composition has been analyzed more comprehensively through the purification of crosslinked telomeric chromatin and analysis by mass spectrometry (Bartocci et al., 2014; Déjardin and Kingston, 2009; Grolimund et al., 2013; Majerska et al., 2018) or through mass spectrometric analyses of proteins that were labeled at telomeres with biotin upon expression of shelterin components fused with a biotin ligase (Garcia-Exposito *et al*, 2016; this study). More than 200 proteins have been identified in these studies and for a subset of them crucial functions have already been documented.

The non-shelterin telomere associated proteins become particularly important during telomere replication or telomere damage. For example, short telomeres change their state during cellular senescence triggering ATM and ATR recruitment and activation to promote permanent cell cycle arrest (d'Adda di Fagagna et al., 2003; Karlseder et al., 1999, 2002). For ATR activation, POT1 is replaced on the single-stranded telomeric DNA by RPA which recruits ATR-ATRIP (Denchi and de Lange, 2007; Zou and Elledge, 2003). Also during semiconservative DNA replication, POT1 is thought to be replaced by RPA (Flynn et al., 2011) which stimulates DNA polymerases. For telomerase-mediated telomere extension in S-phase of the cell cycle (Schmidt and Cech, 2015), telomerase engages with the telomeric 3' overhang upon recruitment by TIN2 associated TPP1 (Abreu et al., 2010; Schmidt and Cech, 2015) and the ATM and ATR kinase activate the extension process (Lee et al., 2015; Tong et al., 2015). The OB-fold containing CST complex associates with the extended telomeric 3' overhang to terminate telomerase-mediated telomere extension promoting fill-in synthesis of the complementary strand (Chen et al., 2012). Finally, though excessive homologous recombination between telomeres is

suppressed in mouse embryonic fibroblasts (MEFs) by contributions of Pot1, Ku and Rap1 (Celli et al., 2006; Palm et al., 2009; Sfeir et al., 2010; Wu et al., 2006), the telomeric 3' overhang can associate with RAD51 and the homology-directed DNA repair (HDR) machinery may contribute to telomere maintenance even in healthy cells (Badie et al., 2010; Verdun and Karlseder, 2006). The HDR involvement in telomere maintenance is most pronounced in ALT cells that maintain their telomeres independently of telomerase (Pickett and Reddel, 2015).

During S-phase for the faithful replication of telomeric DNA, not only the canonical replication machinery must associate with telomeres but additional specialized proteins are recruited to overcome telomere-specific hurdles. For example, the t-loops are unwound by RTEL1 (Sarek et al., 2016; Vannier et al., 2012), G-quadruplex structures which can be formed during replication by the G-rich telomeric strand are counteracted by BLM, RTEL1 and WRN helicases (Crabbe et al., 2004; Sfeir et al., 2009; Vannier et al., 2012). Telomeric R-loops formed between the telomeric long noncoding RNA TERRA and the C-rich telomeric DNA strand are repressed by RNA surveillance factors (Azzalin et al., 2007; Chawla et al., 2011), RNase H (Arora et al., 2014; Graf et al., 2017), FANCM (Silva et al., 2019) and the THO-complex (Pfeiffer et al., 2013). Telomere replication defects become apparent as so-called fragile telomeres which display discontinuities of the telomeric signals in metaphase chromosomes (Sfeir et al., 2009).

Recently, the OB-fold containing protein RADX has been identified to control replication fork protection by antagonizing RAD51 binding to single stranded DNA (Bhat et al., 2018; Dungrawala et al., 2017; Schubert et al., 2017). In this paper, we explore the telomere protein composition by proximity-dependent labeling using TRF1, TRF2 and POT1 as baits. Apart from obtaining comprehensive insights into the telomeric microenvironment we identify RADX with all baits. We demonstrate that RADX associates with telomeres in replicating and non-replicating cells through its DNA binding OB-fold. Concomitant loss of RADX and POT1 leads to RAD51 recruitment and enhanced telomere fragility, which can be suppressed by RAD51 depletion. Thus, RADX contributes to telomere protection in conjunction with POT1.

2.3. Results

2.3.1. BioID Identifies RADX at Telomeres

We employed BioID (Roux et al., 2012) to explore and compare the proteomic microenvironments of TRF1, TRF2 and POT1. In order to express the biotin protein ligase (BirA) tagged shelterin proteins BirA-TRF1, BirA-TRF2 and BirA-POT1 at endogenous levels and to avoid biotinylation artifacts due to overexpression, we used a CRISPR-Cas9 knock-in approach to integrate the BirA sequence into the genomic loci at the N-termini of *TRF1*, *TRF2* and *POT1* in HEK293T cells (Figure 1A). We screened for recombinant clones by PCR with primers flanking the region of integration and sequenced the PCR products (Figure S1A, S1B, S1E and S1G). Expression of the tagged fusion proteins was confirmed on Western blots (Figure S1C, S1F, S1H). Sequencing of the genotyping PCR revealed one tagged and two disrupted alleles for the myc-BirA-TRF1 clone (Figure 1A and S1D), as well as for 3xFlag-BirA-POT1 clone 5 (Figure S1G and S1I). Clone 3xFlag-POT1 84 showed evidence of two unedited alleles (Figure S1I) retaining expression of untagged POT1 (Figure S1H). Of note, HEK293T cells are triploid for chromosomes 7 and 8, which contain the *POT1* and *TRF1* genes, respectively (Figure 1A). The genotyping PCR for clone 3xFlag-BirA-TRF2 88 revealed the tagged allele of *TRF2* and not the unmodified locus (Figure S1E), but the Western blot analysis indicated co-expression of tagged and untagged TRF2 (Figure S1F).

The telomere length of genome-edited cells was clone-specific as typically seen in clonal isolates of human cells and it remained stable during several weeks of growth when assessed by telomere restriction fragment (TRF) analysis indicating normal shelterin function (Figure 1B). Telomere integrity was also analyzed by inspecting telomeric fluorescence in situ hybridization (FISH) signals on metaphase chromosome spreads (Figure S2). Telomere abnormalities did not increase in the analyzed clones. Thus, the tagged proteins showed no interference with telomere maintenance.

Wild type (WT) and genome-edited cells were expanded and labeled during 24 hours with biotin. Nuclei were isolated removing cytoplasm and mitochondria, which contain abundant endogenous biotinylated proteins (Figure 1C). Biotinylated proteins in nuclear extracts were bound to streptavidin beads and fractionated by SDS-PAGE. As expected, the streptavidin-purified fractions contained also the BirA-tagged shelterins due to self-biotinylation (Figure 1D). Analysis of the streptavidin-purified and SDS-PAGE fractionated proteins by mass spectrometry and comparison to the wild type negative control led to the identification of

proteins previously described to associate with telomeres (Déjardin and Kingston, 2009; Garcia-Exposito et al., 2016; Grolimund et al., 2013) as well as novel telomeric proteins (Figure 1E, S3 and Table S1). This included all the shelterin components, proteins involved in the DNA damage response, chromatin remodeling, transcription and nuclear envelope components. POT1 was not detected in the TRF1-BioID, but TRF1 in the POT1-BioID suggesting that the part of POT1 within the biotinylation radius of BirA-TRF1 does not contain primary amines accessible for biotinylation and subsequent pull-down. The overlap of with BirA-TRF1, -TRF2 and -POT1 identified proteins was extensive giving confidence in the specificity of the experimental approach although several proteins involved in transcription regulation and chromatin remodeling were only identified BirA-TRF2. However, this clone also carried shorter telomeres (Figure 1B), which may have influenced the telomeric proteome environment. Overall, we were most intrigued by the identification of RADX in all BioID experiments (Figure 1E), which had not been found in previous proteomic analyses of telomeres.

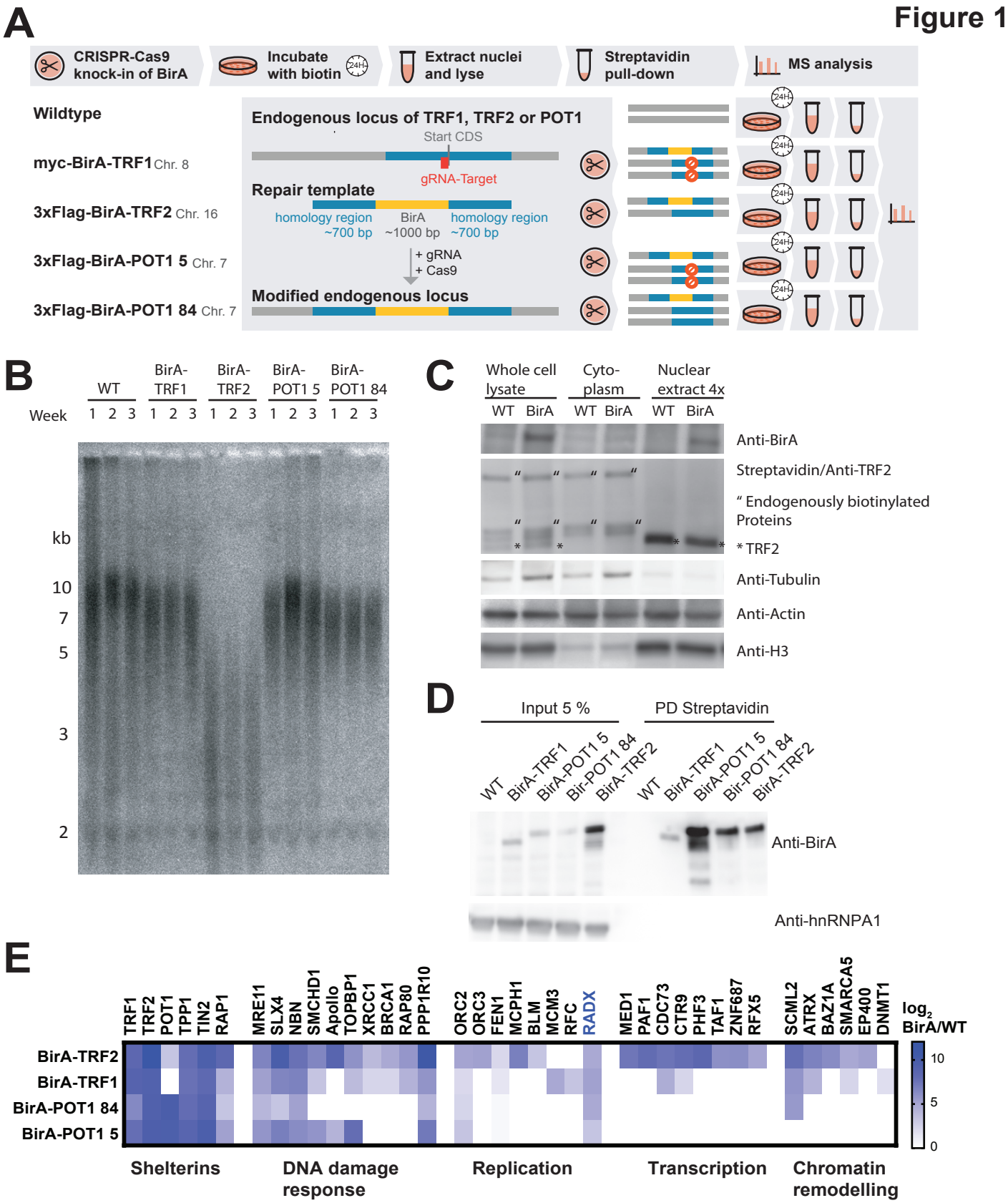

Figure 1. BioID identifies RADX at telomeres

(A) Schematic explaining the CRISPR/Cas9 approach to integrate the BirA sequence into the endogenous loci of TRF1, TRF2 or POT1 in HEK293T cells. Genotypes of selected clones are shown with either intact WT allele, integrated BirA or disrupted WT allele (stop sign).

(B) TRF analysis of indicated clones followed over several weeks in culture.

(C) Western blot showing the fractionation of endogenously biotinylated proteins present in WT and the BirA-tagged TRF1 clone 21.

(D) Immunoprecipitation of BirA-tagged proteins after incubation with Biotin for 24h.

(E) Heatmap showing enrichment ratios, calculated by log2 total spectral counts BirA/WT, for a selection of proteins identified in the corresponding BioID experiments. Proteins were not identified in the WT control IP or at least 3 fold enriched (total spectral counts) in BirA-IP. All proteins in this table, except for RADX had been previously identified at telomeres.

2.3.2. RADX Binds Single-stranded Telomeric DNA in Interphase and S phase

RADX contains three OB-folds (Figure 2A). In previous work, OB2 was identified to be responsible for the binding of single-stranded DNA and the DNA binding activity was abrogated upon mutation of two amino acids (Dungrawala et al., 2017; Schubert et al., 2017) (Figure 2A). To test the mode of RADX association with telomeres, we transiently expressed wild type Flag-tagged RADX (3xFlagRADX) and the DNA binding defective version 3xFlag-RADX OB* in Hela cells (Figure 2A and 2B) and analyzed recruitment to telomeres by immunofluorescence (IF)-FISH. Upon detergent pre-extraction, we detected chromatin-associated 3xFlagRADX in nuclear foci, which to a large extent colocalized with telomeres (Figure 2B and 2C). Very strikingly, the size of foci, the chromatin association and telomere colocalization was strongly diminished when expressing 3xFlag-RADX OB* (Figure 2B and 2C). Consequently, we conclude that RADX associates with telomeres in dependency of its ability to bind single-stranded DNA.

Since RADX was previously described to function at replication forks, we wanted to test if RADX binding to telomeres is more pronounced in S-phase (Dungrawala et al., 2017; Schubert et al., 2017). To distinguish S-phase from interphase cells, we pulse-labeled cells with the thymidine analog EdU which was subsequently fluorescently labeled with a click reaction. We observed that 3xFlagRADX colocalized with telomeres in S-phase and non-S-phase cells to a similar extent (Figure 2D and 2E). This therefore indicates that RADX associates with telomeres in interphase as well as in S-phase. Together, our experiments indicate that RADX binds to the single stranded telomeric G-rich strand which is present at the 3’ overhang of telomeres or present in the displaced G-rich strand which forms when telomeres adopt a t-loop configuration.

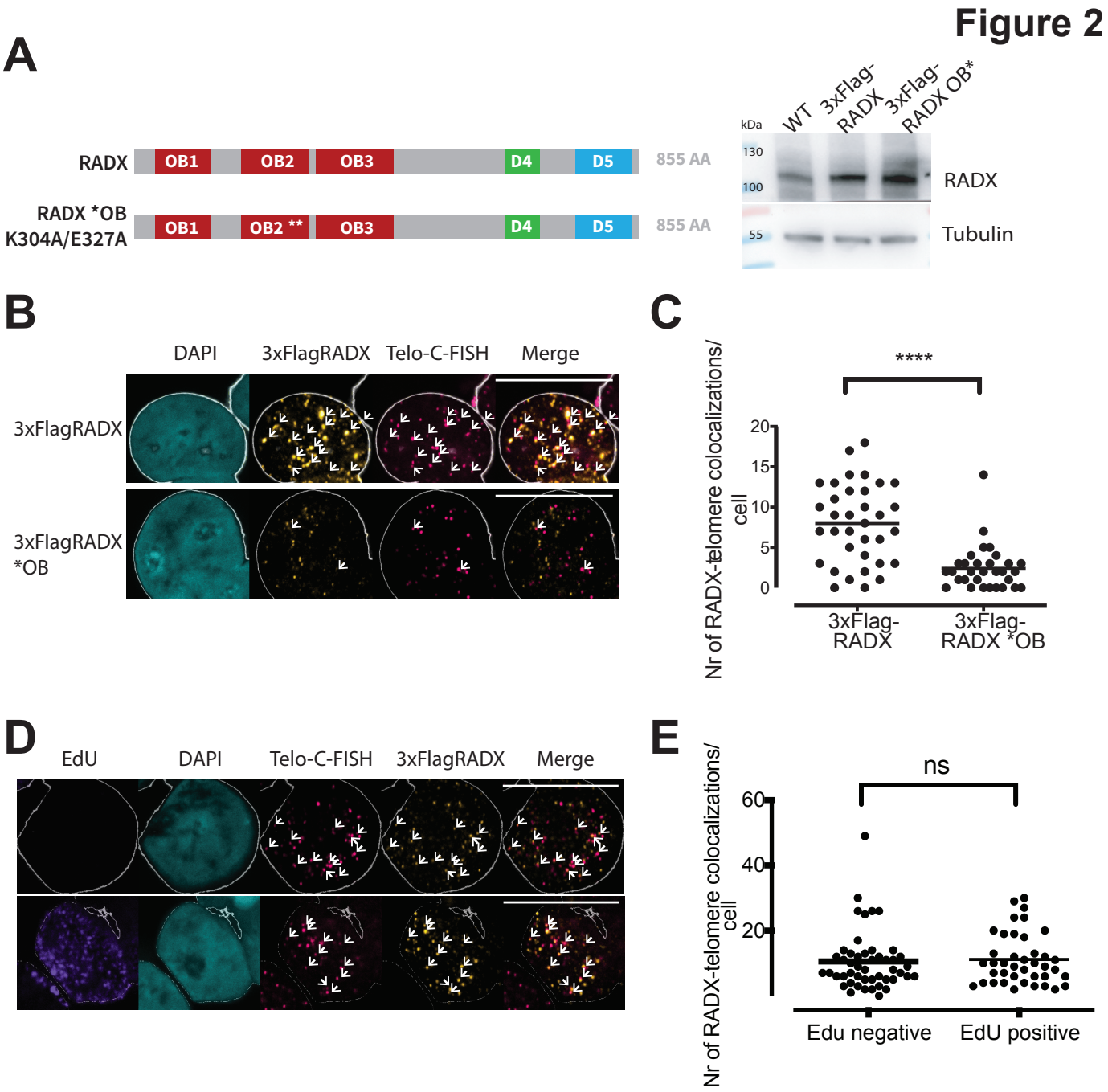

Figure 2. RADX binds single-stranded telomeric DNA throughout the cell cycle
(A)Schematic depicting RADX and RADX*OB with localization of the OB-folds, independent domains D4 and D5 as well as mutations in OB2. Protein levels upon transient transfection in Hela were monitored by Western Blot.
(B) Transiently expressed 3XFlag-RADX (yellow) colocalizes with telomeres (pink), as indicated by white arrows. Scale bar is 10 µm.
(C) Quantification of the number of RADX-telomere colocalizations per cell. At least 30 cells from three independent IF-FISH experiments were analyzed. The mean is displayed and statistical significance was calculated by unpaired t-test with $p<0.0001$.
(D) Representative examples of IF-FISH images showing colocalization of 3XFlag-RADX with telomeres. Cells in S-Phase were determined by incubation with EdU for 10 min and labeling with a Click-it EdU Kit.
(E) Quantification of number of RADX-telomere colocalizations per cell. At least 40 cells from two independent IF-FISH experiments were analyzed, the mean is displayed and statistical significance was calculated by unpaired t-test.

2.3.3. HU Treatment Increases RADX Binding to Telomeres

We next sought to identify conditions which modulate RADX binding to telomeres. We tested by RNA interference (Figure 3A), if depletion of the shelterin components TRF1, TRF2 or POT1 or the RAD51 recombinase influence RADX association with telomeres. RAD51 was previously shown to antagonize RADX binding to stalled replication forks (Dungrawala et al., 2017). In addition, we tested if induction of replication stress induced by hydroxyurea (HU) or induction of DNA double-strand breaks upon zeocin treatment would influence RADX binding to telomeres. Telomere binding by RADX was assessed by chromatin immunoprecipitation (ChIP) using RADX antibodies. As a control for specificity, RADX was deleted using a specific gRNA and CRISPR/Cas9 on the population level. Telomeric DNA was detected by dotblot hybridization and Alu repeat probes were used to compare binding to a chromosome internal locus. The dotblot signal for telomeric DNA was abolished upon *RADX* deletion. RADX binding at telomeres was detected in control cells and it did not change significantly upon depletion of TRF1, TRF2 or POT1 (Figure 3B and 3C). Of note, the depletions of the shelterins were efficient as they impaired telomere function leading to increased presence of γH2AX at telomeres (Figure 3B and 3D). Zeocin treatment and RAD51 depletion increased RADX binding slightly. The most drastic increase of RADX recruitment to telomeres was observed upon HU treatment (Figure 3B and 3C). Significantly, the increased binding was observed only for the telomeric DNA but not the Alu-repeats, even though DNA damage was observed at both loci upon HU or zeocin treatment (Figure 3B and 3D). We also tested in ChIP experiments if depletion of RADX would influence POT1 binding to telomeres but did not observe an effect (Figure S4). Altogether, the results indicated that replication stress and DNA damage stimulate RADX binding at telomeres and that RAD51 counteracts this association.

Figure 3

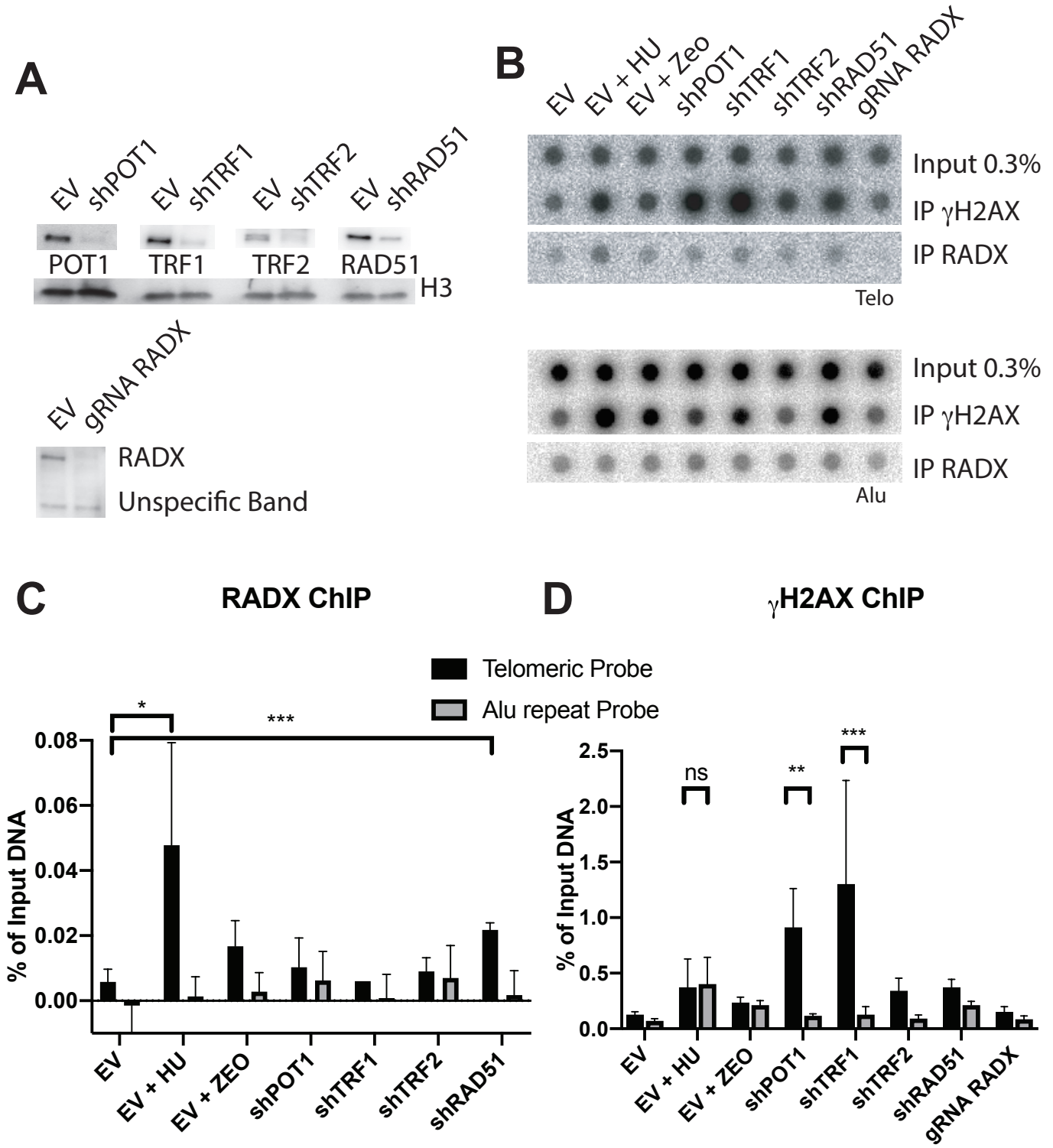

Figure 3. HU treatment increases RADX binding to telomeres
(A) Western blot of one representative experiment showing the efficiency of protein depletions in HEK293T cells.
(B) Dot blot membranes of one representative experiment, hybridized with C-rich telomeric probe, stripped and rehybridized with Alu repeat probe.
(C) and (D) Quantification of three independent ChIP experiments. Significance was determined by ordinary two-way ANOVA with multiple comparison test and $p<0.05$. % Input is displayed and in (C) the signal of the gRNA RADX sample was subtracted for every other sample to account for background binding. Cells were incubated with 1 mM HU or 1mM Zeocin for 14 h.

2.3.4. RADX Cooperates with POT1 to Suppress RAD51-Dependent Telomere Fragility and Telomere Sister-Chromatid Associations

To uncover the biological functions of RADX at telomeres and its putative collaboration with the single-stranded telomeric DNA protein POT1 we carried out depletion studies and determined telomere integrity by staining telomeres in metaphase chromosomes by FISH. In a first series of experiments we depleted RADX with siRNAs in HEK293E cells containing conditional alleles of *POT1*, which could be deleted *via loxP*-sites upon expression of Cre-recombinase (Figure 4A; see accompanying paper by Glousker et al.). Telomere replication defects give rise to fragile telomeres (Sfeir et al., 2009). Telomeres were scored as fragile (white arrows in Figure 4C), when the telomeric signals from one chromosome arm were split into two or when the telomeric signal was elongated and diffuse. RADX depletion on its own did not change the levels of telomere fragility or sister-chromatid associations (Figures 4D and 4E; see red arrows in Figure 4C for sister-chromatid associations). *POT1* deletion increased telomere fragility as well as sister-chromatid associations consistent with published results (Pinzaru et al., 2016). Very strikingly, telomere fragility was drastically aggravated when RADX was depleted in *POT1*-knockout (KO) cells (Figures 4C and 4D). Telomere sister-chromatid associations also increased upon depletion of RADX in *POT1-KO* cells (Figures 4C and 4E). Co-depletion of TRF1 and RADX did not have the same effect (Figure S5). These results suggested that RADX and POT1 cooperate to suppress both of these telomere abnormalities. To test if the putative RADX antagonist RAD51 mediated these phenotypes, we co-depleted RAD51 or the RAD51 loader BRCA2. Indeed, the elevated telomere fragility as well as telomere sister chromatid associations were suppressed upon co-depletion of RAD51 or BRCA2 (Figures 4D and 4E). These results suggested that POT1 and RADX suppress homologous recombination at telomeres which when unleashed mediates sister-telomere associations and telomere fragility.

To further corroborate these findings, we inverted the experimental design by first generating *RADX-KO* clones in HEK2913T cells using CRISPR/Cas9 and depleting POT1 with shRNAs (Figure 5A). Also, in this setting, telomere fragility was more pronounced upon depletion of POT1 in *RADX-KO* cells than in wild type cells and as above, telomere fragility was suppressed upon RAD51 co-depletion (Figures 5B, 5C and 5D). However, depletion of POT1 with shRNA in wild type and *RADX-KO* cells did not lead to an increase in sister-chromatid associations (Figure 5E). This therefore indicates that the small amounts of POT1, which were retained

upon expression of shRNAs (Figure 5B) were sufficient to suppress telomere sister-chromatid associations. Still, these results confirmed that RADX and POT1 cooperate to suppress RAD51-dependent telomere fragility.

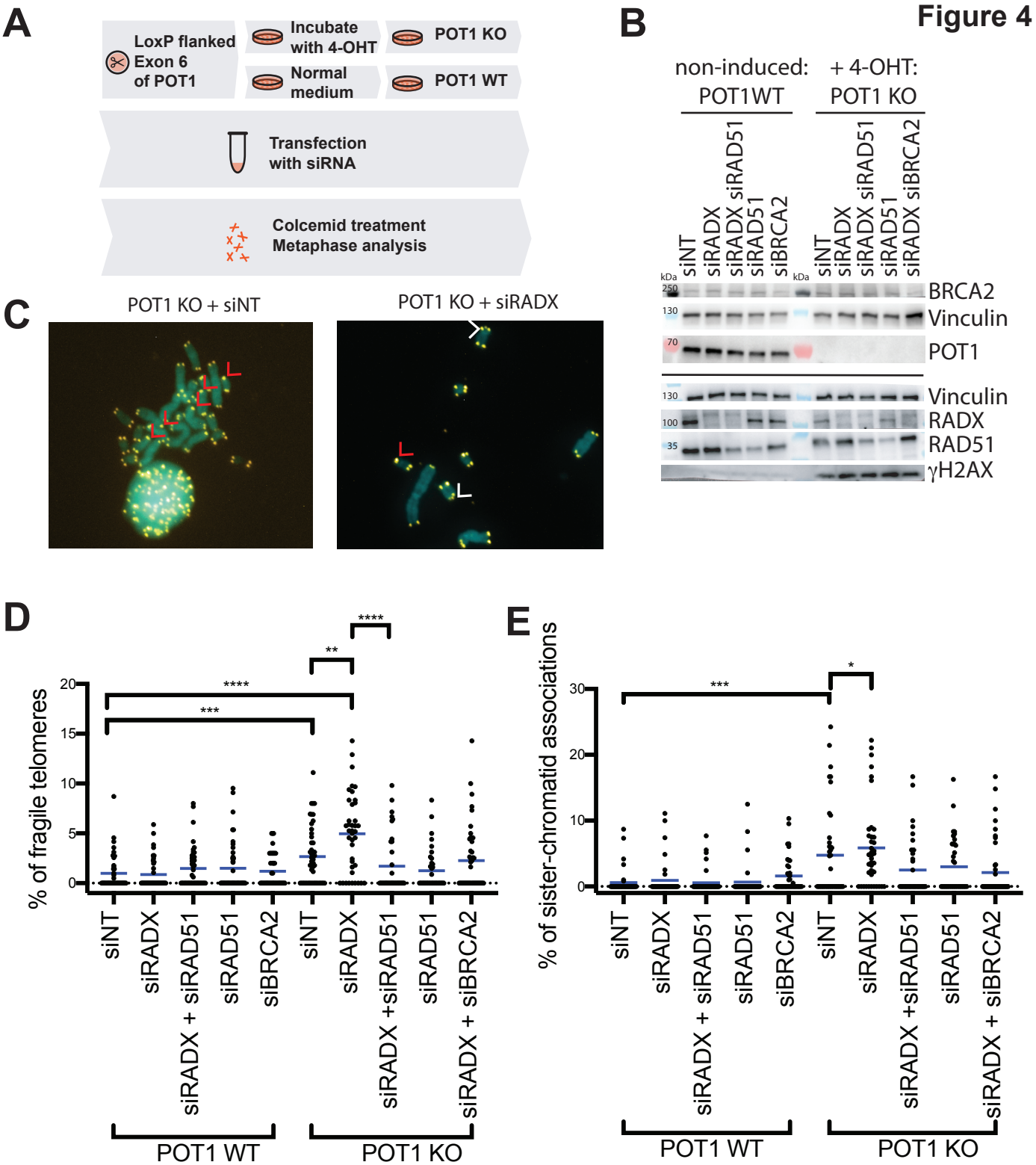

Figure 4. POT1/RADX- double depletion induces telomere fragility and telomere sister-chromatid associations.

(A) Schematic explaining the experimental set-up for protein depletions in HEK293T cells.

(B) Western blot of one representative experiment proving efficient gene deletions and protein depletions. SiRNAs were pools from Dharmacon.

(C) Representative metaphases for induced POT1 KO cells transfected with non-targeting (NT) siRNA or siRADX. White arrows indicate fragile telomeres (smeary dot or two dots on one chromosome arm) and red arrows represent sister chromatid fusions.

(D) and (E) Quantification of >37 metaphases per condition from three independent experiments. The mean is displayed and statistical significance was determined by ordinary one-way ANOVA and TUCKEY'S multiple comparison test, **** $p<0.0001$, *** $p<0.005$, ** $p< 0.001$ and * $p<0.05$.

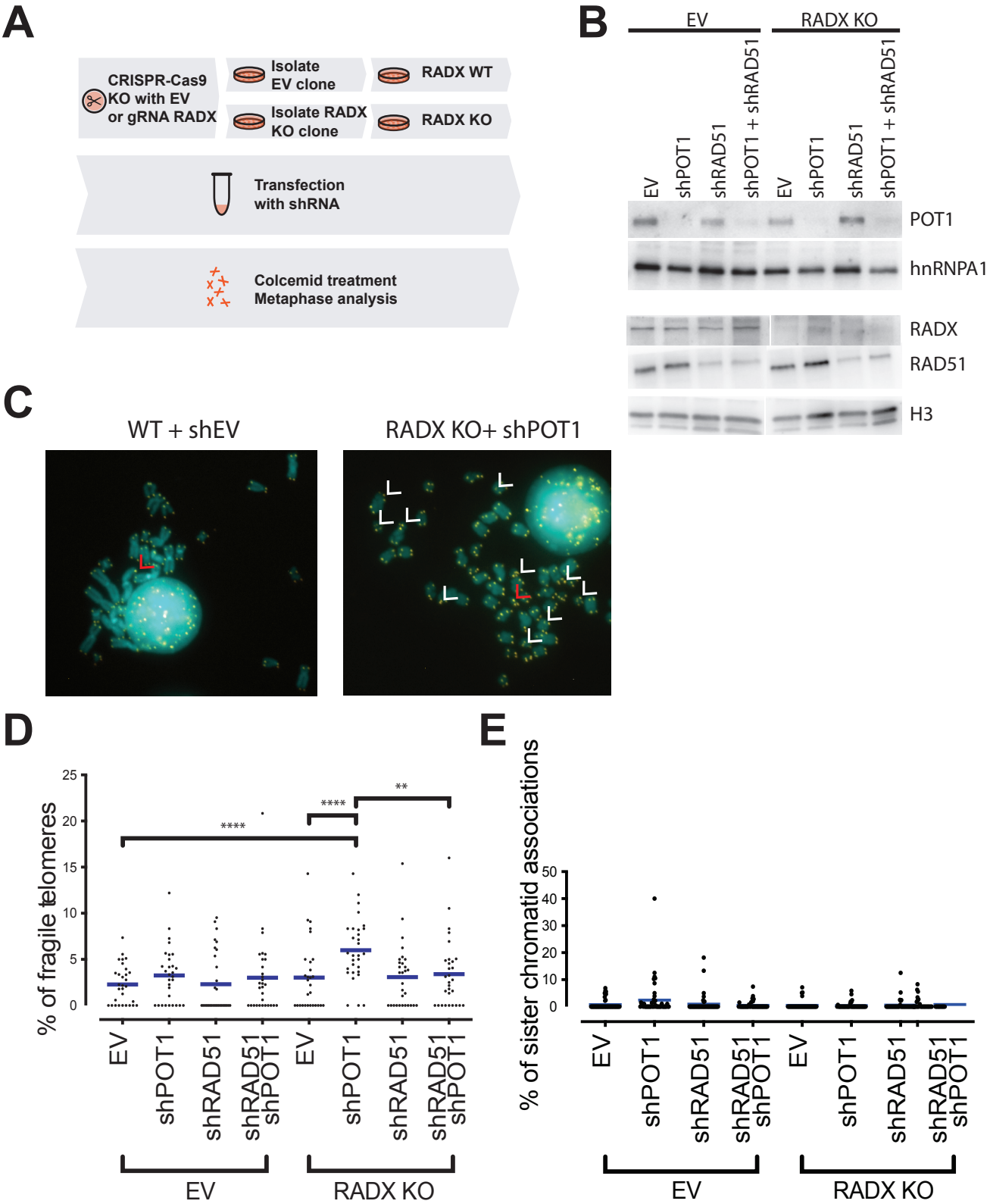

Figure 5. RADX/POT1- double depletions induce telomere fragility.
(A) Schematic explaining the experimental set-up for protein depletions in HEK293T cells.
(B) Western Blot of one representative experiment indicating efficient gene deletions and protein depletions.
(C) Representative metaphases for induced POT1 KO cells transfected with non-targeting (NT) siRNA or siRADX. White arrows represent fragile telomeres (either a smeary dot or two dots on one chromosome arm) and red arrows represent sister chromatid fusions.
(D) and (E) Quantification of >40 metaphases per condition from three independent experiments. The mean is displayed and statistical significance was determined by ordinary one-way ANOVA and TUCKEY's multiple comparison test, **** $p<0.0001$, *** $p<0.005$, ** $p< 0.001$ and * $p<0.05$.

2.3.5. RADX and POT1 suppress RAD51 binding

The above results demonstrated that RADX and POT1 suppress RAD51 dependent telomere damage. To elucidate the underlying mechanism, we tested the hypothesis that RADX and POT1 suppress RAD51 binding at telomeres. We depleted POT1 via shRNAs and deleted *RADX* with CRISPR/Cas9 in Hela cells (Figure 6A). RAD51 association with telomeres was determined by quantifying colocalization of RAD51 with telomeres in IF/FISH experiments (Figure 6B). Deletion of *RADX* on its own did not significantly increase RAD51 abundance at telomeres (Figure 6B and 6C). However, POT1 depletion enhanced RAD51 binding which was further enhanced upon POT1 depletion in *RADX-KO* cells. This experiment therefore indicates that RADX and POT1 cooperate to suppress telomere association of RAD51.

Finally, we determined if *RADX*-deletion affected the telomeric 3' overhang structure or telomere length homeostasis. The telomeric 3' overhang was detected by Southern hybridization of non-denatured DNA and telomere length was determined by Southern hybridization of denatured DNA (Figure S6). In both of these analyses, *RADX* deletion had no impact on telomeric DNA length and structure. However, in the accompanying paper (Glousker et al.) we discovered the *POT1* deletion leads to rapid telomere elongation within seven days of growth. We therefore tested if RADX depletion would affect this phenotype and saw even further telomere elongation (Figure 6D) in cells deprived of POT1 and RADX indicating the cooperation of RADX and POT1 in also suppressing this phenotype.

Figure 6

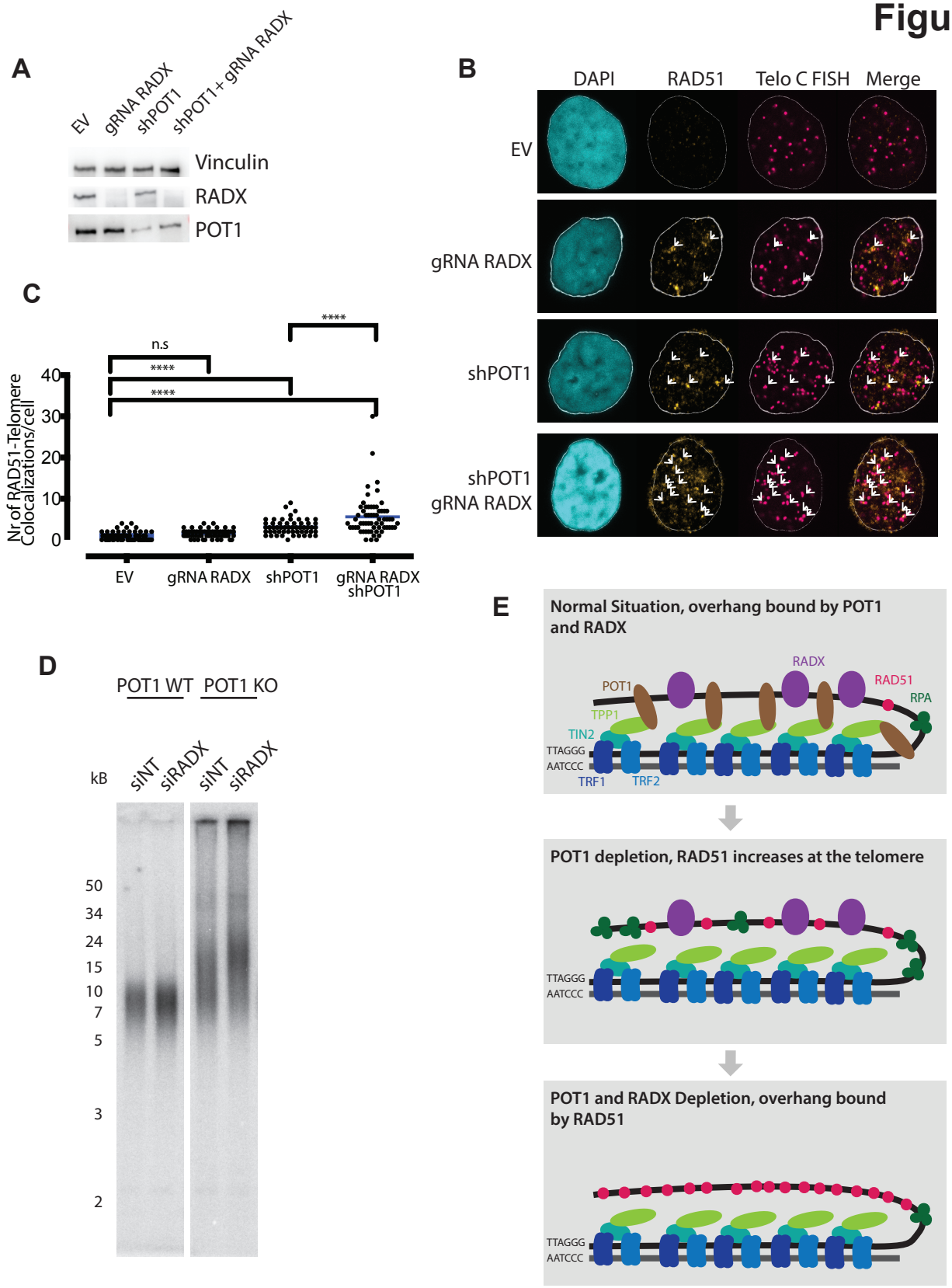

Figure 6. RADX and POT1 suppress RAD51 binding.
(A) Western blot of one representative experiment showing efficient protein depletions in Hela cells.
(B) Representative IF-FISH images of RADX or/and POT1 depletions with RAD51 in yellow and telomeres in pink. White arrows indicate colocalization.
(C) Quantification of one representative experiment with >55 cells analyzed per condition. The mean is displayed and statistical significance was determined by ordinary one-way ANOVA and DUNNETT's multiple comparison test, **** $p<0.0001$ and * $p<0.05$.
(D) TRF of HEK293T cells with the same experimental set-up as for Figure 4, except for the skipping of demecolcine treatment.
(E) Schematic model of RADX, POT1 and RAD51 binding at the telomeric overhang.

2.4. **Discussion**

In this paper we explore the telomeric protein environment of TRF1, TRF2 and POT1 by inserting the BirA sequence at the endogenous loci in frame with the ATG start codons. The fusions did not interfere with telomere function when assessing telomere length maintenance and telomere integrity visualized on metaphase chromosomes. The overlap of the biotinylated proteins identified with all three shelterins was remarkable providing confidence in the biological relevance of identified proteins. Our live-cell labeling results are also consistent with previous data showing a physical association of shelterin components and the formation of functional complexes (Houghtaling et al., 2004; Liu et al., 2004; Ye et al., 2004). Still, slightly more proteins were identified with TRF1 and especially with TRF2 than with POT1 suggesting that the double strand telomere binding proteins may connect to a larger set of cellular processes.

2.4.1. RADX Association with Telomeres

During the course of our studies CxORF57 was identified as an antagonist of RAD51 and re-named RADX (Dungrawala et al., 2017; Schubert et al., 2017). We focused our attention on RADX as it was identified with all three fusion proteins and because it contained OB-folds which are present not only in RPA but also in the important telomere components POT1, TPP1 and CST complex subunits. Our data indicate that RADX binds along with POT1 to the single-stranded G-rich strand at telomeres which is present as 3' overhang or present as displaced strand when telomeres are engaged in t-loops. RADX binding occurs in S-phase as well as interphase. This conclusion is supported by the observation that telomere association is dependent on an intact single-strand-DNA-binding-domain present in OB2 and independent of S-phase. Furthermore, telomere binding was enhanced upon HU treatment, which results in replication fork stalling. In this experiment we observed DNA damage signaling at telomeres and at Alu repeats, but RADX was enriched only at telomeric repeats suggesting there may be preferential binding of RADX to telomeric sequences. Interestingly, TRF1 depletion, which previously was also shown to increase replication fork stalling and replication problems at telomeres (Sfeir et al., 2009) did not induce a comparable rise in RADX telomere binding. We hypothesize that RADX binds specifically to unmanteled G-rich DNA, which is free upon replication fork stalling but forms G4 structures upon TRF1 removal mediated replication fork

stalling due to lack of helicases like BLM which resolve G4 structures (Zimmermann et al., 2014).

2.4.2. RADX Cooperation with POT1 to Suppress Telomere Fragility and Sister-Chromatid Associations

Our results demonstrate that co-depletion of RADX with POT1 but not with TRF1 enhances telomere fragility and sister-telomere associations. It was recently demonstrated that RADX counteracts RAD51 mediated replication fork reversal (Dungrawala et al., 2017) which occurs independently of BRCA2 (Mijic et al., 2017). We tested the involvement of RAD51 and BRCA2 for POT1/RADX depletion mediated telomere fragility and sister-chromatid associations and found that both, RAD51 or BRCA2 depletion, rescued the telomere damage. This suggests that telomere fragility and sister-telomere associations are generated due to activation of homologous recombination, rather than fork reversal at telomeres.

Altogether, our results support a model in which RADX represents next to the more abundant POT1 a second OB-fold containing telomere binding protein that contributes to telomere protection (Figure 6E). Concomitant loss of POT1 and RADX leads to efficient BRCA2-mediated loading of RAD51 at telomeres unleashing RAD51 mediated sister-chromatid association and HDR resulting in telomere fragility. When POT1 is abundantly present at telomeres, the telomeric RADX function is not yet apparent. POT1 is capable to suppress RAD51 binding and the resulting telomere abnormalities on its own, independently of RADX. However, when POT1 becomes scarce at telomeres, RADX function becomes critical to support POT1 in suppressing RAD51 binding (Figure 6E). This function is important also to sustain RPA-ATR-ATRIP mediated damage signaling at telomeres preventing the exchange of RPA by RAD51. We predict that this mechanism becomes particularly critical during cellular senescence when POT1 concentration is lowered at telomeres to guarantee long-lasting RPA-ATR/ATRIP mediated checkpoint signaling. Thus, our results should inspire future investigations to test the roles of RADX for the maintenance of cellular senescence to suppress tumorigenesis.

2.5. Supplemental Information

Supplemental Information includes figures S1-S6 as well as table S1. Table S1 can be found at the end of this thesis.

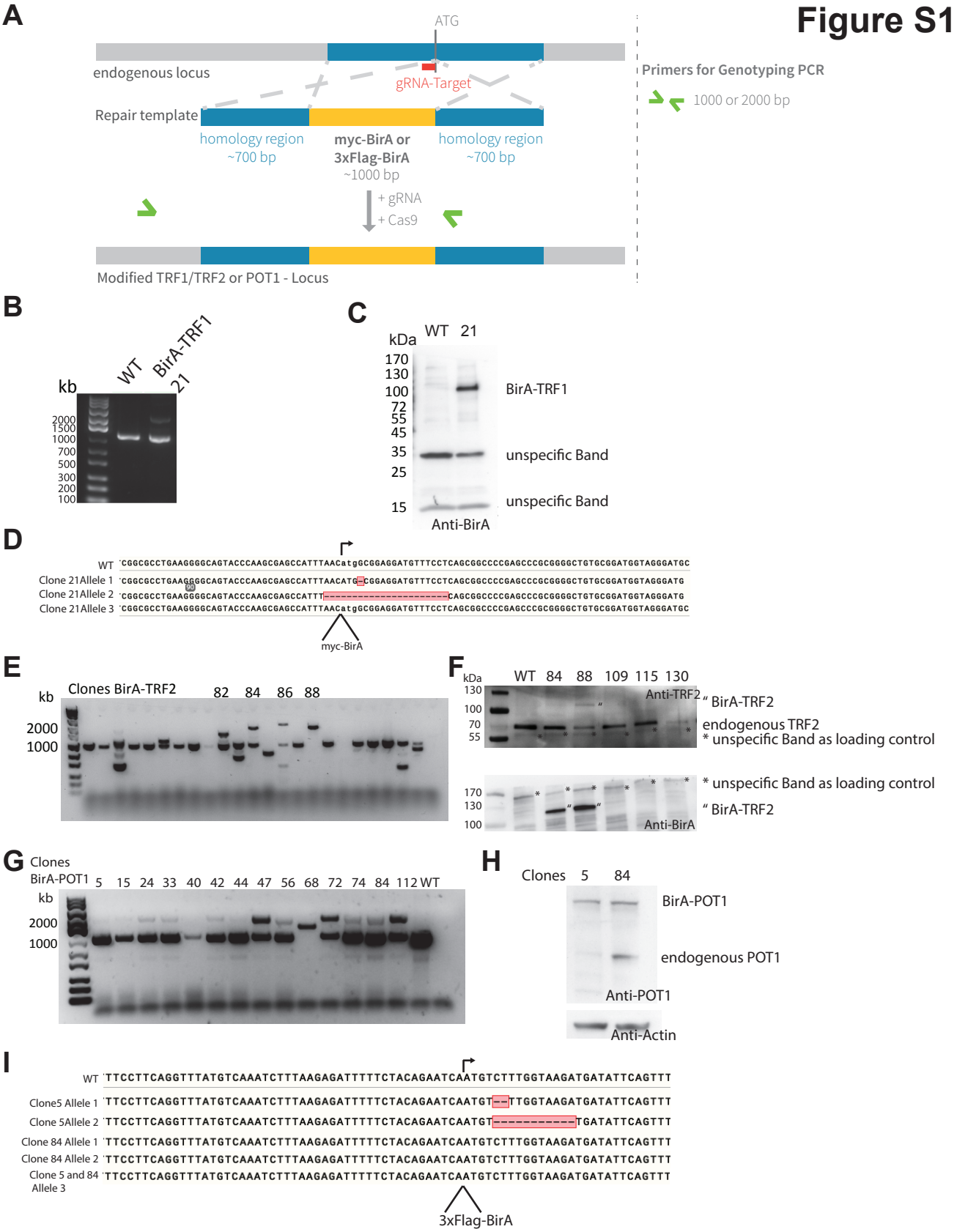

Figure S1. Screening and characterization of BirA-clones

(A) Schematic explaining the PCR approach for screening and genotyping of BirA-tagged clones.
(B) Amplification products for the genotyping PCR showing a band for an untagged WT allele and a larger band for the integration of the BirA sequence at the endogenous TRF1 locus in clone 21.
(C) Western blot showing the expression of BirA-tagged TRF1 in clone 21.
(D) Sequencing results of the subcloned PCR products from (C) for clone 21.
(E) Amplification products for the genotyping PCR for BirA-TRF2 clones.
(F) Western blots for selected BirA-TRF2 clones and a WT control.
(G) Genotyping PCR for BirA-POT1 clones.
(H) Western blot for BirA-POT1 clone 5 and 84 showing endogenous and tagged POT1.
(I) Sequencing results for BirA-POT1 clones 5 and 84

Figure S2

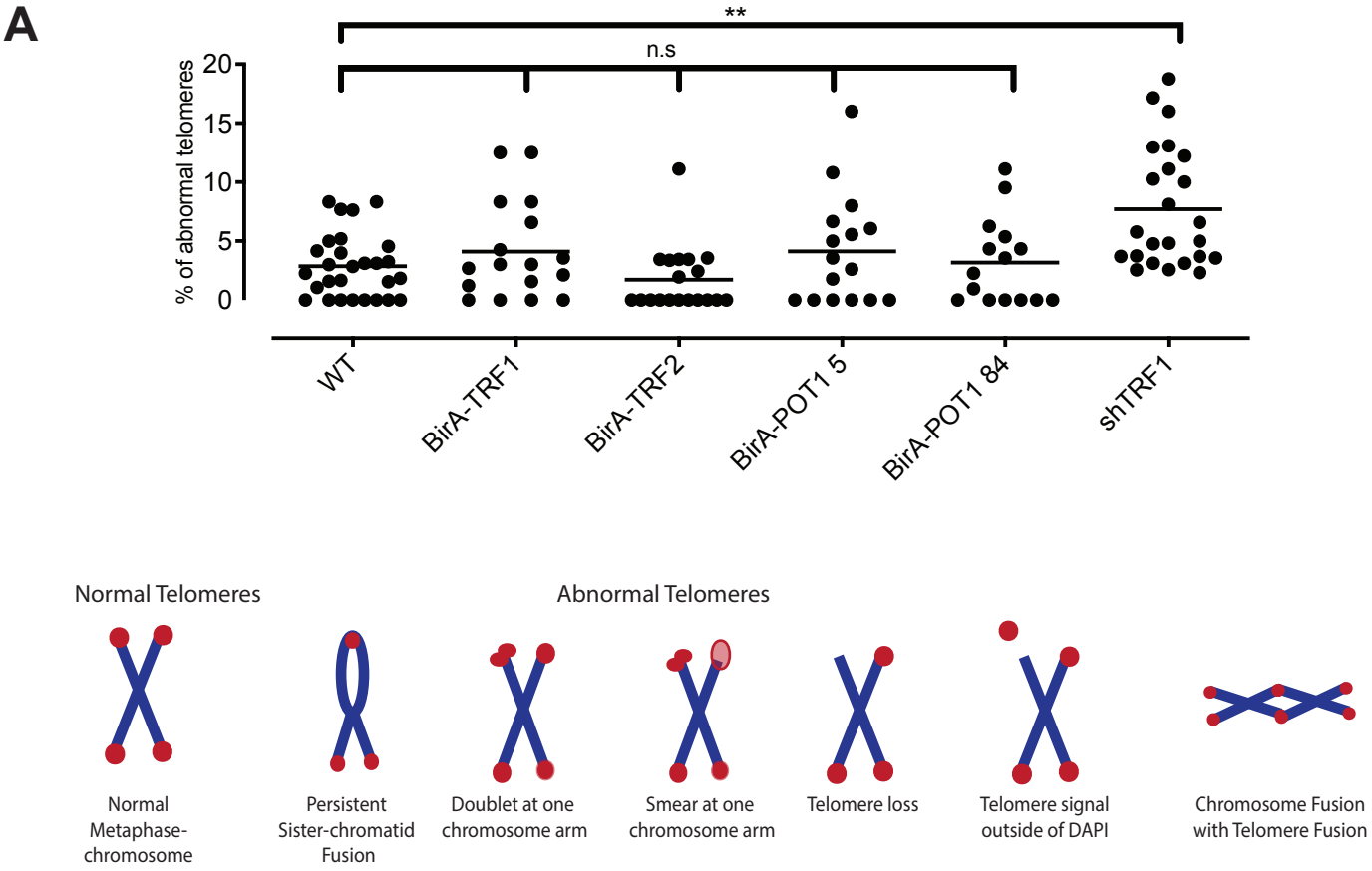

Figure S2. Functional characterization of BirA-clones
(A) WT and BirA clones derived metaphase chromosomes were analyzed for abnormal telomeres and compared to TRF1 depletion as positive control. Statistical significance was determined by one-way-ANOVA and DUNETT's multiple comparison test and **p<0.01%.

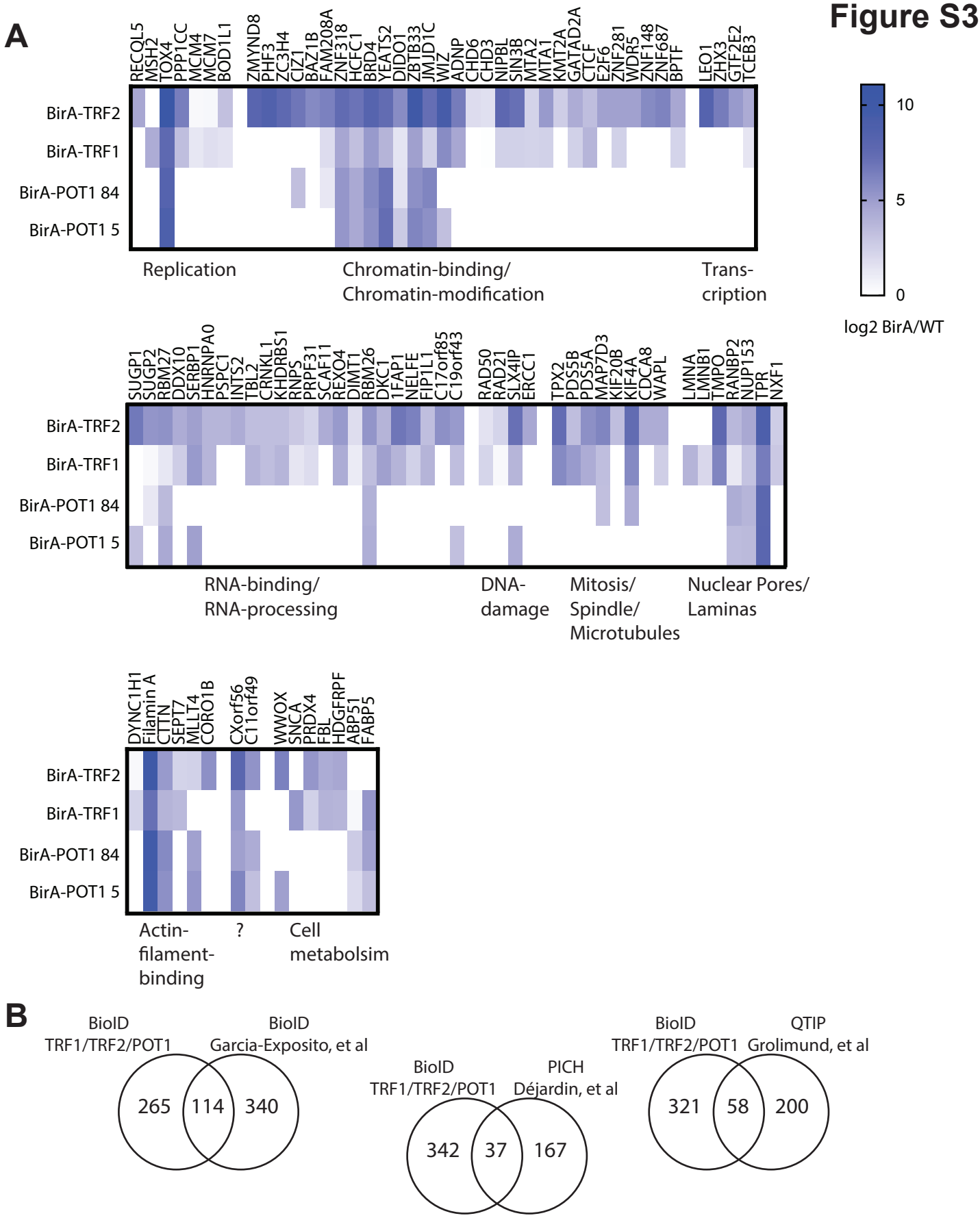

Figure S3. Identified proteins in BioID

(A) Heatmap showing enrichment ratios, calculated by log2 ratios of total spectral counts BirA/WT, for a selection of proteins identified in the corresponding BioIDs. Proteins were not identified in the WT control IP or at least 3 fold enriched (total spectrum counts) in BirA-IP and identified in at least two BirA-IPs.

(B) Comparison of proteins identified in this study to telomeric proteins identified by PICH (Déjardin and Kingston, 2009), TRF1-BioID (Garcia-Exposito et al., 2016) or QTIP (Grolimund et al., 2013).

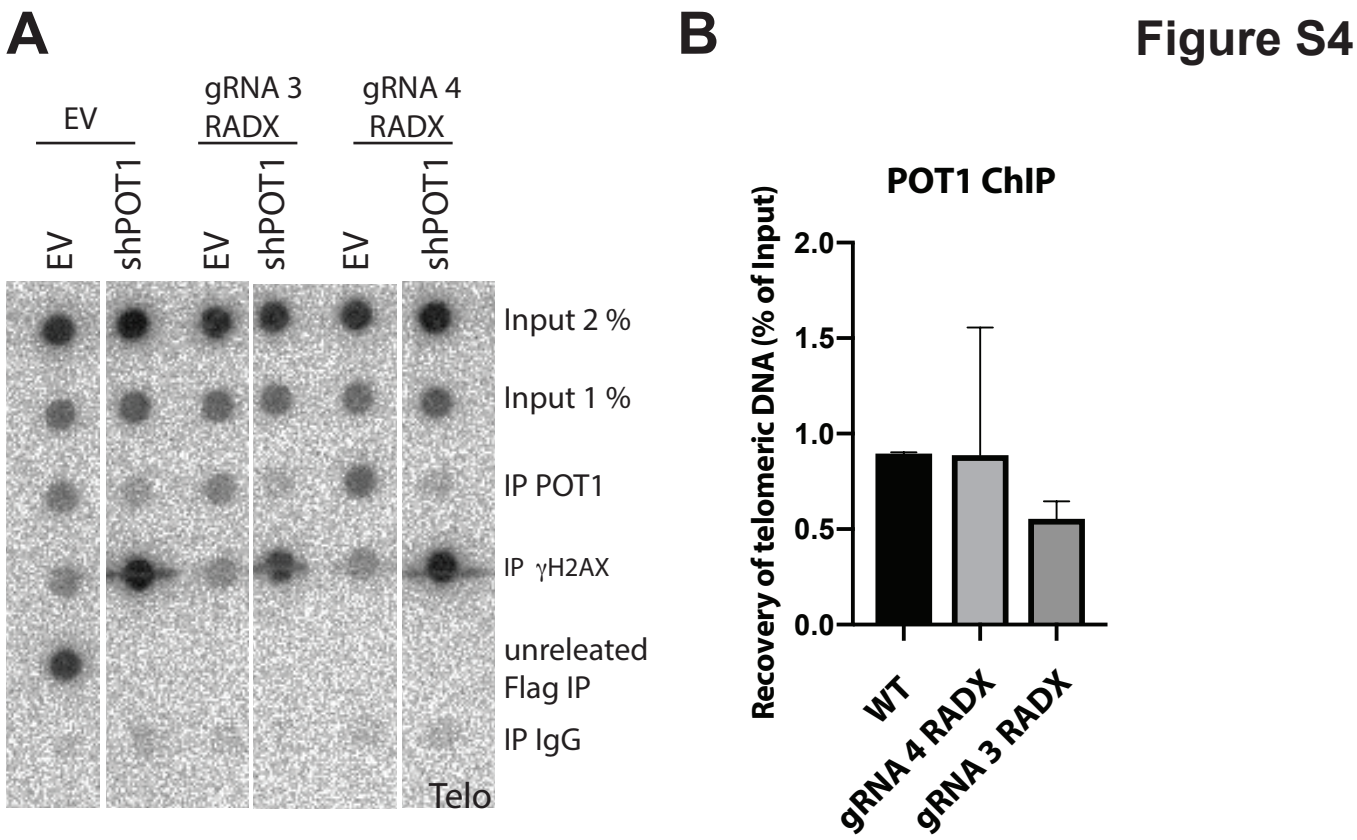

Figure S4: RADX depletion does not change POT1 abundance at the telomere
(A) Dot blot membranes of one representative experiment carried out with HEK293T cells and hybridized with a C-rich telomeric probe.
(B) Quantification of three independent ChIP experiments. Significance was determined by ordinary one-way ANOVA with DUNNETT's multiple comparison test and $p>0.05$.

Figure S5

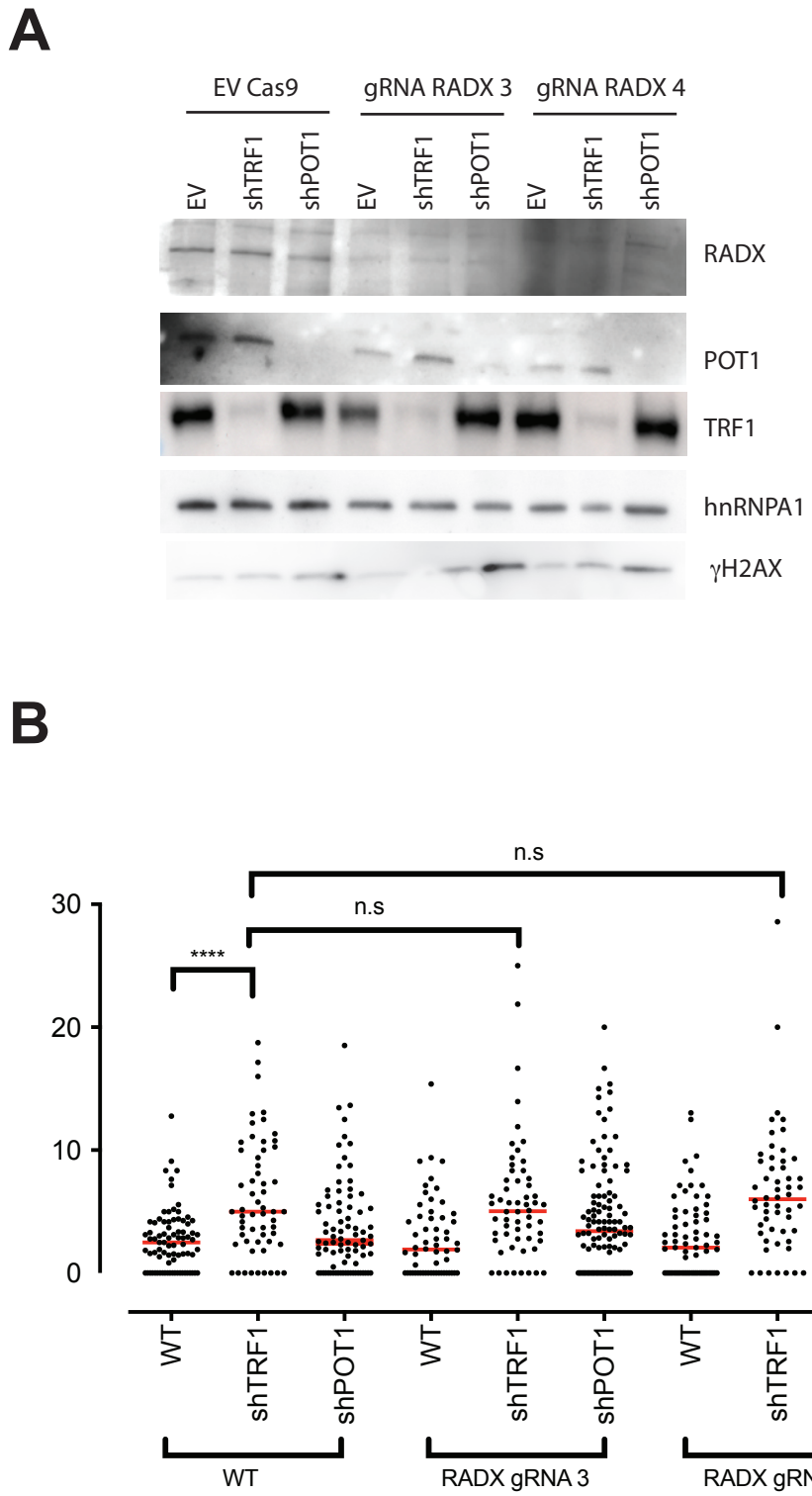

Figure S5. RADX/TRF1 double depletion does not increase telomere fragility.
(A) Western blot of one representative experiment indicating efficient gene deletions and protein depletions in Hek293T cells.
(B) Quantification of >90 metaphases per condition from three independent experiments. The mean is displayed and statistical significance was determined by ordinary one-way ANOVA and TUCKEY's multiple comparison test, **** $p<0.0001$, *** $p<0.005$, ** $p< 0.001$ and * $p<0.05$.

Figure S6

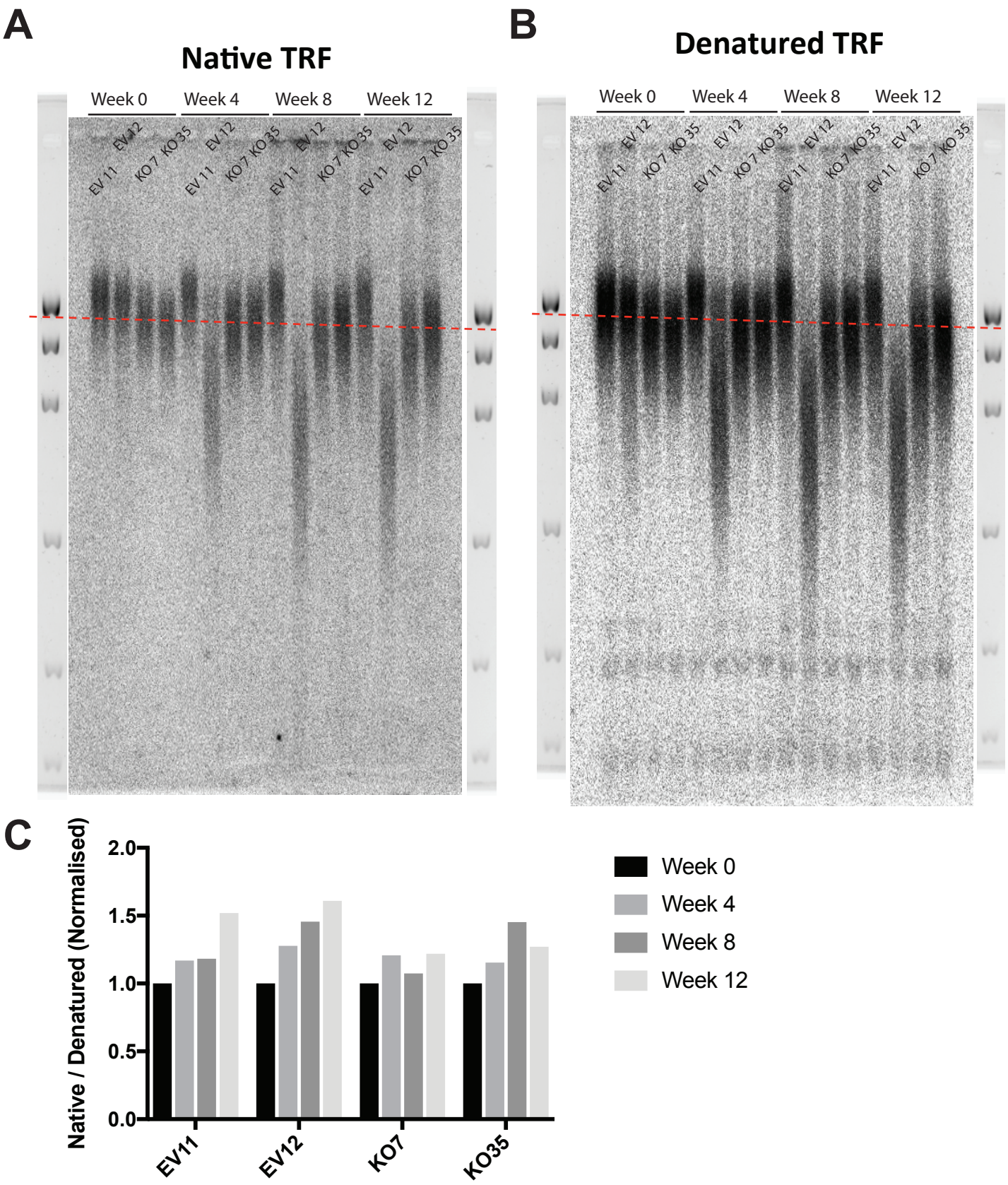

Figure S6. RADX KO does not change telomeric 3'overhang and total telomere length
(A) + (B) Telomere restriction fragment analysis of two isolated HEK293T clones transfected with EV, gRNA3 RADX (KO7) or gRNA4 (KO35). The same gel was hybridized with a 32P-labelled Telo-C-probe with or without denaturation.
(C) Quantification of the native/denatured signal normalized to week 0 from the gel in (A) and (B).

2.6. Experimental Procedures

2.6.1. Cell culture

Hela and HEK293T cells were cultured in Dulbecco's modified Eeagle's medium supplemented with 10% fetal calf serum and 100 U/ml of penicillin/streptomycin. Cells were grown at 37°C in presence of 5% CO_2.

2.6.2. Lipofectamine transfection

0.7 Million HEK293T cells were seeded the day before transfection in a 6-well plate in 2 ml DMEM/FBS/PenStrep. Cells were transfected with 3 µg DNA per plasmid, suspended in 250 µl OptiMEM, combined with 10 µl Lipofectamie 2000 (Invitrogen) in 250 µl OptiMEM. After 15 min incubation the transfection mix was added dropwise to the cells. After 18-24 h the cells were split and transferred to a 10 cm dish and incubated with either blasticidin (5 µg/ml) or puromycin (1 µg/ml) for 3 days. Cells were split again, fresh medium DMEM/FBS/PenStrep was added and cells were harvested after 1-3 days.

2.6.3. siRNA transfection in POT1-inducible KO cells

HEK293E cells were induced with 0.5 µM 4-Hydroxytamoxifen on day 0. On day 2, cells were split and 5 million cells were seeded into 10 cm dishes. On day 3 the medium was changed to 5 ml DMEM/FBS without PenStrep and transfected with 30 pmol siRNA (222 µl H_2O, 25 µl 2.5 M $CaCl_2$, 250 µl 2x HBSS pH 7.04, 3 µl 10 µM siRNA). On day 4, the medium was changed and cells were split into 2-3 10 cm dishes. Cells were harvested on day 6.

2.6.4. Plasmid preparation

For validation of telomeric localization of RADX by IF-FISH, RADX cDNA was amplified from HEK293T cells and cloned into pcDNA6 downstream of three tandemly repeated Flag tags giving rise to pcDNA6-3xFlagRADX. The shRNA expressing vectors were created by ligating the double-stranded DNA oligonucleotides into pSuper-puro or pSuper-Blast-vectors (Oligoengine) digested with BglII and HindIII. gRNAs were generated by ligating the annealed DNA oligonucleotides into the BbsI restriction site of pSpCas9(BB)-2A-Puro (Addgene 48139) as described (Ran et al., 2013). RADX *OB was generated by site-directed-mutagenesis of pcDNA6-3xFlagRADX (QuickChange II Site-directed mutagenesis kit, Agilent).

2.6.5. CRISPR/Cas9 gene editing BirA clone generation

gRNAs to target the genomic loci in proximity to the start codon were selected with the tool provided by Feng Zheng's laboratory (Broad institute, (Shalem et al., 2014)) and were cloned into pSpCas9 (BB)-2A-GFP as described (Ran et al., 2013). The repair template was created by amplifying the homology regions from gDNA of HEK293T cells and the BirA sequence from pcDNA3.1-myc-BioID (Addgene 35700) and combined by overlapping PCR (Bryksin and Matsumura, 2010) and further subcloned into TOPO Zero Blunt for Sequencing (Invitrogen). 1 Million Hek293T cells were transfected in a 6-well plate containing 2 ml DMEM/FBS with 3 µg DNA gRNA and 3 µg repair template, 500 µl OptiMEM and 10 µl Lipofectamine. Cells were split the next day and after 72 h single GFP-positive cells were sorted into 96-well plates. After 2 weeks, cells were split into two 12-well plates. Three days later genomic DNA was extracted from one row of 12 well plates with the Wizard genomic DNA Purification System (Promega). PCR with primers flanking the region of insertion was performed to screen for clones with insertion of the BirA sequence. Positive clones were further expanded and the PCR product was subcloned into TOPO Zero Blunt for sequencing and genotyping.

2.6.6. RADX KO clone generation

gRNAs were selected based on low off-target scores with the tool from Feng Zheng's laboratory (Broad institute, (Shalem et al., 2014)) and cloned into pSpCas9 (BB)-2A-Puro as described before. 1 Million Hek293T cells were transfected in a 6-well plate containing 2 ml DMEM/FBS with 4 µg DNA, either gRNA or EV plasmid, 500 µl OptiMEM and 10 µl Lipofectamine. The next day cells were split and puromycin (1 µg/ml) was added. After 3 additional days cells were diluted to single cells and 1 cell per well was seeded in a 96 well plate. After 2.5 weeks colonies were screened for RADX loss by western blot and validated by sequencing.

2.6.7. Western blot

0.5 million cells were incubated in 2x Laemmli buffer with 100 mM DTT and boiled at 95°C. Proteins were separated on a 4-15% gradient Mini Protean TGC (BioRAD) followed by wet transfer onto a 0.2 µm nitrocellulose membrane (Amersham Protran, GE Healthcare). Membranes were blocked either in 3% BSA in 1x PBS+ 0.1% Tween or 5 % milk in 1x PBS + 0.1% Tween overnight and washed 3x 15 min with PBS + 0.1% Tween the next day. HRP-

conjugated secondary antibodies in combination with ECL spray (Advansta) were used to reveal the signal on a FluorChem 8900 (Alpha Innotech) or Fusion FX (Vilber) detector.

2.6.8. Telomere restriction fragment analysis (TRF)

Genomic DNA from 3 million cells was isolated with the Wizard genomic DNA kit (Promega) following the protocol of the manufacturer. 5 µg genomic DNA was digested with 15 U RsaI and 15 U HinfI (New England Biolabs) overnight at 37°C. Samples were loaded on a 15 cm long 0.8% agarose gel and separated. Alternatively, DNA was separated by pulse field gel electrophoresis on a 1% agarose gel in 0.5 x TBE at 5 V cm^{-1} for 16 h at 14 °C with switch times ramped form 0.5 to 6 seconds. After electrophoresis, the gels were dried for 2h at 50°C, denatured with 0.8 M NaOH, 0.5 M NaCl, neutralized with 0.5 M Tris-HCl pH 7.0 and prehybridized at 50°C in Church buffer (1% BSA, 7% SDS, 1 mM EDTA, 0.5 M Na-phosphate buffer at pH 7.2). Hybridization was overnight at 50°C with a ^{32}P-labeled telomeric probe as described (Grolimund et al., 2013). After hybridization the gel was washed for 1 h with each wash buffer at 50°C containing 2x SSC + 0.1% SDS, 1x SSC + 0.1% SDS, 0.5x SSC + 0.1% SDS and 0.1x SSC. Radioactive signal was detected with Amersham Typhoon.

2.6.9. Telomeric FISH on metaphase chromosomes

Slides were prepared as described (Majerska et al., 2018).

2.6.10. ChIP-dot blot

15 million HEK293T cells were crosslinked for 15 min at room temperature in 1.5 ml 1 % methanol-free formaldehyde in PBS. Formaldehyde was quenched for 5 min with 0.1 M glycine for 5 min. Chromatin enriched fractions were prepared by lysis in SDS lysis buffer (1% SDS, 50 mM Tris-HCl pH 8.0, 10 mM EDTA pH 8.0). Chromatin was resuspended in 1 ml LB3 (10 mM Tris-HCl pH 8.0, 200 mM NaCl, 1 mM EDTA, 0.5 mM EGTA, 0.1 % Na-deoxycholate, 0.25% sodium lauroyl sarcosinate, EDTA-free protease inhibitor complex (Roche) and sonicated for 15 min at 4°C using a Focused-Ultrasonicator (Covaris, E220, duty 5.0, PIP: 140, cycles: 200, amplitude 0, velocity 0, dwell 0, 0.12 x12 mm glass tubes with AFA fiber). Insoluble material was removed by centrifugation for 15 min, 4°C, at 20,000 g. Sonicated extracts were diluted with 5 volumes IP dilution buffer (50 mM Tris-HCl pH 8.0, 0.75% Triton-X-100, 600 mM NaCl, 10 mM EDTA pH 8.0) and precleared with 30 ul sepharose protein G beads (GE Healthcare), which were blocked with 1 mg/ml BSA. Immunoprecipitation was performed with 30 µl blocked sepharose protein G beads and 5 µl of

antibody or serum per precleared lysate corresponding to 200,000 cells. After overnight incubation at 4°C, beads were washed at 4°C for 5 min on a rotating wheel with the following washing buffers: Wash 1 (0.1% SDS, 1% Triton-X-100, 2 mM EDTA pH 8.0, 20 mM Tris-HCl pH 8.0, 300 mM NaCl) for 5 min, wash 2 (0.1% SDS, 1% Triton-X-100, 2 mM EDTA pH 8.0, 20 mM Tris-HCl pH 8.0, 500 mM NaCl) for 5 min, wash 3 (250 mM LiCl, 1% NP-40, 1% Na-deoxycholate, 1 mM EDTA pH 8.0, 10 mM Tris-HCl pH 8.0) for 5 min and twice with TE. Beads were suspended in 100 µl crosslink reversal buffer (20 mM Tris-HCl pH 8.0, 1% SDS, 100 mM $NaHCO_3$, 0.5 mM EDTA, 200 µg/ml RNase-DNase free (Roche)) and incubated 5 h or overnight at 65°C. DNA was purified using the NucleoSpin Gel and PCR Clean-up with buffer NTB (Macherey Nagel) and eluted in 100 µl TE buffer. Afterwards DNA was denatured 5 min at 95°C and chilled immediately on ice before spotting onto a Hybond N+ nylon membrane (GE Healthcare) using a BioRad dot blot apparatus. The membrane was UV-crosslinked, denatured with 0.8 M NaOH, 0.5 M NaCl and neutralized with 0.5 M Tris-HCl pH 7.0 and blocked in Church buffer at 65°C for 1 h. Incubation with a ^{32}P-labeled telomeric probe was done overnight at 65 °C as described (Grolimund et al., 2013). The next day the membrane was washed 3x 30 min with 1x SSC + 0.5% SDS. For Alu probe ((5′-TGATCCGCCCGCCTCGGCCTCCCAAAGTG-3′) incubation, membranes were stripped by boiling at 95°C for 3x 10 min in 0.1x SSC + 1% SDS. Membranes were again prehybridized with Church buffer at 55 °C and hybridized with the Alu repeat probe in Church buffer overnight at 55°C and washed 3x 30 min with 1x SSC + 0.5% SDS.

Radioactive signal was detected with a FujiFilm Fluorescent Image Analyzer (FLA-3000) and the intensity of each dot was calculated using AIDA software. Averages and p-values were calculated using PRISM 8 software.

2.6.11. IF-FISH

Hela cells were grown on coverslips, eventually incubated with 10 mM EdU in DMEM for 10 min at 37°C, washed with PBS, incubated for 7 min on ice with pre-extraction buffer (0.5% Triton-X-100, 20 mM HEPES/KOH pH 7.9, 50 mM NaCl, 3 mM $MgCl_2$, 300 mM sucrose) and fixed with 4% formaldehyde. Then cells were permeabilized for 5 min in 0.1% Triton-X-100/0.02 % SDS/ 1x PBS and pre-blocked with 2% BSA in PBS for 10 min before blocking with 10% goat-serum/ 2 % BSA /1x PBS for 45 min. For EdU-analysis, cells were labeled with a Click-it reaction (20 mM Copper sulfate, 100 mM sodium ascorbate, 2 mM Alexa 488-azide (Invitrogen), PBS 1x) for 30 min before blocking. Afterwards cells were incubated with

primary antibody in blocking solution for 90 min, washed 3x with 2% BSA/PBS and stained with secondary antibody in 2% BSA/PBS for 45 min. Further, cells were washed 3x times with PBS and fixed in 4% formaldehyde for 5 min. For telomeric FISH, coverslips were dehydrated in ethanol series, air dried and hybridized with a Cy3-OO-$(CCCTAA)_3$ PNA probe as described (Majerska et al., 2018). Images were taken with a Zeiss LSM 700 confocal microscope equipped with a 63x oil immersion objective.

2.6.12. BioID

800 million HEK293T cells expressing BirA-TRF1/TRF2 or POT1 were grown in normal Dulbecco's modified Eeagle's medium supplemented with 10% fetal calf serum and 100 U/ml of penicillin/streptomycin. Biotin (Sigma) was added to a final concentration of 50 µM for 24 h. Cells were harvested with trypsin and washed with 1x PBS. Cells were resuspended in 40 mL buffer A (20 mM HEPES, pH 7.5, 10 mM KCl, 1.5 mM $MgCl_2$, 0.34 M sucrose, 10 % glycerol, 1 mM dithiothreitol, 0.2% Triton-X-100, and protease inhibitors (Roche)) and incubated on ice for 5 min. Nuclei were pelleted by centrifugation at 600 g for 5 minutes at 4°C. Then nuclei were washed three times with 200 mL buffer M (10 mM HEPES, pH 7.5, 60 mM KCl, 10 mM NaCl). Pellets were resuspended in 30 mL RIPA buffer (0.5% Na-deoxycholate, 0.1% SDS, 1% NP-40, 150 mM NaCl, 1 mM EDTA, 1mM EGTA, 50 mM Tris-HCl) supplemented with protease inhibitors (Roche) and 150 U/mL of benzonase (Sigma). Samples were incubated for 1 h at 4°C on a rotating wheel. The insoluble fraction was separated by centrifugation at 18,500 g for 15 min at 4°C. The protein concentration of the supernatant was determined using the Bradford assay (Bio-Rad). The amount of protein was adjusted between the different samples. 100 mg of protein and 660 µl of magnetic streptavidin beads (Dynabeads MyOne Streptavidin C1, Thermo Fischer Scientific) were used for the IP. Beads were washed three times with RIPA buffer before being added to the nuclear extracts. Samples were incubated on a wheel overnight at 4°C. Beads were washed for 5 minutes with wash 1 (2% SDS), wash 2 (0.1% Na-deoxycholate, 1% Triton, 1 mM EDTA, 500 mM NaCl, 50 mM HEPES), and twice with wash 3 (0.5 % Na-deoxycholate, 0.5% NP-40, 1 mM EDTA, 250 mM LiCl, 10 mM Tris-HCl pH 8.0). Beads were resuspended in 50 µL of 4x Laemmli buffer with 355 mM of β-mercaptoethanol and run on a 10% Mini Protean TGC (BioRAD) before processing for MS analysis.

2.6.13. MS analysis

In-gel digestion as well as LC-MS/MS analysis were performed by the proteomics core facility at EPFL as in the previously published protocol (Grolimund et al., 2013) with minor modifications. In brief each SDS-PAGE gel lane was entirely sliced. Samples were first washed twice for 20 min in 50% ethanol, 50 mM ammonium bicarbonate (AB, Sigma-Aldrich) and dried down by vacuum centrifugation. Sample reduction was then performed with 10 mM dithioerythritol (DTE, Merck-Millipore) at 56°C for one hour. A washing-drying step was performed as described above prior to samples alkylation with 55 mM Iodoacetamide (IAA, Sigma-Aldrich) for 45 min at 37°C light protected. Samples were then washed-dried and stored on ice. Digestion was performed overnight at 37°C using modified Mass Spectrometry grade trypsin (Trypsin Gold, Promega) at a concentration of 12.5 ng/µl in 50 mM AB and 10 mM CaCl2. Resulting peptides were extracted twice for 20 min in 70% ethanol, 5% formic acid (FA, Merck-Millipore) with permanent shaking. Finally, samples were dried down by vacuum centrifugation. Peptides were desalted on C18 StageTips (Rappsilber et al., 2007) and dried down by vacuum centrifugation again. Samples were resuspended in 2% acetonitrile (ACN, Biosolve), 0.1% FA for LC-MS/MS injections. Nano-flow separations were performed on a Dionex Ultimate 3000 RSLC nano UPLC system (Thermo Fischer Scientific) on-line connected with an Orbitrap Elite Mass-Spectrometer (Thermo Fischer Scientific). A home-made capillary pre-column (Magic AQ C18; 3 µm-200 Å; 2cm x 100 µm ID) was used for sample trapping and cleaning. Analytical separation was then performed using a C18 capillary column (Nikkyo Technos Co; Magic AQ C18; 3µm-100Å; 15cm x 75µm ID) at 250 nl/min. Database search was performed using Mascot (Matrix Science), MS Amanda (Dorfer et al., 2014) and SEQUEST in Proteome Discoverer v.1.4 against the Uniprot Human protein database. Strepativin and BirA sequences were manually added. Searches were performed with trypsin cleavage specificity, ion mass tolerance of 10 ppm for the precursor and 0.5 Da for the fragments. Carbamidomethylation was set as a fixed modification, whereas oxidation (M), acetylation (Protein N-term), phosphorylation (STY) were considered as variable modifications.

Raw MS data was analyzed using Scaffold for filtering and to create a non-redundant list of all replicates. Thresholds of 1% protein and peptide level false discovery rate (FDR) and at least two unique peptides per protein were set.

REAGENTS OR RESSOURCES	SOURCE	IDENTIFIER
Antibodies		
Anti-BirA	Abcam	Ab14002
Anti-Tubulin	Sigma	T9026
Anti-Actin	Santa Cruz	Sc1616
Anti-H3	Abcam	Ab1791
Anti-TRF2	Millipore	05-521
Anti-hnRNPA1	Santa Cruz	Sc32301
Streptavidin-HRP	Invitrogen	43-4323
Anti-RADX	Santa Cruz	sc514563
Anti-POT1	Abcam	Ab124784
Anti-TRF1	Santa Cruz	Sc6165R
Anti-RAD51 Western Blot	Santa Cruz	ScH29
Anti-RAD1 IF-FISH	Abcam	Ab133534
Anti-Vinculin	Abcam	Ab129602
Anti-BRCA2	Millipore	OP95
Anti-γH2AX	Millipore	JBW301
Anti-Flag IF	Sigma	F1804
Anti-Flag-HRP	Sigma	8592
Anti-mouse Alexa 488	Thermo Fisher	A11001
Anti-rabbit Alexa 488	Thermo Fisher	A11034
Chemicals		
Biotin	Sigma	B4501-1G
Hyroxyurea	Fluka Chemica	55291
Zeocin	Life Technologies	R-25001
Dynabeads MyOne C1 Streptavidin beads	Thermo Fisher	65002
Lipofectamine	Thermo Fisher	11668500
Puromycin	Invivo Gen	ant-pr-1
Blastididin	Invivo Gen	ant-bl-1
4-Hydroxytamoxifen	Simga	H2904-5MG
Laemmli buffer	BioRAD	1610747
DTT Biochemica	Applichem	A1101,0005
BSA	Sigma	A9418-100G
ECL Spray	Advansta	K-12049-D50

RsaI	New England Biolabs	R0167S
HinfI	New England Biolabs	R0155L
Sepharose Protein G beads	GE Healthcare	17-0618-02
EdU	Sigma	900584-50MG
Alexa 488 Azide	Thermofisher	A10266
Cy3-OO-(CCCTAA)3-Probe	Pnabio	F1002
Protease Inhibitor Cocktail, EDTA-free	Simge	11873580001
Benzonase	Sigma	E1014-5KU
DAPI	Biochemica	A1001.0025

Recombinant DNA

pcDNA6 3xFlag	(Porro et al., 2014b)	N/A
pSuper-Blast	Oligoengine	VEC-pBS-0008
pSuper-Puro	Oligonengine	VEC-pBS-0008
pSpCas9(BB)-2A-Puro	Addgene	PX459
pSpCas9(BB)-2A-GFP	Addgene	PX458
pcDNA3.1-myc-BioID	Addgene	35700

Commercial Kits

Wizard Genomic DNA Isolation Kit	Promega	A1120
Wizard Genomic DNA Purification system	Promega	A2360
TOPO Zero Blunt for Sequencing Kit	Thermo Fisher	K287520
QuickChange II Site-directed mutagenesis Kit	Agilent	200523
NucleoSpin Gel and PCR Clean-UP	Macherey Nagel	740609.1
NucleoSpin Gel and PCR Clean-UP Buffer NTB	Macherey Nagel	740595.15
Bradford reagent	BioRAD	5000006
Nitrocellulose membrane	Amersham Protran, Sigma	GE10600002
Mini Protean TGC	BioRAD	4561086
N+ nylon membrane	GE Healthcare	RPN1210B

Oligonucleotides

1.Frag for TRF1 Repair template CCCATTTAGAATTTCTTTTTGTGCT	This study	N/A
1.Frag rev TRF1 Repair template gagtttttgttccatGTTAAATGGCTCGCTTGG	This study	N/A

2.Frag for TRF1 Repair template GCGAGCCATTTAACatggaacaaaaactcatctcagaagaggatctcgac	This study	N/A
2.Frag rev TRF1 Repair template CATCTTCCGCcttctctgcgcttctcaggg	This study	N/A
3.Frag for TRF1 Repair template cgcagagaagGCGGAAGATGTTTCCTCAGC	This study	N/A
3.Frag rev TRF1 Repair template TGTAGAGCCAGCAGGCCAAAT	This study	N/A
gRNA N-TRF1 for cacc G CGAGCCATTTAACATGGCGG	This study	N/A
gRNA N-TRF1 rev aaac CCGCCATGTTAAATGGCTCG C	This study	N/A
CRISPR Val TRF1 for AAAAGTGCATAAACGATGTTCAGT	This study	N/A
CRISPR Val TRF1 rev CATCCCTACCATCCGCACAG	This study	N/A
1.Frag for TRF2 Repair template GGTATCACACTGGTCTTTGCTTTATAATTACAGTATTT	This study	N/A
1.Frag frev TRF2 Repair templateAGTCGCTAGCCATGGTTGATAGAAACAGCGTTCCGA GCCG	This study	N/A
2.Frag for TRF2 Repair template ACGCTGTTTCTATCAACCATGGCTAGCGACTACAAAG	This study	N/A
2.Frag rev TRF2 Repair template CCCGCGGCCATcttctctgcgcttctcagggag	This study	N/A
3.Frag for TRF2 Repair template cgcagagaagATGGCCGCGGGAGC	This study	N/A
3.Frag rev TRF2 Repair template CTATCGCACTTTAACCTGGAATCCTTCAG	This study	N/A
gRNA N-TRF2 for caccgTCGGAACGCTGTTTCTATCA	This study	N/A
gRNA N-TRF2 rev aaactgatagaaacagcgttccgac	This study	N/A
CRISPR Val 5' for TRF2 GTGGGGCTGGTAGGACAATC	This study	N/A
CRISPR Val 5'rev TRF2 TGGGTCACGCACGACG	This study	N/A
gRNA NPOT1 for caccgTTCTACAGAATCAATGTCTT	This study	N/A
gRNA NPOT1 rev aaacAAGACATTGATTCTGTAGAAc	This study	N/A
1. Frag POT1 for Repair template AATGAAACTTACAAAACCGCACA	This study	N/A
1. Frag POT1 rev Repair template TCGCTAGCCATTGATTCTGTAGAAAAATCTCTTAAAG	This study	N/A

2. Frag POT1 for Repair template CTACAGAATCAATGGCTAGCGACTACAAAGAC	This study	N/A
2.Frag POT1 rev Repair template ACCAAAGACATcttctctgcgcttctcagg	This study	N/A
3. Frag POT1 for Repair template cgcagagaagATGTCTTTGGTAAGATGATATTCAGT	This study	N/A
3. Frag POT1 rev Repair template AGTAACTGTGTCCTACAGTCATTG	This study	N/A
CRISPR Val 5'rev POT1 CACATGTATCTATGTGTGTGGCAT	This study	N/A
CRISPR Val 5' for POT1 TGAGCTAAAGTGATGGGATTGAAA	This study	N/A
XhoI-CXorf57 for ACTACTCGAGATGTCTGGTGAGTCAGGACAG	This study	N/A
XbaI-CXorf57 rev ACTATCTAGATTAAGAAGTATTCTCTGGACTATAAATCTTG	This study	N/A
CXorf57 gRNA3 f caccGAAATCAAAACTGCGATACTA	This study	N/A
CXorf57 gRNA3 r aaacTAGTATCGCAGTTTTGATTTC	This study	N/A
CXorf57 gRNA4 f caccGTGGTATAAAAGTTTGCGGGT	This study	N/A
CXorf57 gRNA4 raaacACCCGCAAACTTTTATACCAC	This study	N/A
RAD51 shRNA1 for GATCCCCaagggaattagtgaagccaaaTTCAAGAGAtttggcttcactaattcccttTTTTTGGAAA	This study	N/A
RAD51 shRNA1 rev AGCTTTTCCAAAAAaagggaattagtgaagccaaaTCTCTTGAAtttggcttcactaattcccttGGG	This study	N/A
Muta K304A for CTGCTTCAAGACTATTCTGTTGCAAAGAGTTATCCATTCAGAATACAG	This study	N/A
Muta K304A rev CTGTATTCTGAATGGATAACTCTTTGCAACAGAATAGTCTTGAAGCAG	This study	N/A
Mut E327A for CAAACTAATTTCTACAATGGCAATCTGCCTGAATCTTCGAG	This study	N/A
Mut E327A rev CTCGAAGATTCAGGCAGATTGCCATTGTAGAAATTAGTTTG	This study	N/A
siGENOME Human NT UAGCGACUAAACACAUCAA UAAGGCUAUGAAGAGAUAC AUGUAUUGGCCUGUAUUAG AUGAACGUGAAUUGCUCAA	Dharmacon	D-001206-13-20

siGENOME Human RAD51 SMART pool GAAGCUAUGUUCGCCAUUA GCAGUGAUGUCCUGGAUAA CCAACGAUGUGAAGAAAUU AAGCUAUGUUCGCCAUUAA	Dharmacon	5888
siGENOME Human BRCA2 SMART pool GAACGGACUUGCUAUUUA GUAAAGAAAUGCAGAAUUC GGUAUCAGAUGCUUCAUUA GAAGAAUGCAGGUUUAAUA	Dharmacon	675
shPOT1 Target sequence: GATATTGTTCGCTTTCACA	(Hockemeyer et al., 2005)	N/A
shTRF1 Target sequence: GAATATTTGGTGATCCAAA	(McKerlie and Zhu, 2011)	N/A
shTRF2 Target sequence: gcgcatgacaataagcaga	(Porro et al., 2014b)	N/A
Software		
GraphPad Prism 7.0	GraphPad software	https://www.graphpad.com/
Fiji 1.0	Schindelin et al., 2012	https://fiji.sc/
Scaffold	Scaffold proteome software	http://www.proteomesoftware.com/products/scaffold/

2.7. Acknowledgements

We thank Timothy Murray for collecting samples and performing the TRF analysis in Figure S6, as well as Chih-Yi Lin for help with proteomic comparison analysis in Figure S3B. We further thank Romain Hamelin and the proteomics core facility at EPFL for mass spectrometry analysis. We are grateful to Thomas Lunardi for technical help. Current and former members of the Lingner lab are thanked for discussions, technical advice and sharing reagents. Research in J.L.'s laboratory was supported by the Swiss National Science Foundation (SNSF), the SNSF funded NCCR RNA and disease network, an Initial Training Network (ITN) grant (aDDRess) from the European Commission's Seventh Framework Programme, the Swiss Cancer League and EPFL.

2.8. Section References

Abreu, E., Aritonovska, E., Reichenbach, P., Cristofari, G., Culp, B., Terns, R.M., Lingner, J., and Terns, M.P. (2010). TIN2-tethered TPP1 recruits human telomerase to telomeres in vivo. Mol. Cell. Biol. 30, 2971–2982.

Arora, R., Lee, Y., Wischnewski, H., Brun, C.M., Schwarz, T., and Azzalin, C.M. (2014). RNaseH1 regulates TERRA-telomeric DNA hybrids and telomere maintenance in ALT tumour cells. Nat Commun 5, 5220.

Azzalin, C.M., Reichenbach, P., Khoriauli, L., Giulotto, E., and Lingner, J. (2007). Telomeric repeat containing RNA and RNA surveillance factors at mammalian chromosome ends. Science 318, 798–801.

Badie, S., Escandell, J.M., Bouwman, P., Carlos, A.R., Thanasoula, M., Gallardo, M.M., Suram, A., Jaco, I., Benitez, J., Herbig, U., et al. (2010). BRCA2 acts as a RAD51 loader to facilitate telomere replication and capping. Nat. Struct. Mol. Biol. 17, 1461–1469.

Bartocci, C., Diedrich, J.K., Ouzounov, I., Li, J., Piunti, A., Pasini, D., Yates, J.R., and Lazzerini Denchi, E. (2014). Isolation of chromatin from dysfunctional telomeres reveals an important role for Ring1b in NHEJ-mediated chromosome fusions. Cell Rep 7, 1320–1332.

Baumann, P., and Cech, T.R. (2001). Pot1, the putative telomere end-binding protein in fission yeast and humans. Science 292, 1171–1175.

Bhat, K.P., Krishnamoorthy, A., Dungrawala, H., Garcin, E.B., Modesti, M., and Cortez, D. (2018). RADX Modulates RAD51 Activity to Control Replication Fork Protection. Cell Rep 24, 538–545.

Bryksin, A.V., and Matsumura, I. (2010). Overlap extension PCR cloning: a simple and reliable way to create recombinant plasmids. BioTechniques 48, 463–465.

Celli, G.B., Denchi, E.L., and de Lange, T. (2006). Ku70 stimulates fusion of dysfunctional telomeres yet protects chromosome ends from homologous recombination. Nat. Cell Biol. 8, 885–890.

Chawla, R., Redon, S., Raftopoulou, C., Wischnewski, H., Gagos, S., and Azzalin, C.M. (2011). Human UPF1 interacts with TPP1 and telomerase and sustains telomere leading-strand replication. EMBO J. 30, 4047–4058.

Chen, L.-Y., Redon, S., and Lingner, J. (2012). The human CST complex is a terminator of telomerase activity. Nature 488, 540–544.

Crabbe, L., Verdun, R.E., Haggblom, C.I., and Karlseder, J. (2004). Defective telomere lagging strand synthesis in cells lacking WRN helicase activity. Science 306, 1951–1953.

Déjardin, J., and Kingston, R.E. (2009). Purification of proteins associated with specific genomic Loci. Cell 136, 175–186.

Denchi, E.L., and de Lange, T. (2007). Protection of telomeres through independent control of ATM and ATR by TRF2 and POT1. Nature 448, 1068–1071.

Dungrawala, H., Bhat, K.P., Le Meur, R., Chazin, W.J., Ding, X., Sharan, S.K., Wessel, S.R., Sathe, A.A., Zhao, R., and Cortez, D. (2017). RADX Promotes Genome Stability and Modulates Chemosensitivity by Regulating RAD51 at Replication Forks. Mol. Cell 67, 374-386.e5.

d'Adda di Fagagna, F., Reaper, P.M., Clay-Farrace, L., Fiegler, H., Carr, P., Von Zglinicki, T., Saretzki, G., Carter, N.P., and Jackson, S.P. (2003). A DNA damage checkpoint response in telomere-initiated senescence. Nature 426, 194–198.

Flynn, R.L., Centore, R.C., O'Sullivan, R.J., Rai, R., Tse, A., Songyang, Z., Chang, S., Karlseder, J., and Zou, L. (2011). TERRA and hnRNPA1 orchestrate an RPA-to-POT1 switch on telomeric single-stranded DNA. Nature 471, 532–536.

Garcia-Exposito, L., Bournique, E., Bergoglio, V., Bose, A., Barroso-Gonzalez, J., Zhang, S., Roncaioli, J.L., Lee, M., Wallace, C.T., Watkins, S.C., et al. (2016). Proteomic Profiling Reveals a Specific Role for Translesion DNA Polymerase η in the Alternative Lengthening of Telomeres. Cell Rep 17, 1858–1871.

Graf, M., Bonetti, D., Lockhart, A., Serhal, K., Kellner, V., Maicher, A., Jolivet, P., Teixeira, M.T., and Luke, B. (2017). Telomere Length Determines TERRA and R-Loop Regulation through the Cell Cycle. Cell 170, 72-85.e14.

Grolimund, L., Aeby, E., Hamelin, R., Armand, F., Chiappe, D., Moniatte, M., and Lingner, J. (2013). A quantitative telomeric chromatin isolation protocol identifies different telomeric states. Nat Commun 4, 2848.

Houghtaling, B.R., Cuttonaro, L., Chang, W., and Smith, S. (2004). A dynamic molecular link between the telomere length regulator TRF1 and the chromosome end protector TRF2. Curr. Biol. 14, 1621–1631.

Karlseder, J., Broccoli, D., Dai, Y., Hardy, S., and de Lange, T. (1999). p53- and ATM-dependent apoptosis induced by telomeres lacking TRF2. Science 283, 1321–1325.

Karlseder, J., Smogorzewska, A., and de Lange, T. (2002). Senescence induced by altered telomere state, not telomere loss. Science 295, 2446–2449.

de Lange, T. (2018). Shelterin-Mediated Telomere Protection. Annu. Rev. Genet. 52, 223–247.

Lazzerini-Denchi, E., and Sfeir, A. (2016). Stop pulling my strings - what telomeres taught us about the DNA damage response. Nat. Rev. Mol. Cell Biol. 17, 364–378.

Lee, S.S., Bohrson, C., Pike, A.M., Wheelan, S.J., and Greider, C.W. (2015). ATM Kinase Is Required for Telomere Elongation in Mouse and Human Cells. Cell Rep 13, 1623–1632.

Liu, D., O'Connor, M.S., Qin, J., and Songyang, Z. (2004). Telosome, a mammalian telomere-associated complex formed by multiple telomeric proteins. J. Biol. Chem. 279, 51338–51342.

Majerska, J., Feretzaki, M., Glousker, G., and Lingner, J. (2018). Transformation-induced stress at telomeres is counteracted through changes in the telomeric proteome including SAMHD1. Life Sci Alliance 1, e201800121.

Mijic, S., Zellweger, R., Chappidi, N., Berti, M., Jacobs, K., Mutreja, K., Ursich, S., Ray Chaudhuri, A., Nussenzweig, A., Janscak, P., et al. (2017). Replication fork reversal triggers fork degradation in BRCA2-defective cells. Nat Commun 8, 859.

Palm, W., Hockemeyer, D., Kibe, T., and de Lange, T. (2009). Functional dissection of human and mouse POT1 proteins. Mol. Cell. Biol. 29, 471–482.

Pfeiffer, V., Crittin, J., Grolimund, L., and Lingner, J. (2013). The THO complex component Thp2 counteracts telomeric R-loops and telomere shortening. EMBO J. 32, 2861–2871.

Pickett, H.A., and Reddel, R.R. (2015). Molecular mechanisms of activity and derepression of alternative lengthening of telomeres. Nat. Struct. Mol. Biol. 22, 875–880.

Pinzaru, A.M., Hom, R.A., Beal, A., Phillips, A.F., Ni, E., Cardozo, T., Nair, N., Choi, J., Wuttke, D.S., Sfeir, A., et al. (2016). Telomere Replication Stress Induced by POT1 Inactivation Accelerates Tumorigenesis. Cell Rep 15, 2170–2184.

Ran, F.A., Hsu, P.D., Wright, J., Agarwala, V., Scott, D.A., and Zhang, F. (2013). Genome engineering using the CRISPR-Cas9 system. Nat Protoc 8, 2281–2308.

Roux, K.J., Kim, D.I., Raida, M., and Burke, B. (2012). A promiscuous biotin ligase fusion protein identifies proximal and interacting proteins in mammalian cells. J. Cell Biol. 196, 801–810.

Sarek, G., Vannier, J.-B., Panier, S., Petrini, J.H.J., and Boulton, S.J. (2016). TRF2 Recruits RTEL1 to Telomeres in S Phase to Promote T-Loop Unwinding. Mol. Cell 61, 788–789.

Schmidt, J.C., and Cech, T.R. (2015). Human telomerase: biogenesis, trafficking, recruitment, and activation. Genes Dev. 29, 1095–1105.

Schubert, L., Ho, T., Hoffmann, S., Haahr, P., Guérillon, C., and Mailand, N. (2017). RADX interacts with single-stranded DNA to promote replication fork stability. EMBO Rep. 18, 1991–2003.

Sfeir, A., Kosiyatrakul, S.T., Hockemeyer, D., MacRae, S.L., Karlseder, J., Schildkraut, C.L., and de Lange, T. (2009). Mammalian telomeres resemble fragile sites and require TRF1 for efficient replication. Cell 138, 90–103.

Sfeir, A., Kabir, S., van Overbeek, M., Celli, G.B., and de Lange, T. (2010). Loss of Rap1 induces telomere recombination in the absence of NHEJ or a DNA damage signal. Science 327, 1657–1661.

Shalem, O., Sanjana, N.E., Hartenian, E., Shi, X., Scott, D.A., Mikkelson, T., Heckl, D., Ebert, B.L., Root, D.E., Doench, J.G., et al. (2014). Genome-scale CRISPR-Cas9 knockout screening in human cells. Science 343, 84–87.

Silva, B., Pentz, R., Figueira, A.M., Arora, R., Lee, Y.W., Hodson, C., Wischnewski, H., Deans, A.J., and Azzalin, C.M. (2019). FANCM limits ALT activity by restricting telomeric replication stress induced by deregulated BLM and R-loops. Nat Commun 10, 2253.

Tong, A.S., Stern, J.L., Sfeir, A., Kartawinata, M., de Lange, T., Zhu, X.-D., and Bryan, T.M. (2015). ATM and ATR Signaling Regulate the Recruitment of Human Telomerase to Telomeres. Cell Rep 13, 1633–1646.

Vannier, J.-B., Pavicic-Kaltenbrunner, V., Petalcorin, M.I.R., Ding, H., and Boulton, S.J. (2012). RTEL1 dismantles T loops and counteracts telomeric G4-DNA to maintain telomere integrity. Cell 149, 795–806.

Verdun, R.E., and Karlseder, J. (2006). The DNA damage machinery and homologous recombination pathway act consecutively to protect human telomeres. Cell 127, 709–720.

Wu, L., Multani, A.S., He, H., Cosme-Blanco, W., Deng, Y., Deng, J.M., Bachilo, O., Pathak, S., Tahara, H., Bailey, S.M., et al. (2006). Pot1 deficiency initiates DNA damage checkpoint activation and aberrant homologous recombination at telomeres. Cell 126, 49–62.

Ye, J.Z.-S., Donigian, J.R., van Overbeek, M., Loayza, D., Luo, Y., Krutchinsky, A.N., Chait, B.T., and de Lange, T. (2004). TIN2 binds TRF1 and TRF2 simultaneously and stabilizes the TRF2 complex on telomeres. J. Biol. Chem. 279, 47264–47271.

Zimmermann, M., Kibe, T., Kabir, S., and de Lange, T. (2014). TRF1 negotiates TTAGGG repeat-associated replication problems by recruiting the BLM helicase and the TPP1/POT1 repressor of ATR signaling. Genes Dev. 28, 2477–2491.

Zou, L., and Elledge, S.J. (2003). Sensing DNA damage through ATRIP recognition of RPA-ssDNA complexes. Science 300, 1542–1548.

2.9. Section Appendix

As previously shown RADX and POT1 cooperate to suppress RAD51 loading onto telomeres, which leads to telomere fragility and sister-telomere associations. Moreover, telomeres elongate and accumulate complex telomeric secondary structures upon POT1 deletion, a phenotype that was further aggravated upon RADX co-depletion. Since accumulation of fragility and sister-chromatid associations could be reversed by RAD51 and BRCA2 depletion, we sought to test if the same was true for telomere elongation. Indeed, telomere elongation was abolished upon RAD51 and BRCA2 depletions and the smearing up of the telomeric signal to the well caused by complex telomeric structures was greatly diminished (Figure 10).

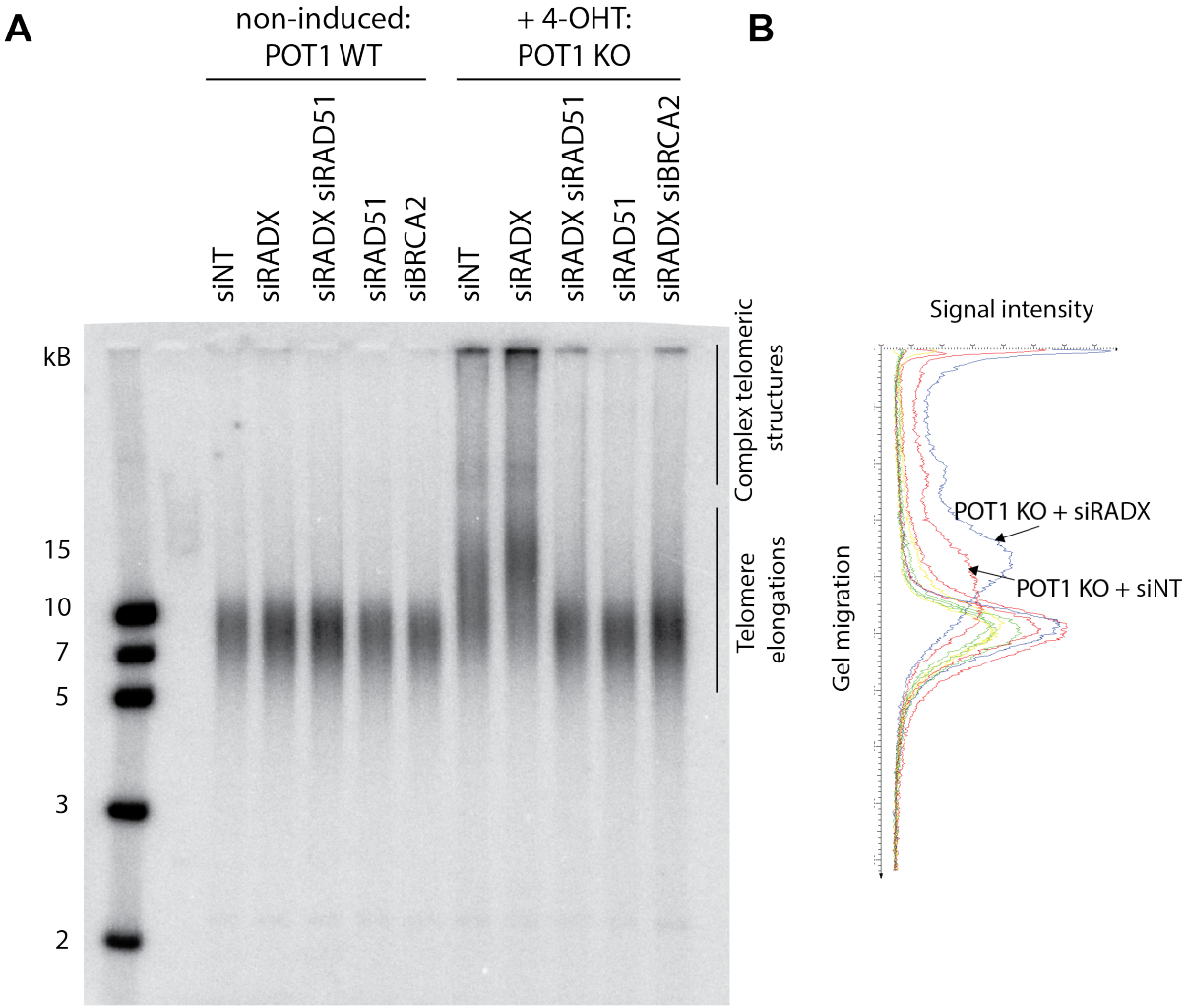

Figure 10. Telomere elongation upon POT1-/RADX-depletion is dependent on homologous recombination.

(A) Telomere restriction fragment analysis of POT1 WT and POT1 KO cells transfected with the indicated siRNA. POT1 KO was induced on day 0, siRNAs were transfected on day 3 and cells were harvested on day 7.

(B) Signal intensity curves from the TRF gel in (A)

Since RADX suppressed RAD51-binding to telomeres upon POT1 loss we became interested in what would happen to RPA binding and ATR-checkpoint-signaling upon RADX/POT1-codepletion. Therefore, we investigated p-CHK1 levels in POT1 WT or POT1 KO and RADX, RAD51 and BRCA2 depletions. As previously described (Denchi and de Lange, 2007) we observed increases levels of p-CHK1 upon POT1 deletion, which were lowered if RADX was co-depleted. Only concomitant depletion of RAD51 and BRCA2 allowed accumulation of p-CHK1 (Figure 11). These results suggest compromised ATR-checkpoint-signaling if RADX is lost in addition to POT1, likely due to the BRCA2-mediated exchange of RPA against RAD51.

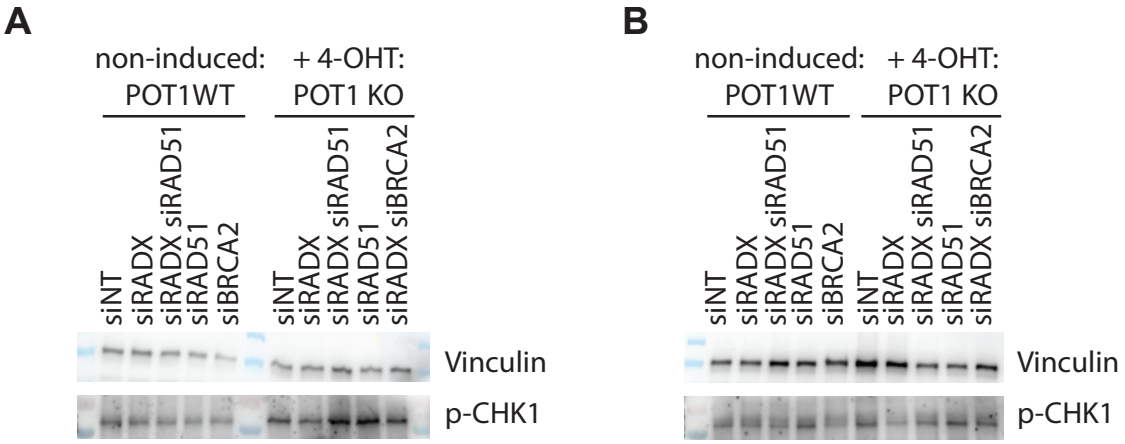

Figure 11. RADX is important to sustain ATR-dependent checkpoint signaling upon POT1 loss

(A) and (B) represent two replicates of western blot analysis of total p-CHK1 levels under the same conditions as in Figure 10. Vinculin serves as loading control.

3. Conclusions and perspectives

The shelterin complex consisting of TRF1, TRF2, POT1, TIN2, TPP1 and RAP1 covers large parts of telomeric DNA, but previous proteomic studies have identified more than 200 proteins to associate with telomeres. The telomeric proteome is present to protect the chromosome end from triggering a DNA damage response and inducing senescence, chromosome fusions leading to genome rearrangements and genome instability as well as nucleolytic processing promoting telomere shortening and telomere loss. Further, suppression of homologous recombination is important to prevent stochastic telomere elongation and shortening events. Certain proteins become particularly important during certain telomere stages, for example at very short or long telomeres, during replication and telomere elongation or help to position telomeres during mitosis and cell division.

The initial aim of this thesis was to identify novel telomeric proteins, which would help us to further characterize the important functions of telomeres.

3.1. Probing the telomere Environment with BioID

We successfully adapted the BioID protocol to work with low abundant, at endogenous level expressed proteins by isolating the nuclei to remove abundant biotinylated proteins in the cytoplasm and mitochondria. We further validated that addition of the BirA-tag by CRISPR/Cas9 genome editing of TRF1, TRF2 and POT1 did not disturb telomere integrity and telomere length maintenance in BirA-tagged clones.

In our BioID results, we discovered a large number of proteins previously described to associate with telomeres validating our approach. In addition, we identified new proteins, which had not been detected at telomeres so far. Most identified proteins were in the vicinity of TRF1, TRF2 and POT1. We could not identify proteins that were uniquely in proximity of POT1. We hypothesize that this approach might not be sensitive enough to detect low abundant proteins, which are only in the vicinity of POT1 and the single-stranded overhang. Indeed the CST complex, which was previously characterized to interact with human POT (Chen et al., 2012) and is recruited to telomeres in MEFs via POT1b (Wu et al., 2012), was not identified.

Several proteins involved in transcription regulation and chromatin remodeling were only identified in the BioID with clone BirA-TRF2 88. This might be due to the overall shorter telomere length in this clone (Figure 1B), arguing for either a distinct proteomic environment at short telomeres or due to a distinct proteomic environment for TRF2 specifically. Additional analysis of more TRF2-tagged clones would be necessary to fully answer this question.

Importantly, our BioID experiments led to the discovery of RADX at telomeres, which was found in the vicinity of TRF1, TRF2 and POT1.

3.2. **RADX-telomere association**

RADX contains three OB-folds resembling the three OB-folds of RPA70 in sequence and structure. It was further shown that the ssDNA-binding of RADX motif is within OB2 and a mutant defective in single-stranded binding was characterized (Dungrawala et al., 2017; Schubert et al., 2017). We could show that RADX WT but not the single-stranded binding defective mutant associates with telomeres and does so throughout the cell cycle in IF-FISH experiments. Therefore, we conclude that RADX binds the single-stranded telomeric overhang or the displaced G-rich strand in the t-loop. This interaction was unaltered when analyzed by chromatin-immunoprecipitation with RADX antibodies upon TRF1, TRF2 or POT1 depletion despite previous studies showing changes in the overhang structure for POT1 KO and TRF2 KO in MEFs. Upon POT1 loss in MEFs the overhang length is thought to increase due to extensive resection via the exonuclease Apollo (Wu et al., 2012) and upon TRF2 loss the overhang is processed to blunt-ends and non-homologous end-joining mediated telomere fusions are observed (Celli and de Lange, 2005). To obtain these changes in telomere overhang structure, protein depletions must be very efficient over a certain period of time. A significant increase in telomere fusions and decrease of the overhang signal intensity are observed only 8 days after continuous inducible shTRF2 expression in human cells (Vančevska et al., 2019). Increase in overhang signal upon POT1 mediated depletion is observed only 9 days after viral infections with POT1 shRNA (Glousker et al, unpublished). TRF2 and POT1 depletions in our experimental set-up persisted only for 6 days and were most likely not long enough to change the overhang structure. Therefore, these ChIP experiments suggest that RADX recruitment to telomeres occurs independently of shelterin proteins. However, the depletion studies cannot distinguish whether RADX binds at telomeres to the 3'overhang or the displaced srtand in the t-loop configuration.

Moreover, RADX associations increased significantly only at telomeres but not at Alu-repeat-containing DNA upon introduction of replication stress with hydroxyurea treatment. We hypothesize that the exposed single-stranded telomeric DNA upon replication fork stalling might be an ideal substrate for RADX and promoting its preferential binding. It would be interesting to test if RADX's single-stranded DNA binding is sequence specific and if it has higher affinity for telomeric DNA.

3.3. **RADX and POT1's combined effort to suppress RAD51 binding**

RADX deletion *per se* did not induce telomere fragility or telomere elongation but we observed increased fragility and sister-chromatid-associations upon POT1- and POT1/RADX depletions. The increased fragility appears to be due to aberrant homologous recombination since it was abolished upon concomitant RAD51 and BRCA2 depletions. The increase of RAD51-telomere associations upon POT1 and POT1/RADX depletions does further strengthen this hypothesis. Finally, we showed that telomere elongation and the accumulation of aberrant telomeric structures in RADX/POT1 loss disappeared upon RAD51 and BRCA2 depletions. To summarize, our data indicates that RADX binds single-stranded G-rich telomeric DNA where it prevents RAD51 binding and homologous recombination in cooperation with POT1 (Figure 12).

HR-dependent telomere elongation upon POT1 loss was not observed previously. POT1 was typically implicated in regulating telomere length by limiting the access of telomerase to telomeres. Studies with the dominant negative ssDNA-binding defective mutant POT1$^{\Delta OB}$ show telomere elongation (Kendellen et al., 2009; Loayza and De Lange, 2003), dependent on telomerase (Zhong et al., 2012). These studies were done with the endogenous POT1 still present, which is most likely enough in cooperation with RADX to suppress homologous recombination, but allows for greater access of telomerase to elongate telomeres.

Some cancer-associated POT1 mutations in the OB-fold domain have also previously been shown to change POT1 affinity for single-stranded telomeric DNA and consequently induced telomere elongation (Gu et al., 2016; Pinzaru et al., 2016). The authors suggested this elongation is dependent on telomerase in a similar way to POT1$^{\Delta OB}$ but did not provide experimental evidence for this. They described OB-fold mutants which differed in their capacity to suppress telomerase activity in vitro (Gu et al., 2016), or binding efficiency of single-stranded telomeric DNA (Pinzaru et al., 2016), yet all these mutants showed similar increase in telomere length. Our work suggests it might important to revisit the issue and test if RADX status and homologous recombination-mediated telomere elongation may contribute to the cancer phenotype.

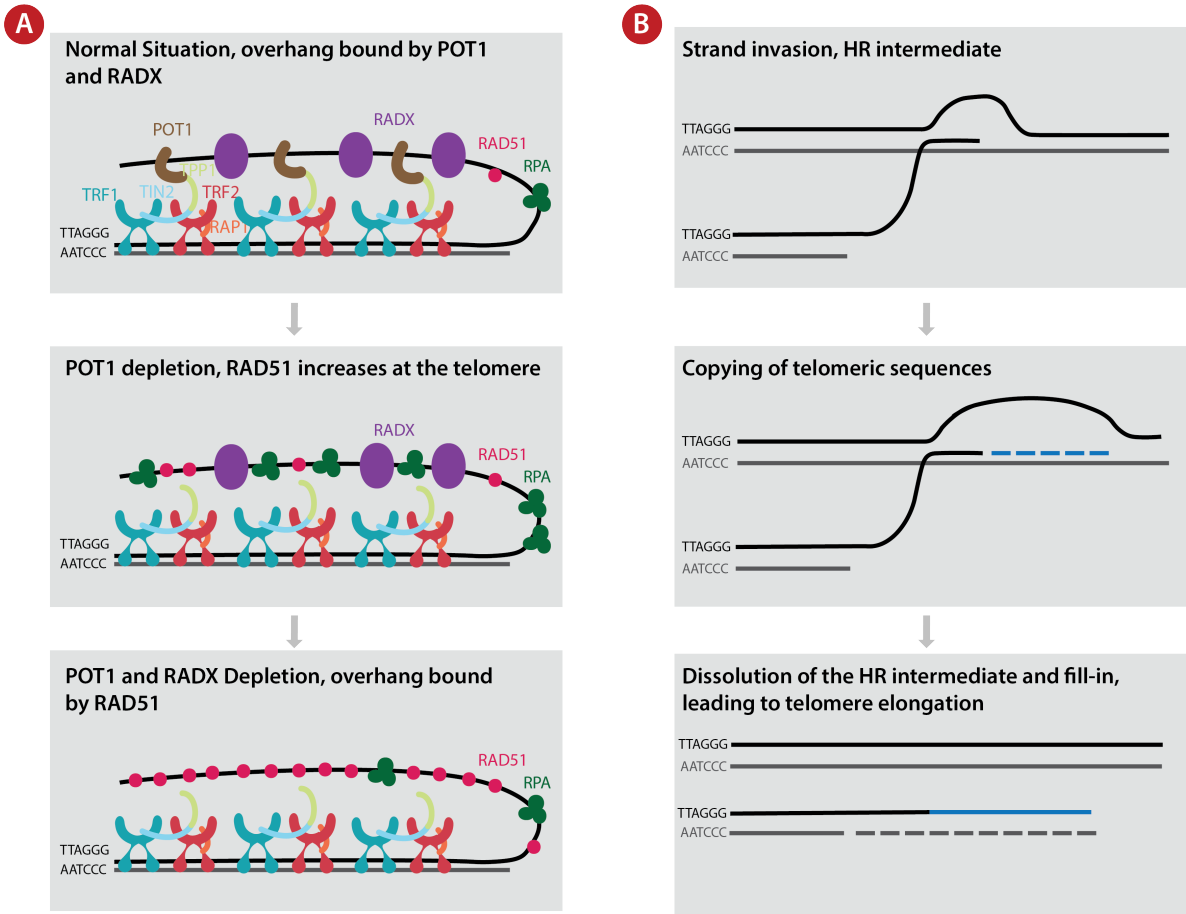

Figure 12. Model for homologous recombination dependent telomere elongation upon RADX and POT1 loss.

(A) In unchallenged situations, we expect the overhang, or the displaced ssDNA in the t-loop, to be bound by POT1 and RADX and small amounts of RAD51 and RPA. Upon POT1 loss, RAD51 and RPA binding increases whereas RADX binding remains unaltered. If RADX is further depleted even more RAD51 can replace RPA and mediate strand-invasion.

(B) The single-stranded overhang can invade double-stranded telomeric DNA and elongation could take place through template-directed synthesis by polymerase δ or ζ. The HR intermediate can be processed by dissolution and fill-in of the C-strand is possible. Proteins on the right side of this image are not displayed (adapted from (Pickett and Reddel, 2015).

3.4. **Homologous recombination in ALT-cell lines**

Homologous recombination is commonly observed in cells relying on ALT for telomere maintenance, which represent 10-15 % of human cancers (Bryan et al., 1997). Previous results have shown that RAD51 is present in ALT-associated PML-bodies (APBs) which are hotspots for telomere clustering and elongation (Yeager et al., 1999). Yet more recent data suggests that the large majority of telomere elongation in these APBs is RAD51-independent and RAD52-dependent. RAD52 is implicated in break-induced-telomere synthesis, which catalyzes long-range-de-novo telomere synthesis induced by DNA-double-strand-breaks and relies on RFC-PCNA-Pol δ replisome (Dilley et al., 2016), whereas RAD51 mediates rapid directional movements of individual telomeres to associate with other telomeres and initiates homologous recombination between them (Cho et al., 2014). Since RAD51 depletion has no effect on telomere synthesis in APBs (Zhang et al., 2019) the homologous recombination mediated telomere elongation in ALT cell lines seems to be different compared to the telomere elongation occurring upon POT1/RADX deletion. In our system excessive RAD51-mediated homologous recombination induces not only telomere elongation but also massive telomere fragility leading to cell death. ALT cell lines also show higher levels of replication stress and DNA damage signaling but this does not impair their viability (Cesare et al., 2009). Therefore, additional features of the ALT phenotype, like increased telomere-sister-chromatid exchanges, increased extra-chromosomal DNA, higher TERRA levels and the clustering of telomeres in APBs might not arise upon POT1/RADX loss. Thus, we plan to confirm this hypothesis and to check for the appearance of telomere-sister-chromatid exchange by Co-FISH and for extra-chromosomal DNA by C-circle assay upon POT1 and RADX loss.

3.5. The interplay between RPA, RAD51, POT1 and RADX

POT1 deletion leads to increased RPA-binding, CHK1 phosphorylation and increased ATR-dependent damage signaling at telomeres (Denchi and de Lange, 2007). In this study we also show that POT1 depletion leads to increased RAD51-loading, which is even more pronounced if RADX is co-depleted. The question arises what happens to RPA and consequent ATR signaling upon POT1 and RADX loss. As expected, we observed higher p-CHK1 levels upon POT1 deletion, but interestingly concomitant RADX depletion resulted in lower p-CHK1 levels suggesting the ATR-checkpoint-signaling is compromised due to replacement of RPA with RAD51. Consequently, only if RAD51 or BRCA2 was depleted together with RADX and POT1 high phosphorylation of CHK1 was detected. This further supports our model in which RADX is necessary to prevent the exchange of RPA with RAD51 at telomeres upon POT1 loss (Figure 12). For that reason, we plan to further investigate ATR-signaling upon POT1 and RADX loss and we will try to directly monitor telomeric RPA-binding by chromatin-immunoprecipitation.

These results further suggest that RADX might have an important role to sustain ATR-checkpoint signaling in senescent cells. So far POT1 levels in senescent cells are not well studied, but there is evidence of lower TRF2 levels in senescent cells (Herbig et al., 2004). Hence, we think the same might be true for POT1, since it is tethered to telomeres via TPP1-TIN2-TRF2. Therefore, it is tempting to speculate that decreasing POT1 levels in senescent cells are important to trigger RPA-ATRIP-ATR sustained checkpoint signaling and consequent cell cycle arrest. It is then, that RADX might become particularly important to inhibit the exchange of RPA against RAD51, which would counteract the checkpoint, lead to telomere elongation, telomere fragility and genome instability. Thus, we plan to test the effects of RADX loss on senescence in primary, telomerase-negative cells.

Along this line of thinking it was observed that POT1 is highly expressed in hematopoietic stem cells but its expression decreases with age (Hosokawa and Arai, 2018) and low POT1 levels are associated with aplastic anemia (Wang et al., 2014). Additionally POT1 single-stranded DNA binding motif is compromised in a number of human cancers (Gu et al., 2016; Pinzaru et al., 2016). Accordingly, RADX telomeric function might be particularly important in these cases of physiologically low POT1 levels and activity. Further studies in the mentioned disease model cell lines will be necessary to answer these questions.

3.6. **Final considerations**

In this thesis I successfully identified a large number of previously unknown proteins to associate with telomeres by an approach combining CRISPR-Cas9 genome editing and proximity dependent biotin labeling. We describe RADX, a novel OB-fold containing protein to bind to telomeric single-stranded DNA and shed light into the regulation of homologous recombination at telomeres. We show how RAD51 loading is suppressed at telomeres and the deleterious effects of increased RAD51 binding for telomere length and integrity. Therefore, this thesis broadens our understanding of how aberrant homologous recombination and associated genome instability are suppressed at telomeres. We also demonstrate that homologous recombination and its intermediates can impair telomere replication and present an explanation for fragility observed upon POT1 loss. Moreover, this thesis and the insights into RADX telomeric function might become particularly relevant to further characterize and understand cellular senescence induced by telomeric ATR-checkpoint signaling and certain cancer-associated POT1 mutations.

References

Abreu, E., Aritonovska, E., Reichenbach, P., Cristofari, G., Culp, B., Terns, R.M., Lingner, J., and Terns, M.P. (2010). TIN2-tethered TPP1 recruits human telomerase to telomeres in vivo. Mol Cell Biol *30*, 2971-2982.

Amiard, S., Doudeau, M., Pinte, S., Poulet, A., Lenain, C., Faivre-Moskalenko, C., Angelov, D., Hug, N., Vindigni, A., Bouvet, P.*, et al.* (2007). A topological mechanism for TRF2-enhanced strand invasion. Nature Structural &Amp; Molecular Biology *14*, 147.

Arnoult, N., and Karlseder, J. (2015). Complex interactions between the DNA-damage response and mammalian telomeres. Nature structural & molecular biology *22*, 859-866.

Arnoult, N., Van Beneden, A., and Decottignies, A. (2012). Telomere length regulates TERRA levels through increased trimethylation of telomeric H3K9 and HP1α. Nature Structural &Amp; Molecular Biology *19*, 948.

Arora, R., Lee, Y., Wischnewski, H., Brun, C.M., Schwarz, T., and Azzalin, C.M. (2014). RNaseH1 regulates TERRA-telomeric DNA hybrids and telomere maintenance in ALT tumour cells. Nat Commun *5*.

Azzalin, C.M., Reichenbach, P., Khoriauli, L., Giulotto, E., and Lingner, J. (2007). Telomeric Repeat–Containing RNA and RNA Surveillance Factors at Mammalian Chromosome Ends. Science *318*, 798-801.

Badie, S., Escandell, J.M., Bouwman, P., Carlos, A.R., Thanasoula, M., Gallardo, M.M., Suram, A., Jaco, I., Benitez, J., Herbig, U.*, et al.* (2010). BRCA2 acts as a RAD51 loader to facilitate telomere replication and capping. Nature structural & molecular biology *17*, 1461-1469.

Balk, B., Maicher, A., Dees, M., Klermund, J., Luke-Glaser, S., Bender, K., and Luke, B. (2013). Telomeric RNA-DNA hybrids affect telomere-length dynamics and senescence. Nature Structural &Amp; Molecular Biology *20*, 1199.

Benarroch-Popivker, D., Pisano, S., Mendez-Bermudez, A., Lototska, L., Kaur, P., Bauwens, S., Djerbi, N., Latrick, C.M., Fraisier, V., Pei, B.*, et al.* (2016). TRF2-Mediated Control of Telomere DNA Topology as a Mechanism for Chromosome-End Protection. Molecular cell *61*, 274-286.

Bhat, K.P., and Cortez, D. (2018). RPA and RAD51: fork reversal, fork protection, and genome stability. Nature structural & molecular biology *25*, 446-453.

Bhat, K.P., Krishnamoorthy, A., Dungrawala, H., Garcin, E.B., Modesti, M., and Cortez, D. (2018). RADX Modulates RAD51 Activity to Control Replication Fork Protection. Cell Reports *24*, 538-545.

Blackburn, E.H., and Gall, J.G. (1978). A tandemly repeated sequence at the termini of the extrachromosomal ribosomal RNA genes in Tetrahymena. Journal of Molecular Biology *120*, 33-53.

Broccoli, D., Smogorzewska, A., Chong, L., and de Lange, T. (1997). Human telomeres contain two distinct Myb-related proteins, TRF1 and TRF2. Nat Genet *17*, 231-235.

Bryan, T.M., Englezou, A., Dalla-Pozza, L., Dunham, M.A., and Reddel, R.R. (1997). Evidence for an alternative mechanism for maintaining telomere length in human tumors and tumor-derived cell lines. Nature Medicine *3*, 1271-1274.

Celli, G.B., Denchi, E.L., and de Lange, T. (2006). Ku70 stimulates fusion of dysfunctional telomeres yet protects chromosome ends from homologous recombination. Nature Cell Biology *8*, 885-890.

Cesare, A.J., Kaul, Z., Cohen, S.B., Napier, C.E., Pickett, H.A., Neumann, A.A., and Reddel, R.R. (2009). Spontaneous occurrence of telomeric DNA damage response in the absence of chromosome fusions. Nature structural & molecular biology *16*, 1244-1251.

Chen, L.-Y., Majerska, J., and Lingner, J. (2013). Molecular basis of telomere syndrome caused by CTC1 mutations. Genes & Development *27*, 2099-2108.

Chen, L.-Y., Redon, S., and Lingner, J. (2012). The human CST complex is a terminator of telomerase activity. Nature *488*, 540-+.

Cho, Nam W., Dilley, Robert L., Lampson, Michael A., and Greenberg, Roger A. (2014). Interchromosomal Homology Searches Drive Directional ALT Telomere Movement and Synapsis. Cell *159*, 108-121.

Colgin, L.M., Baran, K., Baumann, P., Cech, T.R., and Reddel, R.R. (2003). Human POT1 facilitates telomere elongation by telomerase. Current biology : CB *13*, 942-946.

Compton, S.A., Choi, J.-H., Cesare, A.J., Özgür, S., and Griffith, J.D. (2007). Xrcc3 and Nbs1 Are Required for the Production of Extrachromosomal Telomeric Circles in Human Alternative Lengthening of Telomere Cells. Cancer Research *67*, 1513-1519.

Conomos, D., Reddel, R.R., and Pickett, H.A. (2014). NuRD–ZNF827 recruitment to telomeres creates a molecular scaffold for homologous recombination. Nature structural & molecular biology *21*, 760-770.

Crabbe, L., Cesare, Anthony J., Kasuboski, James M., Fitzpatrick, James A.J., and Karlseder, J. (2012). Human Telomeres Are Tethered to the Nuclear Envelope during Postmitotic Nuclear Assembly. Cell Reports *2*, 1521-1529.

Crabbe, L., Verdun, R.E., Haggblom, C.I., and Karlseder, J. (2004). Defective telomere lagging strand synthesis in cells lacking WRN helicase activity. Science *306*, 1951-1953.

de Lange, T. (2005). Shelterin: the protein complex that shapes and safeguards human telomeres. Genes & Development *19*, 2100-2110.

de Lange, T. (2010). How shelterin solves the telomere end-protection problem. Cold Spring Harbor symposia on quantitative biology *75*, 167-177.

de Lange, T. (2018). Shelterin-Mediated Telomere Protection. Annual review of genetics *52*, 223-247.

Déjardin, J., and Kingston, R.E. (2009). Purification of Proteins Associated with Specific Genomic Loci. Cell *136*, 175-186.

Denchi, E.L., and de Lange, T. (2007). Protection of telomeres through independent control of ATM and ATR by TRF2 and POT1. Nature *448*, 1068-1071.

Deng, Z., Norseen, J., Wiedmer, A., Riethman, H., and Lieberman, P.M. (2009). TERRA RNA binding to TRF2 facilitates heterochromatin formation and ORC recruitment at telomeres. Molecular cell *35*, 403-413.

Dilley, R.L., Verma, P., Cho, N.W., Winters, H.D., Wondisford, A.R., and Greenberg, R.A. (2016). Break-induced telomere synthesis underlies alternative telomere maintenance. Nature *advance online publication*.

Doksani, Y., and de Lange, T. (2016). Telomere-Internal Double-Strand Breaks Are Repaired by Homologous Recombination and PARP1/Lig3-Dependent End-Joining. Cell Rep *17*, 1646-1656.

Doksani, Y., Wu, J.Y., de Lange, T., and Zhuang, X. (2013). Super-resolution fluorescence imaging of telomeres reveals TRF2-dependent T-loop formation. Cell *155*, 345-356.

Dorfer, V., Pichler, P., Stranzl, T., Stadlmann, J., Taus, T., Winkler, S., and Mechtler, K. (2014). MS Amanda, a universal identification algorithm optimized for high accuracy tandem mass spectra. Journal of proteome research *13*, 3679-3684.

Dungrawala, H., Bhat, K.P., Le Meur, R., Chazin, W.J., Ding, X., Sharan, S.K., Wessel, S.R., Sathe, A.A., Zhao, R., and Cortez, D. (2017). RADX Promotes Genome Stability and Modulates Chemosensitivity by Regulating RAD51 at Replication Forks. Molecular cell *67*, 374-386 e375.

Fagagna, F.d.A.d., Reaper, P.M., Clay-Farrace, L., Fiegler, H., Carr, P., von Zglinicki, T., Saretzki, G., Carter, N.P., and Jackson, S.P. (2003). A DNA damage checkpoint response in telomere-initiated senescence. Nature *426*, 194-198.

Fairall, L., Chapman, L., Moss, H., de Lange, T., and Rhodes, D. (2001). Structure of the TRFH dimerization domain of the human telomeric proteins TRF1 and TRF2. Molecular cell *8*, 351-361.

Flynn, R.L., Centore, R.C., O'Sullivan, R.J., Rai, R., Tse, A., Songyang, Z., Chang, S., Karlseder, J., and Zou, L. (2011). TERRA and hnRNPA1 orchestrate an RPA-to-POT1 switch on telomeric single-stranded DNA. Nature *471*, 532.

Frank, A.K., Tran, D.C., Qu, R.W., Stohr, B.A., Segal, D.J., and Xu, L. (2015). The Shelterin TIN2 Subunit Mediates Recruitment of Telomerase to Telomeres. PLoS Genet *11*, e1005410.

Gan, W., Guan, Z., Liu, J., Gui, T., Shen, K., Manley, J.L., and Li, X. (2011). R-loop-mediated genomic instability is caused by impairment of replication fork progression. Genes & Development *25*, 2041-2056.

Garcia-Exposito, L., Bournique, E., Bergoglio, V., Bose, A., Barroso-Gonzalez, J., Zhang, S., Roncaioli, Justin L., Lee, M., Wallace, Callen T., Watkins, Simon C.*, et al.* (2016). Proteomic

Profiling Reveals a Specific Role for Translesion DNA Polymerase η in the Alternative Lengthening of Telomeres. Cell Reports *17*, 1858-1871.

Glover, T.W., Berger, C., Coyle, J., and Echo, B. (1984). DNA polymerase α inhibition by aphidicolin induces gaps and breaks at common fragile sites in human chromosomes. Human Genetics *67*, 136-142.

Gocha, A.R.S., Harris, J., and Groden, J. (2013). Alternative mechanisms of telomere lengthening: Permissive mutations, DNA repair proteins and tumorigenic progression. Mutation Research/Fundamental and Molecular Mechanisms of Mutagenesis *743-744*, 142-150.

Gong, Y., and de Lange, T. (2010). A Shld1-Controlled POT1a Provides Support for Repression of ATR Signaling at Telomeres through RPA Exclusion. Molecular cell *40*, 377-387.

Greider, C.W., and Blackburn, E.H. (1985). Identification of a specific telomere terminal transferase activity in Tetrahymena extracts. Cell *43*, 405-413.

Griffith, J.D., Comeau, L., Rosenfield, S., Stansel, R.M., Bianchi, A., Moss, H., and de Lange, T. (1999). Mammalian telomeres end in a large duplex loop. Cell *97*, 503-514.

Grolimund, L., Aeby, E., Hamelin, R., Armand, F., Chiappe, D., Moniatte, M., and Lingner, J. (2013). A quantitative telomeric chromatin isolation protocol identifies different telomeric states. Nature Communications *4*.

Gu, P., Wang, Y., Bisht, K.K., Wu, L., Kukova, L., Smith, E.M., Xiao, Y., Bailey, S.M., Lei, M., Nandakumar, J.*, et al.* (2016). Pot1 OB-fold mutations unleash telomere instability to initiate tumorigenesis. Oncogene.

Herbig, U., Jobling, W.A., Chen, B.P., Chen, D.J., and Sedivy, J.M. (2004). Telomere shortening triggers senescence of human cells through a pathway involving ATM, p53, and p21(CIP1), but not p16(INK4a). Molecular cell *14*, 501-513.

Hockemeyer, D., Daniels, J.-P., Takai, H., and de Lange, T. (2006). Recent expansion of the telomeric complex in rodents: Two distinct POT1 proteins protect mouse telomeres. Cell *126*, 63-77.

Hockemeyer, D., Sfeir, A.J., Shay, J.W., Wright, W.E., and de Lange, T. (2005). POT1 protects telomeres from a transient DNA damage response and determines how human chromosomes end. The EMBO journal *24*, 2667-2678.

Hosokawa, K., and Arai, F. (2018). The role of telomere binding molecules for normal and abnormal hematopoiesis. International Journal of Hematology *107*, 646-655.

Jiao, Y., Shi, C., Edil, B.H., de Wilde, R.F., Klimstra, D.S., Maitra, A., Schulick, R.D., Tang, L.H., Wolfgang, C.L., Choti, M.A.*, et al.* (2011). DAXX/ATRX, MEN1, and mTOR pathway genes are frequently altered in pancreatic neuroendocrine tumors. Science *331*, 1199-1203.

Karlseder, J., Hoke, K., Mirzoeva, O.K., Bakkenist, C., Kastan, M.B., Petrini, J.H., and de Lange, T. (2004). The telomeric protein TRF2 binds the ATM kinase and can inhibit the ATM-dependent DNA damage response. PLoS biology *2*, E240.

Kelleher, C., Kurth, I., and Lingner, J. (2005). Human protection of telomeres 1 (POT1) is a negative regulator of telomerase activity in vitro. Mol Cell Biol *25*, 808-818.

Kendellen, M.F., Barrientos, K.S., and Counter, C.M. (2009). POT1 association with TRF2 regulates telomere length. Mol Cell Biol *29*, 5611-5619.

Kim, D.I., and Roux, K.J. (2016). Filling the Void: Proximity-Based Labeling of Proteins in Living Cells. Trends in Cell Biology *26*, 804-817.

Kim, H., Lee, O.H., Xin, H., Chen, L.Y., Qin, J., Chae, H.K., Lin, S.Y., Safari, A., Liu, D., and Songyang, Z. (2009). TRF2 functions as a protein hub and regulates telomere maintenance by recognizing specific peptide motifs. Nature structural & molecular biology *16*, 372-379.

Kim, N.W., Piatyszek, M.A., Prowse, K.R., Harley, C.B., West, M.D., Ho, P.L., Coviello, G.M., Wright, W.E., Weinrich, S.L., and Shay, J.W. (1994). Specific association of human telomerase activity with immortal cells and cancer. Science *266*, 2011.

Klobutcher, L.A., Swanton, M.T., Donini, P., and Prescott, D.M. (1981). All gene-sized DNA molecules in four species of hypotrichs have the same terminal sequence and an unusual 3' terminus. Proceedings of the National Academy of Sciences of the United States of America *78*, 3015-3019.

Latrick, C.M., and Cech, T.R. (2010). POT1–TPP1 enhances telomerase processivity by slowing primer dissociation and aiding translocation. The EMBO journal *29*, 924-933.

Lazzerini-Denchi, E., and Sfeir, A. (2016). Stop pulling my strings - what telomeres taught us about the DNA damage response. Nature reviews Molecular cell biology *17*, 364-378.

Lee, Stella S., Bohrson, C., Pike, Alexandra M., Wheelan, Sarah J., and Greider, Carol W. (2015). ATM Kinase Is Required for Telomere Elongation in Mouse and Human Cells. Cell Reports *13*, 1623-1632.

Lewis, P.W., Elsaesser, S.J., Noh, K.-M., Stadler, S.C., and Allis, C.D. (2010). Daxx is an H3.3-specific histone chaperone and cooperates with ATRX in replication-independent chromatin assembly at telomeres. Proceedings of the National Academy of Sciences *107*, 14075-14080.

Lingner, J., Cooper, J., and Cech, T. (1995). Telomerase and DNA end replication: no longer a lagging strand problem? Science *269*, 1533-1534.

Loayza, D., and De Lange, T. (2003). POT1 as a terminal transducer of TRF1 telomere length control. Nature *423*, 1013-1018.

Maciejowski, J., and de Lange, T. (2017). Telomeres in cancer: tumour suppression and genome instability. Nature reviews Molecular cell biology *advance online publication*.

McClintock, B. (1941). The Stability of Broken Ends of Chromosomes in Zea Mays. Genetics *26*, 234-282.

McKerlie, M., and Zhu, X.D. (2011). Cyclin B-dependent kinase 1 regulates human TRF1 to modulate the resolution of sister telomeres. Nat Commun *2*, 371.

Meselson, M., and Stahl, F.W. (1958). THE REPLICATION OF DNA IN ESCHERICHIA COLI. Proceedings of the National Academy of Sciences of the United States of America *44*, 671-682.

Muller, H.J. (1938). The remaking of chromosomes. Collect Net *8*, 182-195.

Nandakumar, J., Bell, C.F., Weidenfeld, I., Zaug, A.J., Leinwand, L.A., and Cech, T.R. (2012). The TEL patch of telomere protein TPP1 mediates telomerase recruitment and processivity. Nature *492*, 285.

Okamoto, K., Bartocci, C., Ouzounov, I., Diedrich, J.K., Yates Iii, J.R., and Denchi, E.L. (2013). A two-step mechanism for TRF2-mediated chromosome-end protection. Nature *494*, 502.

Palm, W., Hockemeyer, D., Kibe, T., and de Lange, T. (2009). Functional Dissection of Human and Mouse POT1 Proteins. Molecular and Cellular Biology *29*, 471-482.

Pfeiffer, V., and Lingner, J. (2012). TERRA Promotes Telomere Shortening through Exonuclease 1–Mediated Resection of Chromosome Ends. PLOS Genetics *8*, e1002747.

Pickett, H.A., and Reddel, R.R. (2015). Molecular mechanisms of activity and derepression of alternative lengthening of telomeres. Nature structural & molecular biology *22*, 875-880.

Pinzaru, A.M., Hom, R.A., Beal, A., Phillips, A.F., Ni, E., Cardozo, T., Nair, N., Choi, J., Wuttke, D.S., Sfeir, A.*, et al.* (2016). Telomere Replication Stress Induced by POT1 Inactivation Accelerates Tumorigenesis. Cell Rep *15*, 2170-2184.

Porro, A., Feuerhahn, S., Delafontaine, J., Riethman, H., Rougemont, J., and Lingner, J. (2014a). Functional characterization of the TERRA transcriptome at damaged telomeres. Nature Communications *5*.

Porro, A., Feuerhahn, S., and Lingner, J. (2014b). TERRA-reinforced association of LSD1 with MRE11 promotes processing of uncapped telomeres. Cell Rep *6*, 765-776.

Rai, R., Zheng, H., He, H., Luo, Y., Multani, A., Carpenter, P.B., and Chang, S. (2010). The function of classical and alternative non‐homologous end‐joining pathways in the fusion of dysfunctional telomeres. The EMBO journal *29*, 2598.

Rappsilber, J., Mann, M., and Ishihama, Y. (2007). Protocol for micro-purification, enrichment, pre-fractionation and storage of peptides for proteomics using StageTips. Nature protocols *2*, 1896-1906.

Redon, S., Zemp, I., and Lingner, J. (2013). A three-state model for the regulation of telomerase by TERRA and hnRNPA1. Nucleic Acids Research *41*, 9117-9128.

Ribes-Zamora, A., Indiviglio, Sandra M., Mihalek, I., Williams, Christopher L., and Bertuch, Alison A. (2013). TRF2 Interaction with Ku Heterotetramerization Interface Gives Insight into c-NHEJ Prevention at Human Telomeres. Cell Reports *5*, 194-206.

Roux, K.J., Kim, D.I., Raida, M., and Burke, B. (2012). A promiscuous biotin ligase fusion protein identifies proximal and interacting proteins in mammalian cells. Journal of Cell Biology *196*, 801-810.

Sarek, G., Vannier, J.B., Panier, S., Petrini, J.H., and Boulton, S.J. (2015). TRF2 Recruits RTEL1 to Telomeres in S Phase to Promote T-Loop Unwinding. Molecular cell.

Sarthy, J., Bae, N.S., Scrafford, J., and Baumann, P. (2009). Human RAP1 inhibits non‐homologous end joining at telomeres. The EMBO journal *28*, 3390-3399.

Schmidt, J.C., and Cech, T.R. (2015). Human telomerase: biogenesis, trafficking, recruitment, and activation. Genes & Development *29*, 1095-1105.

Schubert, L., Ho, T., Hoffmann, S., Haahr, P., Guérillon, C., and Mailand, N. (2017). RADX interacts with single-stranded DNA to promote replication fork stability. EMBO reports *18*, 1991-2003.

Sfeir, A., and de Lange, T. (2012). Removal of Shelterin Reveals the Telomere End-Protection Problem. Science *336*, 593-597.

Sfeir, A., Kosiyatrakul, S.T., Hockemeyer, D., MacRae, S.L., Karlseder, J., Schildkraut, C.L., and de Lange, T. (2009). Mammalian Telomeres Resemble Fragile Sites and Require TRF1 for Efficient Replication. Cell *138*, 90-103.

Smogorzewska, A., and de Lange, T. (2004). Regulation of telomerase by telomeric proteins. Annual Review of Biochemistry *73*, 177-208.

Smogorzewska, A., Van Steensel, B., Bianchi, A., Oelmann, S., Schaefer, M.R., Schnapp, G., and De Lange, T. (2000). Control of human telomere length by TRF1 and TRF2. Molecular and Cellular Biology *20*, 1659-1668.

Stewart, J.A., Wang, F., Chaiken, M.F., Kasbek, C., Chastain, P.D., Wright, W.E., and Price, C.M. (2012). Human CST promotes telomere duplex replication and general replication restart after fork stalling. The EMBO journal *31*, 3537-3549.

Streaker, E.D., and Beckett, D. (2006). Nonenzymatic biotinylation of a biotin carboxyl carrier protein: Unusual reactivity of the physiological target lysine. Protein Science *15*, 1928-1935.

Takai, K.K., Hooper, S., Blackwood, S., Gandhi, R., and de Lange, T. (2010). In Vivo Stoichiometry of Shelterin Components. Journal of Biological Chemistry *285*, 1457-1467.

Takai, Kaori K., Kibe, T., Donigian, Jill R., Frescas, D., and de Lange, T. (2011). Telomere Protection by TPP1/POT1 Requires Tethering to TIN2. Molecular cell *44*, 647-659.

Tong, A.S., Stern, J.L., Sfeir, A., Kartawinata, M., de Lange, T., Zhu, X.D., and Bryan, T.M. (2015). ATM and ATR Signaling Regulate the Recruitment of Human Telomerase to Telomeres. Cell Rep *13*, 1633-1646.
van Overbeek, M., and de Lange, T. (2006). Apollo, an Artemis-Abreu, E., Aritonovska, E., Reichenbach, P., Cristofari, G., Culp, B., Terns, R.M., Lingner, J., and Terns, M.P. (2010). TIN2-tethered TPP1 recruits human telomerase to telomeres in vivo. Mol. Cell. Biol. *30*, 2971–2982.

Arora, R., Lee, Y., Wischnewski, H., Brun, C.M., Schwarz, T., and Azzalin, C.M. (2014). RNaseH1 regulates TERRA-telomeric DNA hybrids and telomere maintenance in ALT tumour cells. Nat. Commun. *5*, 5220.

Azzalin, C.M., Reichenbach, P., Khoriauli, L., Giulotto, E., and Lingner, J. (2007). Telomeric repeat containing RNA and RNA surveillance factors at mammalian chromosome ends. Science *318*, 798–801.

Badie, S., Escandell, J.M., Bouwman, P., Carlos, A.R., Thanasoula, M., Gallardo, M.M., Suram, A., Jaco, I., Benitez, J., Herbig, U., et al. (2010). BRCA2 acts as a RAD51 loader to facilitate telomere replication and capping. Nat. Struct. Mol. Biol. *17*, 1461–1469.

Bailey, S.M., Cornforth, M.N., Kurimasa, A., Chen, D.J., and Goodwin, E.H. (2001). Strand-Specific Postreplicative Processing of Mammalian Telomeres. Science *293*, 2462–2465.

Bartocci, C., Diedrich, J.K., Ouzounov, I., Li, J., Piunti, A., Pasini, D., Yates, J.R., and Lazzerini Denchi, E. (2014). Isolation of chromatin from dysfunctional telomeres reveals an important role for Ring1b in NHEJ-mediated chromosome fusions. Cell Rep. *7*, 1320–1332.

Baumann, P., and Cech, T.R. (2001). Pot1, the putative telomere end-binding protein in fission yeast and humans. Science *292*, 1171–1175.

Bhat, K.P., Krishnamoorthy, A., Dungrawala, H., Garcin, E.B., Modesti, M., and Cortez, D. (2018). RADX Modulates RAD51 Activity to Control Replication Fork Protection. Cell Rep. *24*, 538–545.

Bryksin, A.V., and Matsumura, I. (2010). Overlap extension PCR cloning: a simple and reliable way to create recombinant plasmids. BioTechniques *48*, 463–465.

Celli, G.B., and de Lange, T. (2005). DNA processing is not required for ATM-mediated telomere damage response after TRF2 deletion. Nat. Cell Biol. *7*, 712-U110.

Celli, G.B., Denchi, E.L., and de Lange, T. (2006). Ku70 stimulates fusion of dysfunctional telomeres yet protects chromosome ends from homologous recombination. Nat. Cell Biol. *8*, 885–890.

Chawla, R., Redon, S., Raftopoulou, C., Wischnewski, H., Gagos, S., and Azzalin, C.M. (2011). Human UPF1 interacts with TPP1 and telomerase and sustains telomere leading-strand replication. EMBO J. *30*, 4047–4058.

Chen, L.-Y., Redon, S., and Lingner, J. (2012). The human CST complex is a terminator of telomerase activity. Nature *488*, 540–544.

Crabbe, L., Verdun, R.E., Haggblom, C.I., and Karlseder, J. (2004). Defective telomere lagging strand synthesis in cells lacking WRN helicase activity. Science *306*, 1951–1953.

Déjardin, J., and Kingston, R.E. (2009). Purification of proteins associated with specific genomic Loci. Cell *136*, 175–186.

Denchi, E.L., and de Lange, T. (2007). Protection of telomeres through independent control of ATM and ATR by TRF2 and POT1. Nature *448*, 1068–1071.

Dungrawala, H., Bhat, K.P., Le Meur, R., Chazin, W.J., Ding, X., Sharan, S.K., Wessel, S.R., Sathe, A.A., Zhao, R., and Cortez, D. (2017). RADX Promotes Genome Stability and Modulates Chemosensitivity by Regulating RAD51 at Replication Forks. Mol. Cell *67*, 374-386.e5.

d'Adda di Fagagna, F., Reaper, P.M., Clay-Farrace, L., Fiegler, H., Carr, P., Von Zglinicki, T., Saretzki, G., Carter, N.P., and Jackson, S.P. (2003). A DNA damage checkpoint response in telomere-initiated senescence. Nature *426*, 194–198.

Flynn, R.L., Centore, R.C., O'Sullivan, R.J., Rai, R., Tse, A., Songyang, Z., Chang, S., Karlseder, J., and Zou, L. (2011). TERRA and hnRNPA1 orchestrate an RPA-to-POT1 switch on telomeric single-stranded DNA. Nature *471*, 532–536.

Garcia-Exposito, L., Bournique, E., Bergoglio, V., Bose, A., Barroso-Gonzalez, J., Zhang, S., Roncaioli, J.L., Lee, M., Wallace, C.T., Watkins, S.C., et al. (2016). Proteomic Profiling Reveals a Specific Role for Translesion DNA Polymerase η in the Alternative Lengthening of Telomeres. Cell Rep. *17*, 1858–1871.

Graf, M., Bonetti, D., Lockhart, A., Serhal, K., Kellner, V., Maicher, A., Jolivet, P., Teixeira, M.T., and Luke, B. (2017). Telomere Length Determines TERRA and R-Loop Regulation through the Cell Cycle. Cell *170*, 72-85.e14.

Grolimund, L., Aeby, E., Hamelin, R., Armand, F., Chiappe, D., Moniatte, M., and Lingner, J. (2013). A quantitative telomeric chromatin isolation protocol identifies different telomeric states. Nat. Commun. *4*, 2848.

Houghtaling, B.R., Cuttonaro, L., Chang, W., and Smith, S. (2004). A dynamic molecular link between the telomere length regulator TRF1 and the chromosome end protector TRF2. Curr. Biol. CB *14*, 1621–1631.

Karlseder, J., Broccoli, D., Dai, Y., Hardy, S., and de Lange, T. (1999). p53- and ATM-dependent apoptosis induced by telomeres lacking TRF2. Science *283*, 1321–1325.

Karlseder, J., Smogorzewska, A., and de Lange, T. (2002). Senescence induced by altered telomere state, not telomere loss. Science *295*, 2446–2449.

de Lange, T. (2018). Shelterin-Mediated Telomere Protection. Annu. Rev. Genet. *52*, 223–247.

Lazzerini-Denchi, E., and Sfeir, A. (2016). Stop pulling my strings - what telomeres taught us about the DNA damage response. Nat. Rev. Mol. Cell Biol. *17*, 364–378.

Lee, S.S., Bohrson, C., Pike, A.M., Wheelan, S.J., and Greider, C.W. (2015). ATM Kinase Is Required for Telomere Elongation in Mouse and Human Cells. Cell Rep. *13*, 1623–1632.

Liu, D., O'Connor, M.S., Qin, J., and Songyang, Z. (2004). Telosome, a mammalian telomere-associated complex formed by multiple telomeric proteins. J. Biol. Chem. *279*, 51338–51342.

Majerska, J., Feretzaki, M., Glousker, G., and Lingner, J. (2018). Transformation-induced stress at telomeres is counteracted through changes in the telomeric proteome including SAMHD1. Life Sci. Alliance *1*, e201800121.

Mijic, S., Zellweger, R., Chappidi, N., Berti, M., Jacobs, K., Mutreja, K., Ursich, S., Ray Chaudhuri, A., Nussenzweig, A., Janscak, P., et al. (2017). Replication fork reversal triggers fork degradation in BRCA2-defective cells. Nat. Commun. *8*, 859.

Palm, W., Hockemeyer, D., Kibe, T., and de Lange, T. (2009). Functional dissection of human and mouse POT1 proteins. Mol. Cell. Biol. *29*, 471–482.

Pfeiffer, V., Crittin, J., Grolimund, L., and Lingner, J. (2013). The THO complex component Thp2 counteracts telomeric R-loops and telomere shortening. EMBO J. *32*, 2861–2871.

Pickett, H.A., and Reddel, R.R. (2015). Molecular mechanisms of activity and derepression of alternative lengthening of telomeres. Nat. Struct. Mol. Biol. *22*, 875–880.

Pinzaru, A.M., Hom, R.A., Beal, A., Phillips, A.F., Ni, E., Cardozo, T., Nair, N., Choi, J., Wuttke, D.S., Sfeir, A., et al. (2016). Telomere Replication Stress Induced by POT1 Inactivation Accelerates Tumorigenesis. Cell Rep. *15*, 2170–2184.

Ran, F.A., Hsu, P.D., Wright, J., Agarwala, V., Scott, D.A., and Zhang, F. (2013). Genome engineering using the CRISPR-Cas9 system. Nat. Protoc. *8*, 2281–2308.

Roux, K.J., Kim, D.I., Raida, M., and Burke, B. (2012). A promiscuous biotin ligase fusion protein identifies proximal and interacting proteins in mammalian cells. J. Cell Biol. *196*, 801–810.

Sarek, G., Vannier, J.-B., Panier, S., Petrini, J.H.J., and Boulton, S.J. (2016). TRF2 Recruits RTEL1 to Telomeres in S Phase to Promote T-Loop Unwinding. Mol. Cell *61*, 788–789.

Schmidt, J.C., and Cech, T.R. (2015). Human telomerase: biogenesis, trafficking, recruitment, and activation. Genes Dev. *29*, 1095–1105.

Schubert, L., Ho, T., Hoffmann, S., Haahr, P., Guérillon, C., and Mailand, N. (2017). RADX interacts with single-stranded DNA to promote replication fork stability. EMBO Rep. *18*, 1991–2003.

Sfeir, A., Kosiyatrakul, S.T., Hockemeyer, D., MacRae, S.L., Karlseder, J., Schildkraut, C.L., and de Lange, T. (2009). Mammalian telomeres resemble fragile sites and require TRF1 for efficient replication. Cell *138*, 90–103.

Sfeir, A., Kabir, S., van Overbeek, M., Celli, G.B., and de Lange, T. (2010). Loss of Rap1 induces telomere recombination in the absence of NHEJ or a DNA damage signal. Science *327*, 1657–1661.

Shalem, O., Sanjana, N.E., Hartenian, E., Shi, X., Scott, D.A., Mikkelson, T., Heckl, D., Ebert, B.L., Root, D.E., Doench, J.G., et al. (2014). Genome-scale CRISPR-Cas9 knockout screening in human cells. Science *343*, 84–87.

Silva, B., Pentz, R., Figueira, A.M., Arora, R., Lee, Y.W., Hodson, C., Wischnewski, H., Deans, A.J., and Azzalin, C.M. (2019). FANCM limits ALT activity by restricting telomeric replication stress induced by deregulated BLM and R-loops. Nat. Commun. *10*, 2253.

Tong, A.S., Stern, J.L., Sfeir, A., Kartawinata, M., de Lange, T., Zhu, X.-D., and Bryan, T.M. (2015). ATM and ATR Signaling Regulate the Recruitment of Human Telomerase to Telomeres. Cell Rep. *13*, 1633–1646.

Vančevska, A., Pfeiffer, V., Feretzaki, M., Ahmed, W., and Lingner, J. (2019). SMCHD1 Promotes ATM-dependent DNA Damage Signaling and Repair of Uncapped Telomeres. BioRxiv 669119.

Vannier, J.-B., Pavicic-Kaltenbrunner, V., Petalcorin, M.I.R., Ding, H., and Boulton, S.J. (2012). RTEL1 dismantles T loops and counteracts telomeric G4-DNA to maintain telomere integrity. Cell *149*, 795–806.

Verdun, R.E., and Karlseder, J. (2006). The DNA damage machinery and homologous recombination pathway act consecutively to protect human telomeres. Cell *127*, 709–720.

Wu, L., Multani, A.S., He, H., Cosme-Blanco, W., Deng, Y., Deng, J.M., Bachilo, O., Pathak, S., Tahara, H., Bailey, S.M., et al. (2006). Pot1 deficiency initiates DNA damage checkpoint activation and aberrant homologous recombination at telomeres. Cell *126*, 49–62.

Wu, P., Takai, H., and de Lange, T. (2012). Telomeric 3′ Overhangs Derive from Resection by Exo1 and Apollo and Fill-In by POT1b-Associated CST. Cell *150*, 39–52.

Ye, J.Z.-S., Donigian, J.R., van Overbeek, M., Loayza, D., Luo, Y., Krutchinsky, A.N., Chait, B.T., and de Lange, T. (2004). TIN2 binds TRF1 and TRF2 simultaneously and stabilizes the TRF2 complex on telomeres. J. Biol. Chem. *279*, 47264–47271.

Zimmermann, M., Kibe, T., Kabir, S., and de Lange, T. (2014). TRF1 negotiates TTAGGG repeat-associated replication problems by recruiting the BLM helicase and the TPP1/POT1 repressor of ATR signaling. Genes Dev. *28*, 2477–2491.

Zou, L., and Elledge, S.J. (2003). Sensing DNA damage through ATRIP recognition of RPA-ssDNA complexes. Science *300*, 1542–1548.

related nuclease, interacts with TRF2 and protects human telomeres in S phase. Current biology : CB *16*, 1295-1302.

van Steensel, B., Smogorzewska, A., and de Lange, T. (1998). TRF2 protects human telomeres from end-to-end fusions. Cell *92*, 401-413.

Vannier, J.-B., Sandhu, S., Petalcorin, M.I.R., Wu, X., Nabi, Z., Ding, H., and Boulton, S.J. (2013). RTEL1 Is a Replisome-Associated Helicase That Promotes Telomere and Genome-Wide Replication. Science *342*, 239.

vanSteensel, B., and deLange, T. (1997). Control of telomere length by the human telomeric protein TRF1. Nature *385*, 740-743.

Wang, R.C., Smogorzewska, A., and de Lange, T. (2004). Homologous Recombination Generates T-Loop-Sized Deletions at Human Telomeres. Cell *119*, 355-368.

Wang, T., Mei, S.-C., Fu, R., Wang, H.-Q., and Shao, Z.-H. (2014). Expression of Shelterin Component POT1 Is Associated with Decreased Telomere Length and Immunity Condition in Humans with Severe Aplastic Anemia. Journal of immunology research *2014*.

Wang, Y., Ghosh, G., and Hendrickson, E.A. (2009). Ku86 represses lethal telomere deletion events in human somatic cells. Proceedings of the National Academy of Sciences *106*, 12430-12435.

Watson, J.D. (1972). Origin of concatemeric T7 DNA. Nature: New biology *239*, 197-201.

Watson, J.D., and Crick, F.H.C. (1953). Molecular Structure of Nucleic Acids: A Structure for Deoxyribose Nucleic Acid. Nature *171*, 737-738.

West, S.C., Blanco, M.G., Chan, Y.W., Matos, J., Sarbajna, S., and Wyatt, H.D. (2015). Resolution of Recombination Intermediates: Mechanisms and Regulation. Cold Spring Harbor symposia on quantitative biology *80*, 103-109.

Wu, L., Multani, A.S., He, H., Cosme-Blanco, W., Deng, Y., Deng, J.M., Bachilo, O., Pathak, S., Tahara, H., Bailey, S.M., *et al.* (2006). Pot1 deficiency initiates DNA damage checkpoint activation and aberrant homologous recombination at telomeres. Cell *126*, 49-62.

Wu, P., Takai, H., and de Lange, T. (2012). Telomeric 3′ Overhangs Derive from Resection by Exo1 and Apollo and Fill-In by POT1b-Associated CST. Cell *150*, 39-52.

Ye, J.Z., Donigian, J.R., van Overbeek, M., Loayza, D., Luo, Y., Krutchinsky, A.N., Chait, B.T., and de Lange, T. (2004). TIN2 binds TRF1 and TRF2 simultaneously and stabilizes the TRF2 complex on telomeres. The Journal of biological chemistry *279*, 47264-47271.

Yeager, T.R., Neumann, A.A., Englezou, A., Huschtscha, L.I., Noble, J.R., and Reddel, R.R. (1999). Telomerase-negative immortalized human cells contain a novel type of promyelocytic leukemia (PML) body. Cancer Res *59*, 4175-4179.

Zhang, J.M., Yadav, T., Ouyang, J., Lan, L., and Zou, L. (2019). Alternative Lengthening of Telomeres through Two Distinct Break-Induced Replication Pathways. Cell Rep *26*, 955-968 e953.

Zhao, W., Wiese, C., Kwon, Y., Hromas, R., and Sung, P. (2019). The BRCA Tumor Suppressor Network in Chromosome Damage Repair by Homologous Recombination. Annual Review of Biochemistry *88*, 221-245.

Zhao, Y., Sfeir, A.J., Zou, Y., Buseman, C.M., Chow, T.T., Shay, J.W., and Wright, W.E. (2009). Telomere extension occurs at most chromosome ends and is uncoupled from fill-in in human cancer cells. Cell *138*, 463-475.

Zhong, Franklin L., Batista, Luis F.Z., Freund, A., Pech, Matthew F., Venteicher, Andrew S., and Artandi, Steven E. (2012). TPP1 OB-Fold Domain Controls Telomere Maintenance by Recruiting Telomerase to Chromosome Ends. Cell *150*, 481-494.

Zimmermann, M., Kibe, T., Kabir, S., and de Lange, T. (2014). TRF1 negotiates TTAGGG repeat-associated replication problems by recruiting the BLM helicase and the TPP1/POT1 repressor of ATR signaling. Genes & development *28*.

Zou, L., and Elledge, S.J. (2003). Sensing DNA damage through ATRIP recognition of RPA-ssDNA complexes. Science *300*, 1542-1548.

Anna-Sophia Briod

I'm passionate about understanding complex molecular phenomenons and sharing this knowledge with my peers and the general public.

Laboratory skills

- **Cell culture** of mammalian and bacterial cells
- **Genome Editing** approaches: **CRISPR/-Cas9** and viral transductions
- **Fluorescence microscopy**: Sample preparation and imaging of fixed cells and chromosomes
- **DNA Biology Methods**: PCR, southern blotting, cloning strategies
- **Protein Biology Methods**: western blotting, immunoprecipitations, chroma-tin-immunoprecipitations, proteomic analysis
- **Flow cytometry**

The languages I speak fluently

German, **French** and **English**

Computer skills

Image analysis software: **ImageJ**, **Prism**
Softwares to create illustrations: **Illustrator, Photoshop**
Interactive presentations: **Prezi**
Word, **Excel** and **Powerpoint**

How to get in touch

anna-sophia.briod@gmail.com

+41 78 920 10 42

Ch. du Reposoir 5b
1007 Lausanne
Switzerland

Doctorate Student — 2014 - 2019

EPFL - Life Science Faculty — Lausanne

Inside one of the leading research labs on telomere biology, I conducted my own project while contributing to the research activities of my colleagues with two research papers currently in preparation. I also accomplished morer than 300 hours of teaching. dergraduates.

PhD Thesis - RADX: A NOVEL SINGLE-STRANDED DNA-BINDING PROTEIN REGULATING TELOMERE RECOMBINATION

Prof. **J. Lingner**

Public defense scheduled for the 4th of October 2019

Research Assistant — 7 months - 2013

Geneva University — Geneva

Development and characterization of a liposomal formulation for cancer treatment

Pharmacist — 2012 - 2013

Apotheke in der Metropole — Berlin

First practical experience in a public pharmacy. Key aspect of my work was pharmaceutical consulting.

Teaching assistant — 2010 - 2012

Freie Universität Berlin — Berlin

Teaching a course for pharmacy students in general and analytical chemistry

Pharmacy studies — 2008- 2012

Freie Universität Berlin — Berlin

2nd state examination (2. Staatsexamen der Pharmazie) received with an average of 1,4 (maximal possible grade 1,0)

Supplemental Table S1

Proteins are at least 3-fold enriched in the BirA-IP over WT control, or not identified in WT control. For BirA-TRF1 and BirA-TRF2 the average of total spectral counts of two replicates and for WT control the average of three replicates was taken to calculate the $\log_2$ (BirA/WT). If proteins were not identified in one replicate 0.1 spectral counts were set as arbitrary value to calculate the enrichment ratios.

		log2 ratios of total spectral counts			
Identified Proteins (741)	Accession Number	BirA-POT1 5/WT	BirA-POT1 84/WT	BirA-TRF1/WT	BirA-TRF2/WT
Telomeric repeat-binding factor 2 OS=Homo sapiens GN=TERF2 PE=1 SV=3	Q15554	10	9	9	12
Nucleoprotein TPR OS=Homo sapiens GN=TPR PE=1 SV=3	P12270	8	8	7	9
TOX high mobility group box family member 4 OS=Homo sapiens GN=TOX4 PE=1 SV=1	O94842 (+2)	9	8	8	11
Chromodomain-helicase-DNA-binding protein 4 OS=Homo sapiens GN=CHD4 PE=1 SV=1	A0A0C4DGG9 (+2)	0	0	0	2
BirA	PBirA	5	6	6	8
Antigen KI-67 OS=Homo sapiens GN=MKI67 PE=1 SV=2	P46013	0	0	3	5
Serine/threonine-protein phosphatase 1 regulatory subunit 10 OS=Homo sapiens GN=PPP1R10 PE=1 SV=1	Q96QC0	7	4	6	11
Filamin-A OS=Homo sapiens GN=FLNA PE=1 SV=4	P21333 (+1)	9	10	7	10
Death-inducer obliterator 1 OS=Homo sapiens GN=DIDO1 PE=1 SV=5	Q9BTC0	3	2	1	6
TERF1-interacting nuclear factor 2 OS=Homo sapiens GN=TINF2 PE=1 SV=1	Q9BSI4	10	9	8	10
PHD finger protein 3 OS=Homo sapiens GN=PHF3 PE=1 SV=3	Q92576 (+1)	-2	-2	-2	9
Chromodomain-helicase-DNA-binding protein 8 OS=Homo sapiens GN=CHD8 PE=1 SV=5	Q9HCK8	3	2	1	5

Neuroblast differentiation-associated protein AHNAK OS=Homo sapiens GN=AHNAK PE=1 SV=2	Q09666	2	3	1	2
Nuclear mitotic apparatus protein 1 OS=Homo sapiens GN=NUMA1 PE=1 SV=2	Q14980 (+1)	0	1	2	4
Telomeric repeat-binding factor 1 OS=Homo sapiens GN=TERF1 PE=1 SV=3	P54274	8	6	9	8
Structure-specific endonuclease subunit SLX4 OS=Homo sapiens GN=SLX4 PE=1 SV=3	Q8IY92	7	3	7	10
Transcriptional regulator Kaiso OS=Homo sapiens GN=ZBTB33 PE=1 SV=2	Q86T24	6	6	5	10
Lamina-associated polypeptide 2, isoform alpha OS=Homo sapiens GN=TMPO PE=1 SV=2	P42166	1	0	1	2
MAX gene-associated protein OS=Homo sapiens GN=MGA PE=1 SV=3	Q8IWI9 (+1)	-1	0	2	3
Zinc finger CCCH domain-containing protein 11A OS=Homo sapiens GN=ZC3H11A PE=1 SV=3	O75152	1	1	1	3
Protection of telomeres protein 1 OS=Homo sapiens GN=POT1 PE=1 SV=1	Q9NUX5	10	10	0	3
Host cell factor 1 OS=Homo sapiens GN=HCFC1 PE=1 SV=2	P51610	4	4	3	7
E3 SUMO-protein ligase RanBP2 OS=Homo sapiens GN=RANBP2 PE=1 SV=2	P49792	4	4	1	4
Double-strand break repair protein MRE11A OS=Homo sapiens GN=MRE11A PE=1 SV=3	P49959	6	4	5	7
Adrenocortical dysplasia protein homolog OS=Homo sapiens GN=ACD PE=1 SV=3	Q96AP0 (+1)	9	8	8	8
Isoform 3 of Protein Wiz OS=Homo sapiens GN=WIZ	O95785-3	3	0	6	9
Non-POU domain-containing octamer-binding protein OS=Homo sapiens GN=NONO PE=1 SV=4	Q15233	0	-1	1	2
Origin recognition complex subunit 2 OS=Homo sapiens GN=ORC2 PE=1 SV=2	Q13416	3	2	2	5
U4/U6.U5 tri-snRNP-associated protein 1 OS=Homo sapiens GN=SART1 PE=1 SV=1	O43290	0	-1	1	2
General transcription factor II-I OS=Homo sapiens GN=GTF2I PE=1 SV=2	P78347 (+3)	1	0	1	3
RNA-binding protein 26 OS=Homo sapiens GN=RBM26 PE=1 SV=1	A0A087X0H9	4	4	3	5
Msx2-interacting protein OS=Homo sapiens GN=SPEN PE=1 SV=1	Q96T58	-3	-3	1	5
Splicing factor 3B subunit 2 OS=Homo sapiens GN=SF3B2 PE=1 SV=2	Q13435	0	0	1	2
Biorientation of chromosomes in cell division protein 1-like 1 OS=Homo sapiens GN=BOD1L1 PE=1 SV=2	Q8NFC6	0	-1	2	3
Bromodomain-containing protein 4 OS=Homo sapiens GN=BRD4 PE=1 SV=2	O60885	6	6	5	8
5' exonuclease Apollo OS=Homo sapiens GN=DCLRE1B PE=1 SV=1	Q9H816	4	0	0	9
Nipped-B-like protein OS=Homo sapiens GN=NIPBL PE=1 SV=2	Q6KC79	0	0	2	8
Microtubule-associated protein OS=Homo sapiens GN=MAP4 PE=1 SV=1	E7EVA0	3	3	2	2
Nibrin OS=Homo sapiens GN=NBN PE=1 SV=1	O60934	6	5	7	8
Zinc finger protein 318 OS=Homo sapiens GN=ZNF318 PE=1 SV=2	Q5VUA4	5	5	5	7
RNA binding motif protein 10, isoform CRA_d OS=Homo sapiens GN=RBM10 PE=1 SV=1	A0A0A0MR66	1	1	1	2
Protein FAM208A OS=Homo sapiens GN=FAM208A PE=1 SV=3	Q9UK61	-2	1	2	6
Telomere-associated protein RIF1 OS=Homo sapiens GN=RIF1 PE=1 SV=2	Q5UIP0	-3	-3	1	4

Sex comb on midleg-like protein 2 OS=Homo sapiens GN=SCML2 PE=1 SV=1	Q9UQR0	0	6	6	8
Isoform 3 of Regulation of nuclear pre-mRNA domain-containing protein 2 OS=Homo sapiens GN=RPRD2	Q5VT52-3	1	3	2	5
Slit homolog 2 protein OS=Homo sapiens GN=SLIT2 PE=1 SV=1	O94813 (+1)	0	2	3	-4
YEATS domain-containing protein 2 OS=Homo sapiens GN=YEATS2 PE=1 SV=2	Q9ULM3	7	7	4	7
Spliceosome RNA helicase DDX39B OS=Homo sapiens GN=DDX39B PE=1 SV=1	Q13838 (+1)	-6	-2	2	0
Isoform 3 of Wings apart-like protein homolog OS=Homo sapiens GN=WAPAL	Q7Z5K2-3	0	0	3	4
Lamina-associated polypeptide 2, isoforms beta/gamma OS=Homo sapiens GN=TMPO PE=1 SV=2	P42167	1	0	1	2
HIV Tat-specific factor 1 OS=Homo sapiens GN=HTATSF1 PE=1 SV=1	O43719	0	-5	1	2
Pre-mRNA-processing factor 6 OS=Homo sapiens GN=PRPF6 PE=1 SV=1	O94906	-5	-5	2	-2
Telomeric repeat-binding factor 2-interacting protein 1 OS=Homo sapiens GN=TERF2IP PE=1 SV=1	Q9NYB0	5	3	4	8
THO complex subunit 2 OS=Homo sapiens GN=THOC2 PE=1 SV=2	Q8NI27	-3	-3	2	4
Targeting protein for Xklp2 OS=Homo sapiens GN=TPX2 PE=1 SV=2	Q9ULW0	0	0	6	7
Histone-lysine N-methyltransferase 2A OS=Homo sapiens GN=KMT2A PE=1 SV=5	Q03164 (+2)	-1	-4	-2	3
Isoform 13 of Protein kinase C-binding protein 1 OS=Homo sapiens GN=ZMYND8	Q9ULU4-13 (+1)	0	0	0	8
RNA polymerase-associated protein LEO1 OS=Homo sapiens GN=LEO1 PE=1 SV=1	Q8WVC0	0	0	0	8
UPF0428 protein CXorf56 OS=Homo sapiens GN=CXorf56 PE=1 SV=1	Q9H5V9	6	5	5	8
Nucleosome-remodeling factor subunit BPTF OS=Homo sapiens GN=BPTF PE=1 SV=3	Q12830 (+1)	-2	-2	2	5
ATP-dependent RNA helicase DDX42 OS=Homo sapiens GN=DDX42 PE=1 SV=1	Q86XP3	-1	-1	1	3
Transcriptional regulator ATRX OS=Homo sapiens GN=ATRX PE=1 SV=5	P46100 (+1)	0	0	4	7
Probable JmjC domain-containing histone demethylation protein 2C OS=Homo sapiens GN=JMJD1C PE=1 SV=2	Q15652	6	6	2	7
U4/U6 small nuclear ribonucleoprotein Prp3 OS=Homo sapiens GN=PRPF3 PE=1 SV=2	O43395	0	0	3	4
DNA topoisomerase 2-binding protein 1 OS=Homo sapiens GN=TOPBP1 PE=1 SV=3	Q92547	8	0	4	6
Isoform 2 of DNA (cytosine-5)-methyltransferase 1 OS=Homo sapiens GN=DNMT1	P26358-2	-3	-3	2	3
Splicing factor 45 OS=Homo sapiens GN=RBM17 PE=1 SV=1	Q96I25	-5	-1	1	3
Protein RCC2 OS=Homo sapiens GN=RCC2 PE=1 SV=2	Q9P258	-5	-5	1	2
RNA polymerase-associated protein CTR9 homolog OS=Homo sapiens GN=CTR9 PE=1 SV=1	Q6PD62	0	0	2	8
RNA-binding motif protein, X-linked 2 OS=Homo sapiens GN=RBMX2 PE=1 SV=2	Q9Y388	-5	0	0	2
Heterochromatin protein 1-binding protein 3 OS=Homo sapiens GN=HP1BP3 PE=1 SV=1	Q5SSJ5	-4	-4	1	2
RNA polymerase II-associated factor 1 homolog OS=Homo sapiens GN=PAF1 PE=1 SV=2	Q8N7H5	0	0	0	8
Cytoplasmic dynein 1 heavy chain 1 OS=Homo sapiens GN=DYNC1H1 PE=1 SV=5	Q14204	-2	-2	2	0

Chromosome-associated kinesin KIF4A OS=Homo sapiens GN=KIF4A PE=1 SV=3	O95239	0	4	6	7
Dedicator of cytokinesis protein 6 OS=Homo sapiens GN=DOCK6 PE=1 SV=3	Q96HP0-DECOY	-2	1	-2	2
Bloom syndrome protein OS=Homo sapiens GN=BLM PE=1 SV=1	P54132	-2	-2	-2	3
Helicase, lymphoid-specific, isoform CRA_b OS=Homo sapiens GN=HELLS PE=1 SV=1	A0A0B4J1V9	-4	-4	2	2
Apoptotic chromatin condensation inducer in the nucleus OS=Homo sapiens GN=ACIN1 PE=1 SV=1	S4R3H4	-2	-2	2	4
Replication factor C subunit 1 OS=Homo sapiens GN=RFC1 PE=1 SV=4	P35251 (+1)	-4	-4	2	1
RNA-binding protein 27 OS=Homo sapiens GN=RBM27 PE=1 SV=2	Q9P2N5	4	4	1	6
Parafibromin OS=Homo sapiens GN=CDC73 PE=1 SV=1	Q6P1J9	0	0	5	8
Zinc finger CCCH domain-containing protein 4 OS=Homo sapiens GN=ZC3H4 PE=1 SV=3	Q9UPT8	0	0	0	8
Cyclin-dependent kinase 12 OS=Homo sapiens GN=CDK12 PE=1 SV=2	Q9NYV4 (+1)	-4	-4	1	2
Chromosome alignment-maintaining phosphoprotein 1 OS=Homo sapiens GN=CHAMP1 PE=1 SV=2	Q96JM3	-3	-3	1	4
Dachshund homolog 1 OS=Homo sapiens GN=DACH1 PE=1 SV=1	A0A087WZP2 (+2)	3	3	2	5
Isoform 3 of Nuclear pore complex protein Nup153 OS=Homo sapiens GN=NUP153	P49790-3	4	4	3	5
Isoform 2 of DNA repair protein RAD50 OS=Homo sapiens GN=RAD50	Q92878-2	-3	-3	2	2
Pre-mRNA-splicing factor CWC25 homolog OS=Homo sapiens GN=CWC25 PE=1 SV=1	Q9NXE8	1	0	1	2
Centromere protein F OS=Homo sapiens GN=CENPF PE=1 SV=2	P49454	0	0	0	6
RRP12-like protein OS=Homo sapiens GN=RRP12 PE=1 SV=2	Q5JTH9	-4	-1	-1	2
SURP and G-patch domain-containing protein 2 OS=Homo sapiens GN=SUGP2 PE=1 SV=1	M0R2Z9 (+3)	-2	1	0	5
Probable ATP-dependent RNA helicase DDX10 OS=Homo sapiens GN=DDX10 PE=1 SV=2	Q13206	-2	-2	3	4
Corepressor interacting with RBPJ 1 OS=Homo sapiens GN=CIR1 PE=1 SV=1	Q86X95	2	1	-1	-5
Isoform 3 of Transcription initiation factor TFIID subunit 1 OS=Homo sapiens GN=TAF1	P21675-3 (+4)	0	0	0	6
Lamin-B1 OS=Homo sapiens GN=LMNB1 PE=1 SV=2	P20700	-4	-4	2	0
Mediator of RNA polymerase II transcription subunit 1 OS=Homo sapiens GN=MED1 PE=1 SV=4	Q15648	0	0	0	7
Paired amphipathic helix protein Sin3b OS=Homo sapiens GN=SIN3B PE=1 SV=2	O75182 (+1)	0	0	2	7
Flap endonuclease 1 OS=Homo sapiens GN=FEN1 PE=1 SV=1	P39748	1	1	2	2
Kinectin OS=Homo sapiens GN=KTN1 PE=1 SV=1	Q86UP2	-3	-3	2	-3
Structural maintenance of chromosomes flexible hinge domain-containing protein 1 OS=Homo sapiens GN=SMCHD1 PE=1 SV=2	A6NHR9	6	0	3	7
Activity-dependent neuroprotector homeobox protein OS=Homo sapiens GN=ADNP PE=1 SV=1	Q9H2P0	0	0	5	7
Alpha-synuclein OS=Homo sapiens GN=SNCA PE=1 SV=1	E7EPV7 (+2)	-2	-2	5	-2
Microcephalin OS=Homo sapiens GN=MCPH1 PE=1 SV=1	A0A075B6F8 (+1)	0	0	0	7

Zinc finger CCCH domain-containing protein 14 OS=Homo sapiens GN=ZC3H14 PE=1 SV=1	Q6PJT7	-2	-2	3	3
Protein SLX4IP OS=Homo sapiens GN=SLX4IP PE=1 SV=1	Q5VYV7	4	0	4	7
E3 ubiquitin-protein ligase MYCBP2 OS=Homo sapiens GN=MYCBP2 PE=1 SV=3	O75592-DECOY	0	0	3	0
Sister chromatid cohesion protein PDS5 homolog B OS=Homo sapiens GN=PDS5B PE=1 SV=1	Q9NTI5 (+1)	0	0	5	3
Isoform 2 of Kinesin-like protein KIF20B OS=Homo sapiens GN=KIF20B	Q96Q89-2	0	0	0	3
Cell division cycle 5-like protein OS=Homo sapiens GN=CDC5L PE=1 SV=2	Q99459	-3	-3	2	1
Eukaryotic initiation factor 4A-III OS=Homo sapiens GN=EIF4A3 PE=1 SV=4	P38919	-4	-4	2	1
Protein Red OS=Homo sapiens GN=IK PE=1 SV=3	Q13123	3	3	4	7
Uncharacterized protein CXorf57 OS=Homo sapiens GN=CXorf57 PE=1 SV=2	Q6NSI4	3	5	5	5
Kinesin-like protein KIF22 OS=Homo sapiens GN=KIF22 PE=1 SV=5	Q14807	1	-2	0	3
Tyrosine-protein kinase BAZ1B OS=Homo sapiens GN=BAZ1B PE=1 SV=2	Q9UIG0 (+1)	0	0	0	6
Zinc finger protein 687 OS=Homo sapiens GN=ZNF687 PE=1 SV=1	Q8N1G0	0	0	0	6
Heterogeneous nuclear ribonucleoprotein L OS=Homo sapiens GN=HNRNPL PE=1 SV=2	P14866	-1	-4	2	0
Cactin OS=Homo sapiens GN=CACTIN PE=1 SV=3	Q8WUQ7 (+1)	-3	1	1	2
Protein ELYS OS=Homo sapiens GN=AHCTF1 PE=1 SV=3	Q8WYP5 (+2)	0	0	0	6
ESF1 homolog OS=Homo sapiens GN=ESF1 PE=1 SV=1	Q9H501	1	-3	-1	2
Isoform 4 of Double-stranded RNA-specific adenosine deaminase OS=Homo sapiens GN=ADAR	P55265-4	-3	-3	2	2
Bromodomain adjacent to zinc finger domain protein 1A OS=Homo sapiens GN=BAZ1A PE=1 SV=2	Q9NRL2	0	0	0	6
Microfibrillar-associated protein 1 OS=Homo sapiens GN=MFAP1 PE=1 SV=2	P55081	0	0	4	7
Lysozyme OS=Homo sapiens GN=LYZ PE=1 SV=1	A0A0B4J259 (+2)	1	2	0	0
Structural maintenance of chromosomes protein 1A OS=Homo sapiens GN=SMC1A PE=1 SV=2	Q14683	-3	-3	2	-3
Chromodomain-helicase-DNA-binding protein 6 OS=Homo sapiens GN=CHD6 PE=1 SV=4	Q8TD26	-1	-5	-1	2
Pinin OS=Homo sapiens GN=PNN PE=1 SV=4	Q9H307	-3	4	2	3
Apoptosis inhibitor 5 OS=Homo sapiens GN=API5 PE=1 SV=3	Q9BZZ5	-4	-4	1	3
Small subunit processome component 20 homolog OS=Homo sapiens GN=UTP20 PE=1 SV=3	O75691	0	0	0	3
Angiomotin OS=Homo sapiens GN=AMOT PE=1 SV=1	Q4VCS5	-4	3	0	-4
MAP7 domain-containing protein 3 OS=Homo sapiens GN=MAP7D3 PE=1 SV=2	Q8IWC1	0	3	3	6
Exosome complex exonuclease RRP44 OS=Homo sapiens GN=DIS3 PE=1 SV=2	Q9Y2L1	-4	-4	2	-4
Pescadillo homolog OS=Homo sapiens GN=PES1 PE=1 SV=1	B5MCF9 (+2)	-3	-3	2	3
Zinc finger protein 768 OS=Homo sapiens GN=ZNF768 PE=1 SV=2	Q9H5H4	-2	-2	2	-2

Transcription elongation factor B (SIII), polypeptide 3 (110kDa, elongin A), isoform CRA_a OS=Homo sapiens GN=TCEB3 PE=1 SV=1	A0A024RAC6	-2	-2	1	4
Polymerase delta-interacting protein 3 OS=Homo sapiens GN=POLDIP3 PE=1 SV=2	Q9BY77	-3	-3	1	2
ATP-dependent DNA helicase Q5 OS=Homo sapiens GN=RECQL5 PE=1 SV=2	O94762 (+1)	0	0	0	5
Cornifin-B OS=Homo sapiens GN=SPRR1B PE=1 SV=2	P22528	1	2	1	0
Pre-mRNA cleavage complex 2 protein Pcf11 OS=Homo sapiens GN=PCF11 PE=1 SV=3	O94913	0	0	3	6
Uncharacterized protein C16orf46 OS=Homo sapiens GN=C16orf46 PE=2 SV=2	Q6P387	2	-2	2	3
Pre-mRNA-splicing factor SLU7 OS=Homo sapiens GN=SLU7 PE=1 SV=2	O95391	-3	-3	1	2
Zinc fingers and homeoboxes protein 3 (Fragment) OS=Homo sapiens GN=ZHX3 PE=1 SV=1	H0Y6F5	0	0	0	7
Dolichyl-diphosphooligosaccharide--protein glycosyltransferase subunit 1 OS=Homo sapiens GN=RPN1 PE=1 SV=1	P04843	-3	-3	2	2
AP-2 complex subunit mu OS=Homo sapiens GN=AP2M1 PE=1 SV=1	A0A087WY71 (+3)	0	0	5	6
Histone-lysine N-methyltransferase, H3 lysine-36 and H4 lysine-20 specific OS=Homo sapiens GN=NSD1 PE=1 SV=1	Q96L73 (+1)	0	0	0	5
Ankyrin repeat domain-containing protein 11 OS=Homo sapiens GN=ANKRD11 PE=1 SV=3	Q6UB99	0	0	0	4
Sister chromatid cohesion protein PDS5 homolog A OS=Homo sapiens GN=PDS5A PE=1 SV=1	Q29RF7	0	0	4	6
Probable 28S rRNA (cytosine(4447)-C(5))-methyltransferase OS=Homo sapiens GN=NOP2 PE=1 SV=2	P46087 (+1)	-4	-4	2	-2
Actin-binding protein anillin OS=Homo sapiens GN=ANLN PE=1 SV=2	Q9NQW6 (+1)	0	0	0	5
DNA replication licensing factor MCM7 OS=Homo sapiens GN=MCM7 PE=1 SV=4	P33993	-3	-3	2	1
SURP and G-patch domain-containing protein 1 OS=Homo sapiens GN=SUGP1 PE=1 SV=2	Q8IWZ8	3	0	0	7
Probable G-protein-coupled receptor 179 OS=Homo sapiens GN=GPR179 PE=1 SV=1	A0A087WW83 (+2)	-2	-2	2	-2
Cytoskeleton-associated protein 5 OS=Homo sapiens GN=CKAP5 PE=1 SV=3	Q14008 (+2)	0	4	0	2
Chromodomain-helicase-DNA-binding protein 3 OS=Homo sapiens GN=CHD3 PE=1 SV=3	Q12873 (+1)	-1	-6	0	2
U2 small nuclear ribonucleoprotein A' OS=Homo sapiens GN=SNRPA1 PE=1 SV=2	P09661	-4	-4	1	2
Exosome component 10 OS=Homo sapiens GN=EXOSC10 PE=1 SV=2	Q01780	-4	-4	2	1
Src substrate cortactin OS=Homo sapiens GN=CTTN PE=1 SV=2	Q14247	6	6	4	5
Signal recognition particle subunit SRP72 OS=Homo sapiens GN=SRP72 PE=1 SV=3	O76094	-3	-3	2	-1
Polyadenylate-binding protein OS=Homo sapiens GN=PABPC1 PE=1 SV=1	E7EQV3 (+1)	-3	-3	2	-3
Breast cancer type 1 susceptibility protein OS=Homo sapiens GN=BRCA1 PE=1 SV=2	P38398 (+1)	0	0	2	5
Formin-binding protein 4 OS=Homo sapiens GN=FNBP4 PE=1 SV=3	Q8N3X1 (+1)	0	-3	2	1
Protein EMSY OS=Homo sapiens GN=EMSY PE=1 SV=2	Q7Z589 (+3)	0	0	0	5

Putative pre-mRNA-splicing factor ATP-dependent RNA helicase DHX16 OS=Homo sapiens GN=DHX16 PE=1 SV=2	O60231	0	-3	2	1
Metastasis-associated protein MTA1 OS=Homo sapiens GN=MTA1 PE=1 SV=2	Q13330 (+1)	0	0	2	5
Negative elongation factor A OS=Homo sapiens GN=NELFA PE=1 SV=1	A0A0C4DFX9	-2	-2	2	2
Emerin OS=Homo sapiens GN=EMD PE=1 SV=1	P50402	1	1	0	2
X-ray repair cross-complementing protein 6 OS=Homo sapiens GN=XRCC6 PE=1 SV=2	P12956	-3	-3	2	1
PAX3- and PAX7-binding protein 1 OS=Homo sapiens GN=PAXBP1 PE=1 SV=2	Q9Y5B6	-3	-3	2	-3
SWI/SNF-related matrix-associated actin-dependent regulator of chromatin subfamily A member 5 OS=Homo sapiens GN=SMARCA5 PE=1 SV=1	O60264	0	0	2	5
SNW domain-containing protein 1 OS=Homo sapiens GN=SNW1 PE=1 SV=1	Q13573	-3	-3	2	2
Cip1-interacting zinc finger protein OS=Homo sapiens GN=CIZ1 PE=1 SV=2	F5H2X7 (+4)	0	3	0	7
Fatty acid-binding protein, epidermal OS=Homo sapiens GN=FABP5 PE=1 SV=3	Q01469	3	5	5	0
Negative elongation factor E OS=Homo sapiens GN=NELFE PE=1 SV=3	P18615	0	0	2	6
Chromodomain-helicase-DNA-binding protein 7 OS=Homo sapiens GN=CHD7 PE=1 SV=3	Q9P2D1	-4	-4	1	3
DNA mismatch repair protein Msh2 OS=Homo sapiens GN=MSH2 PE=1 SV=1	P43246	0	0	4	0
Clathrin heavy chain OS=Homo sapiens GN=CLTC PE=1 SV=1	A0A087WVQ6 (+2)	-3	-3	2	-3
Nuclear pore complex protein Nup98-Nup96 OS=Homo sapiens GN=NUP98 PE=1 SV=4	P52948 (+1)	-4	1	1	-4
AP-2 complex subunit alpha-1 OS=Homo sapiens GN=AP2A1 PE=1 SV=3	O95782 (+1)	-3	-3	1	-1
Isoform 4 of Signal recognition particle subunit SRP68 OS=Homo sapiens GN=SRP68	Q9UHB9-4	0	0	4	2
60S ribosomal protein L26-like 1 OS=Homo sapiens GN=RPL26L1 PE=1 SV=1	Q9UNX3	0	0	0	0
Scaffold attachment factor B2 OS=Homo sapiens GN=SAFB2 PE=1 SV=1	Q14151	0	0	4	2
SWI/SNF complex subunit SMARCC1 OS=Homo sapiens GN=SMARCC1 PE=1 SV=3	Q92922	-2	-2	3	1
Afadin OS=Homo sapiens GN=MLLT4 PE=1 SV=2	A8MQ02	5	5	0	2
Cyclin-dependent kinase 11B OS=Homo sapiens GN=CDK11B PE=4 SV=1	A0A0D9SER5	-3	-3	1	1
Methyl-CpG-binding domain protein 3 OS=Homo sapiens GN=MBD3 PE=1 SV=1	O95983	-3	-3	2	0
E3 ubiquitin-protein ligase TTC3 OS=Homo sapiens GN=TTC3 PE=1 SV=2	P53804	0	0	3	2
Prelamin-A/C OS=Homo sapiens GN=LMNA PE=1 SV=1	P02545 (+3)	0	0	4	0
Isoform 2 of MICOS complex subunit MIC60 OS=Homo sapiens GN=IMMT	Q16891-2	-3	-3	2	-3
ATP-dependent RNA helicase DDX1 OS=Homo sapiens GN=DDX1 PE=1 SV=2	Q92499	-3	-3	2	-3
Splicing factor 3B subunit 3 OS=Homo sapiens GN=SF3B3 PE=1 SV=4	Q15393	-2	-2	4	-2
Probable ATP-dependent RNA helicase DDX23 OS=Homo sapiens GN=DDX23 PE=1 SV=3	Q9BUQ8	-3	-3	3	-3

Serine/threonine-protein phosphatase OS=Homo sapiens GN=PPP1CC PE=1 SV=1	F8W0W8 (+1)	0	0	3	6
Probable dimethyladenosine transferase OS=Homo sapiens GN=DIMT1 PE=1 SV=1	Q9UNQ2	-3	-3	1	2
Insulin-like growth factor 2 mRNA-binding protein 1 OS=Homo sapiens GN=IGF2BP1 PE=1 SV=2	Q9NZI8	-3	-3	1	-3
Protein-glutamine gamma-glutamyltransferase K OS=Homo sapiens GN=TGM1 PE=1 SV=4	P22735	-3	1	1	2
Annexin A1 OS=Homo sapiens GN=ANXA1 PE=1 SV=2	P04083	2	1	-4	-4
Plasminogen activator inhibitor 1 RNA-binding protein OS=Homo sapiens GN=SERBP1 PE=1 SV=2	Q8NC51	5	0	5	5
Centrosomal protein of 170 kDa OS=Homo sapiens GN=CEP170 PE=1 SV=1	Q5SW79	0	4	0	2
Transcriptional repressor p66-alpha OS=Homo sapiens GN=GATAD2A PE=1 SV=1	Q86YP4 (+1)	0	0	2	5
RNA exonuclease 4 OS=Homo sapiens GN=REXO4 PE=1 SV=2	Q9GZR2	0	0	4	5
Glutamine and serine-rich protein 1 OS=Homo sapiens GN=QSER1 PE=1 SV=3	Q2KHR3 (+1)	0	0	0	5
Eukaryotic translation initiation factor 2 subunit 2 OS=Homo sapiens GN=EIF2S2 PE=1 SV=2	P20042	-3	-3	2	-1
Lamin B2, isoform CRA_a OS=Homo sapiens GN=LMNB2 PE=1 SV=1	J9JID7	-3	-3	2	-3
E1A-binding protein p400 OS=Homo sapiens GN=EP400 PE=1 SV=4	Q96L91	0	0	0	5
DNA-binding protein RFX5 (Fragment) OS=Homo sapiens GN=RFX5 PE=1 SV=1	F8W689 (+1)	0	0	0	5
Polypyrimidine tract-binding protein 1 OS=Homo sapiens GN=PTBP1 PE=1 SV=1	P26599 (+2)	-3	-3	2	0
Peptidyl-prolyl cis-trans isomerase-like 4 OS=Homo sapiens GN=PPIL4 PE=1 SV=1	Q8WUA2	-2	-2	3	3
BRCA1-A complex subunit RAP80 OS=Homo sapiens GN=UIMC1 PE=1 SV=2	Q96RL1 (+1)	0	0	4	6
Protein SCAF11 OS=Homo sapiens GN=SCAF11 PE=1 SV=2	Q99590	0	0	0	4
Zinc finger protein 148 OS=Homo sapiens GN=ZNF148 PE=1 SV=2	Q9UQR1	0	0	0	6
Nuclear RNA export factor 1 OS=Homo sapiens GN=NXF1 PE=1 SV=1	Q9UBU9	-2	-2	3	3
Hexokinase-1 OS=Homo sapiens GN=HK1 PE=1 SV=3	P19367 (+3)	0	0	4	0
Isoform 2 of Inner centromere protein OS=Homo sapiens GN=INCENP	Q9NQS7-2 (+1)	0	0	2	5
Metastasis-associated protein MTA2 OS=Homo sapiens GN=MTA2 PE=1 SV=1	O94776	-2	-2	2	2
Poly(rC)-binding protein 1 OS=Homo sapiens GN=PCBP1 PE=1 SV=2	Q15365	-2	1	2	3
Nuclear valosin-containing protein-like OS=Homo sapiens GN=NVL PE=1 SV=1	O15381 (+1)	-3	-3	2	1
Protein LYRIC OS=Homo sapiens GN=MTDH PE=1 SV=2	Q86UE4	-4	-4	1	-2
Septin-7 OS=Homo sapiens GN=SEPT7 PE=1 SV=2	E7EPK1	-2	-2	4	2
DNA replication licensing factor MCM6 OS=Homo sapiens GN=MCM6 PE=1 SV=1	Q14566	-2	-2	3	-2
Myelin basic protein OS=Homo sapiens GN=MBP PE=1 SV=1	A8MZH3	0	7	2	0
WW domain-containing oxidoreductase OS=Homo sapiens GN=WWOX PE=1 SV=1	Q9NZC7 (+1)	5	0	0	6
Nuclear pore complex protein Nup50 OS=Homo sapiens GN=NUP50 PE=1 SV=2	Q9UKX7 (+1)	0	-3	1	2

Probable ATP-dependent RNA helicase DDX47 OS=Homo sapiens GN=DDX47 PE=1 SV=1	Q9H0S4 (+1)	-4	-4	0	1
Exocyst complex component 4 OS=Homo sapiens GN=EXOC4 PE=1 SV=1	Q96A65	0	3	3	0
Helicase-like transcription factor OS=Homo sapiens GN=HLTF PE=1 SV=2	Q14527	0	0	4	4
Interleukin enhancer-binding factor 2 OS=Homo sapiens GN=ILF2 PE=1 SV=1	B4DY09 (+1)	-3	-3	2	-3
Zinc finger and BTB domain-containing protein 9 OS=Homo sapiens GN=ZBTB9 PE=1 SV=1	Q96C00	0	0	0	6
Isoform 1 of Histone-lysine N-methyltransferase, H3 lysine-79 specific OS=Homo sapiens GN=DOT1L	Q8TEK3-2	3	0	0	3
Spliceosome-associated protein CWC15 homolog OS=Homo sapiens GN=CWC15 PE=1 SV=2	Q9P013	1	-2	0	3
Pre-mRNA 3'-end-processing factor FIP1 OS=Homo sapiens GN=FIP1L1 PE=1 SV=1	A0A0B4J203	0	0	4	3
YLP motif-containing protein 1 OS=Homo sapiens GN=YLPM1 PE=1 SV=3	P49750 (+1)	0	0	0	4
Isoform 4 of U4/U6 small nuclear ribonucleoprotein Prp31 OS=Homo sapiens GN=PRPF31	Q8WWY3-4	-2	-2	2	2
Splicing factor 3A subunit 1 OS=Homo sapiens GN=SF3A1 PE=1 SV=1	Q15459	3	0	2	5
Isoform 5 of Dynamin-2 OS=Homo sapiens GN=DNM2	P50570-5	-2	-2	2	-2
Pre-mRNA-splicing factor SYF1 OS=Homo sapiens GN=XAB2 PE=1 SV=2	Q9HCS7	0	0	0	5
DNA replication licensing factor MCM3 OS=Homo sapiens GN=MCM3 PE=1 SV=3	P25205 (+1)	0	0	5	0
Sentrin-specific protease 6 OS=Homo sapiens GN=SENP6 PE=1 SV=2	Q9GZR1 (+1)	0	0	0	4
Probable ATP-dependent RNA helicase DDX52 OS=Homo sapiens GN=DDX52 PE=1 SV=3	Q9Y2R4	0	0	3	2
Eukaryotic translation initiation factor 2 subunit 3 OS=Homo sapiens GN=EIF2S3 PE=1 SV=3	P41091	-2	-2	3	0
Uncharacterized protein C19orf43 OS=Homo sapiens GN=C19orf43 PE=1 SV=1	Q9BQ61	3	0	3	5
RNA-binding protein 5 OS=Homo sapiens GN=RBM5 PE=1 SV=2	P52756	0	0	4	3
NF-kappa-B-repressing factor OS=Homo sapiens GN=NKRF PE=1 SV=2	O15226 (+1)	0	0	3	0
Apolipoprotein D (Fragment) OS=Homo sapiens GN=APOD PE=1 SV=1	C9JF17 (+1)	-3	-3	0	2
28S ribosomal protein S5, mitochondrial OS=Homo sapiens GN=MRPS5 PE=1 SV=2	P82675	1	1	3	-2
Ubinuclein-2 OS=Homo sapiens GN=UBN2 PE=1 SV=2	Q6ZU65	0	0	0	3
Transcription initiation factor IIE subunit beta OS=Homo sapiens GN=GTF2E2 PE=1 SV=1	P29084	0	0	0	5
WD repeat-containing protein 76 OS=Homo sapiens GN=WDR76 PE=1 SV=2	Q9H967	0	0	0	5
T-complex protein 1 subunit alpha OS=Homo sapiens GN=TCP1 PE=1 SV=1	P17987	-2	-2	2	2
Isoform 3 of Septin-2 OS=Homo sapiens GN=SEPT2	Q15019-3	-2	-2	3	0
Uncharacterized protein (Fragment) OS=Homo sapiens PE=1 SV=1	H0YHG0	0	0	2	6
Eukaryotic translation initiation factor 3 subunit L OS=Homo sapiens GN=EIF3L PE=1 SV=1	B0QY89 (+1)	-2	-2	3	-2
SAP30-binding protein (Fragment) OS=Homo sapiens GN=SAP30BP PE=1 SV=1	J3QQJ0	0	0	4	5
Nuclear pore complex protein Nup107 OS=Homo sapiens GN=NUP107 PE=1 SV=1	P57740	-2	-2	2	-2

Fanconi anemia group J protein OS=Homo sapiens GN=BRIP1 PE=1 SV=1	Q9BX63	5	0	0	2
Kinesin-like protein KIFC1 OS=Homo sapiens GN=KIFC1 PE=1 SV=2	Q9BW19	0	0	0	4
AT-rich interactive domain-containing protein 3B OS=Homo sapiens GN=ARID3B PE=1 SV=2	Q8IVW6 (+1)	0	0	0	6
RNA-binding protein with serine-rich domain 1 OS=Homo sapiens GN=RNPS1 PE=1 SV=1	Q15287 (+1)	-2	-2	1	3
Hepatoma-derived growth factor-related protein 2 OS=Homo sapiens GN=HDGFRP2 PE=1 SV=1	Q7Z4V5 (+1)	0	0	4	5
Cell division cycle-associated protein 2 OS=Homo sapiens GN=CDCA2 PE=1 SV=2	Q69YH5	0	0	0	4
Zinc finger CCCH-type antiviral protein 1 OS=Homo sapiens GN=ZC3HAV1 PE=1 SV=1	C9J6P4	0	0	3	0
Heterogeneous nuclear ribonucleoprotein A0 OS=Homo sapiens GN=HNRNPA0 PE=1 SV=1	Q13151	0	0	4	4
Peroxiredoxin-4 OS=Homo sapiens GN=PRDX4 PE=1 SV=1	Q13162	0	0	2	5
Chromobox protein homolog 8 OS=Homo sapiens GN=CBX8 PE=1 SV=3	Q9HC52	0	0	2	4
KH domain-containing, RNA-binding, signal transduction-associated protein 1 OS=Homo sapiens GN=KHDRBS1 PE=1 SV=1	Q07666	0	0	4	3
Coiled-coil domain-containing protein 86 OS=Homo sapiens GN=CCDC86 PE=1 SV=1	Q9H6F5	0	0	5	2
Protein capicua homolog OS=Homo sapiens GN=CIC PE=1 SV=1	I3L2J0	0	0	0	4
UPF0705 protein C11orf49 OS=Homo sapiens GN=C11orf49 PE=1 SV=2	Q9H6J7	3	4	0	5
Uncharacterized protein C17orf85 OS=Homo sapiens GN=C17orf85 PE=1 SV=2	Q53F19	0	0	0	6
Poly(rC)-binding protein 2 OS=Homo sapiens GN=PCBP2 PE=1 SV=1	F8VZX2 (+9)	-3	0	2	2
Cyclin-T1 OS=Homo sapiens GN=CCNT1 PE=1 SV=1	O60563	0	0	0	4
Histidine ammonia-lyase OS=Homo sapiens GN=HAL PE=1 SV=1	P42357	-2	1	1	2
Transcriptional repressor p66-beta OS=Homo sapiens GN=GATAD2B PE=1 SV=1	Q8WXI9	0	0	2	4
Borealin OS=Homo sapiens GN=CDCA8 PE=1 SV=2	Q53HL2	0	0	0	4
U3 small nucleolar RNA-associated protein 18 homolog OS=Homo sapiens GN=UTP18 PE=1 SV=3	Q9Y5J1	0	0	4	3
H/ACA ribonucleoprotein complex subunit 4 OS=Homo sapiens GN=DKC1 PE=1 SV=3	O60832	0	0	5	4
T-complex protein 1 subunit theta OS=Homo sapiens GN=CCT8 PE=1 SV=4	P50990	0	0	0	4
Proliferation-associated protein 2G4 OS=Homo sapiens GN=PA2G4 PE=1 SV=3	Q9UQ80	0	0	3	2
Mitochondrial 2-oxoglutarate/malate carrier protein (Fragment) OS=Homo sapiens GN=SLC25A11 PE=1 SV=1	I3L1P8 (+1)	-3	1	1	2
Pogo transposable element with ZNF domain OS=Homo sapiens GN=POGZ PE=1 SV=2	Q7Z3K3 (+5)	0	0	2	3
Isoform 2 of Bromodomain-containing protein 2 OS=Homo sapiens GN=BRD2	P25440-2	-2	-2	2	-2
Probable ATP-dependent RNA helicase DDX41 OS=Homo sapiens GN=DDX41 PE=1 SV=2	Q9UJV9	0	0	0	3
Mitotic checkpoint protein BUB3 (Fragment) OS=Homo sapiens GN=BUB3 PE=1 SV=1	J3QT28 (+2)	0	0	5	3

Phenylalanine--tRNA ligase alpha subunit OS=Homo sapiens GN=FARSA PE=1 SV=1	K7ER00	0	0	4	0
Coronin-1B OS=Homo sapiens GN=CORO1B PE=1 SV=1	Q9BR76	0	0	0	6
rRNA 2'-O-methyltransferase fibrillarin OS=Homo sapiens GN=FBL PE=1 SV=2	P22087	0	0	4	4
Origin recognition complex subunit 3 OS=Homo sapiens GN=ORC3 PE=1 SV=1	Q9UBD5 (+1)	0	0	0	5
Neutrophil defensin 1 OS=Homo sapiens GN=DEFA1 PE=1 SV=1	P59665 (+1)	2	3	1	-3
Crooked neck-like protein 1 OS=Homo sapiens GN=CRNKL1 PE=1 SV=4	Q9BZJ0	0	0	3	3
T-complex protein 1 subunit delta OS=Homo sapiens GN=CCT4 PE=1 SV=4	P50991	0	0	3	0
Translation initiation factor eIF-2B subunit delta OS=Homo sapiens GN=EIF2B4 PE=1 SV=1	A0A087WTA5 (+4)	-2	-2	2	1
Isoform 2 of Protein IWS1 homolog OS=Homo sapiens GN=IWS1	Q96ST2-2	0	0	0	5
Protein KRI1 homolog OS=Homo sapiens GN=KRI1 PE=1 SV=3	Q8N9T8	-2	-2	2	1
Leukocyte receptor cluster member 8 OS=Homo sapiens GN=LENG8 PE=1 SV=1	A0A087WTE7	0	0	0	4
Transcriptional repressor CTCF OS=Homo sapiens GN=CTCF PE=1 SV=1	P49711	0	0	4	3
Eukaryotic translation initiation factor 3 subunit B OS=Homo sapiens GN=EIF3B PE=1 SV=3	P55884 (+1)	-2	-2	2	-2
Caldesmon OS=Homo sapiens GN=CALD1 PE=1 SV=3	Q05682	4	3	0	2
60S ribosomal protein L35a OS=Homo sapiens GN=RPL35A PE=1 SV=2	P18077	-4	-4	0	-4
ELAV-like protein 1 OS=Homo sapiens GN=ELAVL1 PE=1 SV=2	Q15717 (+1)	-3	-3	2	-3
Histone-lysine N-methyltransferase EHMT1 OS=Homo sapiens GN=EHMT1 PE=1 SV=4	Q9H9B1 (+1)	-2	-2	-2	2
Isoform 2 of ATP-citrate synthase OS=Homo sapiens GN=ACLY	P53396-2	0	0	3	0
HCG2039996 OS=Homo sapiens GN=PPAN-P2RY11 PE=1 SV=1	A0A0B4J1V8	0	0	0	3
ELM2 and SANT domain-containing protein 1 OS=Homo sapiens GN=ELMSAN1 PE=1 SV=2	Q6PJG2	0	0	0	3
Actin-like protein 6A OS=Homo sapiens GN=ACTL6A PE=1 SV=1	O96019	-2	-2	3	-2
Ribosome biogenesis protein BRX1 homolog OS=Homo sapiens GN=BRIX1 PE=1 SV=2	Q8TDN6	0	0	5	0
Ribonucleoprotein PTB-binding 1 OS=Homo sapiens GN=RAVER1 PE=1 SV=1	A0A087WZ13 (+1)	-2	-2	3	0
Pre-mRNA-processing factor 19 OS=Homo sapiens GN=PRPF19 PE=1 SV=1	Q9UMS4	0	0	3	0
Peptidyl-prolyl cis-trans isomerase-like 2 OS=Homo sapiens GN=PPIL2 PE=1 SV=1	Q13356	0	0	0	4
Transcription initiation factor TFIID subunit 9B OS=Homo sapiens GN=TAF9B PE=1 SV=1	Q9HBM6	0	0	0	5
Isoform 3 of Cleavage and polyadenylation specificity factor subunit 7 OS=Homo sapiens GN=CPSF7	Q8N684-3	0	0	5	0
Collagen alpha-1(I) chain OS=Homo sapiens GN=COL1A1 PE=1 SV=5	P02452	1	3	-2	-2
Transducin beta-like protein 2 OS=Homo sapiens GN=TBL2 PE=1 SV=1	E9PF19	0	0	4	3
Poly(A) polymerase gamma OS=Homo sapiens GN=PAPOLG PE=1 SV=2	Q9BWT3	0	0	0	4
Protein phosphatase 1D OS=Homo sapiens GN=PPM1D PE=1 SV=1	O15297	0	0	0	5

Calcium-binding mitochondrial carrier protein Aralar2 OS=Homo sapiens GN=SLC25A13 PE=1 SV=2	Q9UJS0 (+1)	-2	-2	3	2
Integrin-linked kinase-associated serine/threonine phosphatase 2C OS=Homo sapiens GN=ILKAP PE=1 SV=1	Q9H0C8	0	0	0	5
Cleavage stimulation factor subunit 2 OS=Homo sapiens GN=CSTF2 PE=1 SV=1	P33240 (+1)	0	0	0	5
Peroxisomal multifunctional enzyme type 2 OS=Homo sapiens GN=HSD17B4 PE=1 SV=3	P51659	0	0	4	0
Isoform 2 of Kelch-like protein 13 OS=Homo sapiens GN=KLHL13	Q9P2N7-2-DECOY	0	0	0	3
DNA repair protein XRCC1 OS=Homo sapiens GN=XRCC1 PE=1 SV=2	F5H8D7	0	0	2	4
WD repeat-containing protein 5 OS=Homo sapiens GN=WDR5 PE=1 SV=1	P61964	0	0	0	5
5'-3' exoribonuclease 2 OS=Homo sapiens GN=XRN2 PE=1 SV=1	Q9H0D6	0	0	4	0
X-ray repair cross-complementing protein 5 OS=Homo sapiens GN=XRCC5 PE=1 SV=3	P13010	-2	-2	2	-2
Eukaryotic translation initiation factor 3 subunit F OS=Homo sapiens GN=EIF3F PE=1 SV=1	O00303	-2	-2	3	-2
Double-strand-break repair protein rad21 homolog OS=Homo sapiens GN=RAD21 PE=1 SV=2	O60216	-2	-2	0	2
RuvB-like 1 OS=Homo sapiens GN=RUVBL1 PE=1 SV=1	Q9Y265	0	0	0	5
PC4 and SFRS1-interacting protein OS=Homo sapiens GN=PSIP1 PE=1 SV=1	O75475	0	0	0	3
WD repeat-containing protein 43 OS=Homo sapiens GN=WDR43 PE=1 SV=3	Q15061	0	0	0	3
Large subunit GTPase 1 homolog OS=Homo sapiens GN=LSG1 PE=1 SV=2	Q9H089	0	0	0	3
Heterogeneous nuclear ribonucleoprotein A3 OS=Homo sapiens GN=HNRNPA3 PE=1 SV=2	P51991 (+1)	0	0	4	0
Semenogelin-1 OS=Homo sapiens GN=SEMG1 PE=1 SV=2	P04279 (+1)	0	0	0	4
Zinc finger protein 281 OS=Homo sapiens GN=ZNF281 PE=1 SV=1	Q9Y2X9 (+1)	0	0	2	5
Isoform 2 of DNA-3-methyladenine glycosylase OS=Homo sapiens GN=MPG	P29372-2	0	0	0	4
Isoform 2 of ETS-related transcription factor Elf-2 OS=Homo sapiens GN=ELF2	Q15723-2 (+1)	0	0	0	4
HMG domain-containing protein 4 OS=Homo sapiens GN=HMGXB4 PE=1 SV=2	Q9UGU5	0	0	0	5
Isoform 3 of Transcription initiation factor TFIID subunit 6 OS=Homo sapiens GN=TAF6	P49848-3	0	0	0	4
Zinc finger MYM-type protein 2 OS=Homo sapiens GN=ZMYM2 PE=1 SV=1	Q9UBW7	0	0	0	4
Zinc finger protein 830 OS=Homo sapiens GN=ZNF830 PE=1 SV=2	Q96NB3	0	0	0	4
Dolichyl-diphosphooligosaccharide--protein glycosyltransferase 48 kDa subunit OS=Homo sapiens GN=DDOST PE=1 SV=1	A0A0C4DGS1 (+1)	-2	-2	3	-2
RNA-binding protein Raly (Fragment) OS=Homo sapiens GN=RALY PE=1 SV=1	Q5QPL9 (+1)	0	0	5	0
Polyadenylate-binding protein 2 OS=Homo sapiens GN=PABPN1 PE=1 SV=3	Q86U42 (+1)	-2	-2	-2	2
40S ribosomal protein S25 OS=Homo sapiens GN=RPS25 PE=1 SV=1	P62851	-2	-2	2	0
Protein lin-54 homolog OS=Homo sapiens GN=LIN54 PE=1 SV=3	Q6MZP7	0	0	0	4
RNA-binding protein 33 OS=Homo sapiens GN=RBM33 PE=1 SV=3	Q96EV2	0	0	0	4

Telomere repeats-binding bouquet formation protein 1 OS=Homo sapiens GN=CCDC79 PE=2 SV=3	Q8NA31-DECOY	0	0	0	3
Isoform 2 of Nuclear receptor subfamily 2 group C member 2 OS=Homo sapiens GN=NR2C2	P49116-2	0	0	0	4
Trifunctional enzyme subunit beta, mitochondrial OS=Homo sapiens GN=HADHB PE=1 SV=3	P55084	0	0	4	0
Exosome complex component RRP45 OS=Homo sapiens GN=EXOSC9 PE=1 SV=3	Q06265 (+1)	0	0	3	4
RNA demethylase ALKBH5 OS=Homo sapiens GN=ALKBH5 PE=1 SV=2	Q6P6C2 (+1)	0	0	0	4
Ribosomal biogenesis protein LAS1L OS=Homo sapiens GN=LAS1L PE=1 SV=2	Q9Y4W2 (+1)	0	0	4	0
Isoform 3 of AP-2 complex subunit beta OS=Homo sapiens GN=AP2B1	P63010-3	-2	-2	2	-2
Isoform 2 of Clathrin interactor 1 OS=Homo sapiens GN=CLINT1	Q14677-2	0	0	4	0
Eukaryotic translation initiation factor 3 subunit G (Fragment) OS=Homo sapiens GN=EIF3G PE=1 SV=5	K7EL20	0	0	4	0
Coiled-coil domain containing 55, isoform CRA_a OS=Homo sapiens GN=CCDC55 PE=1 SV=1	A0A024QZ33 (+1)	0	0	0	3
40S ribosomal protein SA OS=Homo sapiens GN=RPSA PE=1 SV=1	A0A0C4DG17 (+3)	-2	-2	2	-2
WW domain-containing adapter protein with coiled-coil OS=Homo sapiens GN=WAC PE=1 SV=3	Q9BTA9	0	0	0	4
G patch domain and KOW motifs-containing protein OS=Homo sapiens GN=GPKOW PE=1 SV=2	Q92917	0	0	0	5
Isoform 3 of Cold shock domain-containing protein E1 OS=Homo sapiens GN=CSDE1	O75534-3 (+1)	0	0	3	0
Septin-11 OS=Homo sapiens GN=SEPT11 PE=1 SV=1	D6RER5 (+3)	0	0	5	0
Putative methyltransferase C9orf114 OS=Homo sapiens GN=C9orf114 PE=1 SV=3	Q5T280	0	-3	1	-3
Integrator complex subunit 12 OS=Homo sapiens GN=INTS12 PE=1 SV=1	A0A087WXN4 (+1)	0	0	0	4
Casein kinase II subunit alpha OS=Homo sapiens GN=CSNK2A1 PE=1 SV=1	E7EU96	0	0	3	0
Cleavage stimulation factor subunit 3 OS=Homo sapiens GN=CSTF3 PE=1 SV=1	Q12996	0	0	3	0
Transcription factor E2F6 OS=Homo sapiens GN=E2F6 PE=1 SV=1	O75461	0	0	0	5
Paraspeckle component 1 OS=Homo sapiens GN=PSPC1 PE=1 SV=1	Q8WXF1 (+1)	0	0	0	4
Transcription elongation factor SPT6 OS=Homo sapiens GN=SUPT6H PE=1 SV=2	Q7KZ85	0	0	0	3
Replication factor C subunit 3 OS=Homo sapiens GN=RFC3 PE=1 SV=2	P40938	0	0	3	0
Loricrin OS=Homo sapiens GN=LOR PE=1 SV=2	P23490	0	0	0	3
Alpha-adducin OS=Homo sapiens GN=ADD1 PE=1 SV=1	E7ENY0 (+6)	0	0	3	0
Eukaryotic translation initiation factor 2A OS=Homo sapiens GN=EIF2A PE=1 SV=3	Q9BY44 (+2)	0	0	4	0
Isoform 3 of Calponin-3 OS=Homo sapiens GN=CNN3	Q15417-3	0	0	0	3
Nuclear receptor subfamily 2 group C member 1 OS=Homo sapiens GN=NR2C1 PE=1 SV=2	P13056	0	0	0	3
Inner nuclear membrane protein Man1 OS=Homo sapiens GN=LEMD3 PE=1 SV=2	Q9Y2U8	0	0	0	5
T-complex protein 1 subunit eta OS=Homo sapiens GN=CCT7 PE=1 SV=2	Q99832	0	0	3	0
Proline-rich protein 11 (Fragment) OS=Homo sapiens GN=PRR11 PE=1 SV=1	J3QKY4	0	0	3	0

Isoform sGi2 of Guanine nucleotide-binding protein G(i) subunit alpha-2 OS=Homo sapiens GN=GNAI2	P04899-4	-3	-3	2	-3
U4/U6 small nuclear ribonucleoprotein Prp4 OS=Homo sapiens GN=PRPF4 PE=1 SV=2	O43172	0	0	4	0
Protein pelota homolog OS=Homo sapiens GN=PELO PE=1 SV=2	Q9BRX2	0	0	3	0
DNA excision repair protein ERCC-1 (Fragment) OS=Homo sapiens GN=ERCC1 PE=1 SV=1	K7ES46 (+3)	0	0	0	5
Lamina-associated polypeptide 2, isoforms beta/gamma (Fragment) OS=Homo sapiens GN=TMPO PE=1 SV=1	H0YJH7	0	0	6	8
ARP2 actin-related protein 2 homolog (Yeast), isoform CRA_d OS=Homo sapiens GN=ACTR2 PE=1 SV=2	F5H6T1 (+2)	0	0	3	0
Myocyte-specific enhancer factor 2D OS=Homo sapiens GN=MEF2D PE=1 SV=1	Q14814 (+1)	0	0	0	3
MAP3K12-binding inhibitory protein 1 OS=Homo sapiens GN=MBIP PE=1 SV=1	A0A087X1L0 (+5)	0	0	0	4
Cilia- and flagella-associated protein 20 OS=Homo sapiens GN=CFAP20 PE=1 SV=1	Q9Y6A4	0	0	0	3

Ce document a été imprimé au Centre d'impression EPFL,
imprimerie climatiquement neutre, certifiée myClimate.